République Algérienne Démocratique et Populaire
Ministère de l'Enseignement Supérieur et de la Recherche Scientifique
Université A.MIRA-BEJAIA

جامعة بجاية
Tasdawit n'Bgayet
Université de Béjaïa

Faculté de technologie

Département génie des procédés

THÈSE

Présentée par

IMESSAOUDENE Ali

Pour l'obtention du grade de

DOCTEUR EN SCIENCES

Filière : Génie des procédés

Option : Génie chimique

Thème

Couplage photocatalyseurs-adsorption sur des zéolites: dépollution organique des rejets liquides pollués

Soutenue le : 06/12/2025 Devant le Jury composé de :

Nom et Prénom	Grade		
Mr. Bey Said	Professeur	Univ. de Béjaia	Président
Mr. Mouni Lotfi	Professeur	Univ. de Bouira	Rapporteur
Mme. Ait Braham Laila	Professeur	Univ. de Béjaia	Examinatrice
Mr. Aoudjit Farid	MCA	Univ. de Bouira	Examinateur

Année Universitaire: 2025/2026

Democratic and Popular Republic of Algeria
Ministry of Higher Education and Scientific Research University of Bejaia

جامعة بجاية
Tasdawit n'Bgayet
Université de Béjaïa

Faculty of Technology
Department of Process Engineering

THESIS

Presented by:

Mr. IMESSAOUDENE Ali

In view of obtaining the diploma of

DOCTORAT IN SCIENCES

Sector: Process Engineering

Option: Chemical Engineering

Thesis Title

Photocatalysts coupled with zeolites adsorption: organic depollution of contaminated liquid effluents

Supported on: 06/12/2025 In front of the jury:

First and last Name	Grade		
Mr. Bey Said	Professor	Univ. of Bejaia	Chairman
Mr. Mouni Lotfi	Professor	Univ. of Bouira	Supervisor
Mrs. Ait Braham Laila	Professor	Univ. of Bejaia	Examiner
Mr. Aoudjit Farid	Senior lecturer A class	Univ. of Bouira	Examiner

Academic Year: 2025/2026

Dedication

I dedicate this work to the memory of **my FATHER**, to **my MOTHER**, and to **my entire FAMILY**.

Acknowledgement

I would like to begin by expressing my sincere gratitude to my thesis advisor, Professor Lotfi Mouni of the University of Bouira, for his guidance throughout my research, his insightful ideas, his valuable advice, his kindness, the time he dedicated to me, as well as for his support during the writing of the articles and the revision of this thesis.

I would also like to extend my heartfelt gratitude to Mr. **Jean-Claude Bollinger**, Emeritus Professor at the University of Limoges, to Mr. **Abdelkrim Bouzaza**, Professor at the University of Rennes, to Mr. **Abdeltif Amrane**, Professor at the University of Rennes, as well as to Mr. **Aymen Assadi**, Professor at Imam Mohammad Ibn Saud Islamic University, for their kindness, their human qualities, as well as for their valuable advice and invaluable support during the revision of the articles.

I would like to thank the members of the jury for having done me the honor of accepting to evaluate my work, to their head the president of the jury Mr. **Said Bey**, Professor at University of Bejaia as well as the examiners Mrs. **Leila Ait Brahem** Professor at University of Bejaia and Mr. **Farid Aoudjit** Senior lecturer A class at University of Bouira.

Figures list

Chapter I.

Chapter II.

Chapter III.

Chapter IV.

Tables list

Chapter I.

Chapter II.

Chapter III.

Chapter IV.

Chapter V.

Chapter VI.

Summary

Section II. Investigation of the adsorption performance of zeolite and its synergistic effect with the TiO_2 photocatalyst for textile dye removal

General introduction:

Background, objectives, and thesis outline

General introduction: Background, objectives, and thesis outline.

Access to safe water is vital for life. Securing a reliable supply to meet the daily needs of the population, along with agricultural and industrial demands, remains one of the most significant challenges today [1]. Protecting clean water resources from any threat of pollution and ensuring their rational use is a shared responsibility of individuals and authorities worldwide. However, as the United Nations has highlighted in recent years, more than 80% of wastewater produced by human activities is released into water bodies without undergoing any form of treatment [2].

The global annual production of synthetic dyes is estimated at approximately 7×10^5 tons, with over 10,000 tons used by the textile industry [3,4]. Additionally, this sector consumes around 100 to 150 liters of water to produce just one kilogram of fabric [5]. As a result, the textile industry generates around 17-20% of all industrial effluents [6], with nearly 80% discharged untreated into the environment [7]. Given these figures, textile effluents are regarded as one of the primary sources of dye pollution in the hydrosphere. From a physicochemical perspective, this type of wastewater is distinguished by elevated levels of biochemical oxygen demand, chemical oxygen demand, total suspended solids, total suspended solids, toxic metals, emulsifiers, color, pH variations, and elevated temperatures [8,9]. Their discharge into aquatic environments poses serious environmental hazards, imparting undesirable color and odor to receiving water bodies, reducing dissolved oxygen levels, blocking sunlight penetration, and limiting photosynthetic activity. This deterioration of water's physicochemical properties can cause severe imbalances in aquatic ecosystems [10]. Furthermore, the carcinogenic, genotoxic, and mutagenic effects of dyes on aquatic organisms, as well as their potential risks to human health, are well documented [11]. For these reasons, the management and control of such liquid waste require special attention, both in terms of enforcing environmental regulations and monitoring pollution, and in advancing technological solutions for effective remediation.

Numerous methods have been introduced for treating dye-containing effluents, including ion-exchange resin [12], coagulation-flocculation [13], electrochemical [14], adsorption [15], biodegradation [16], ozonation [17], photocatalysis [18], fenton oxidation [19], and membrane separation [20]. However, these techniques have their own limitations, such as inefficacy for all dyes, high sludge production, high energy consumption, contaminant transfer, environmental constraints, short technology lifespan, slow kinetics, by-product formation, and economic undesirability [21,22]. Among all these techniques, adsorption may be the most suitable solution, as it offers several advantages compared to its few shortcomings. The major

benefits of this process include its simplicity, eco-friendliness, ability to treat effluents with high pollutant loads, effectiveness in removing various types of organic and inorganic contaminants, high process stability, low cost, and the possibility of reusing the adsorbent after regeneration [23]. The main limitation of this method is that, during effluent treatment, pollutants are transferred from the liquid phase to the solid phase without being degraded. Photocatalysis is a treatment technology known for its ability to degrade organic pollutants. However, its main drawback is that its application is limited to effluents with low contaminant concentrations, and the degradation reactions proceed with relatively slow kinetics [18]. A hybrid process coupling adsorption and photocatalysis in a single unit operation, working synergistically, may be one of the most effective solutions for purifying dye effluents. The key of this hybrid process lies in a composite material, designed with a high-performance adsorbent that acts as a support for a suitable semiconductor deposited on its surface. Using this innovative technology, we can achieve multiple objectives simultaneously when treating textile effluents: (i) the concurrent removal of organic pollutants (dyes) and mineral contaminants such as toxic metals, (ii) the photodegradation of dye molecules, (iii) a reduced risk of photocatalyst poisoning, as intermediate products of photocatalytic reactions can attach to the adsorbent surface, (iv) enhanced photocatalytic performance by increasing the contact area between the catalyst and the liquid phase, and (v) improved adsorption capacity, as dye molecules adsorbed on the composite surface are continuously degraded by photocatalytic sites, shifting the adsorption-desorption equilibrium in favor of further dye adsorption.

Against this background, this thesis aims to develop a versatile and sustainable composite using a simple method, designed to function simultaneously and efficiently as both an adsorbent and a photocatalyst for the effective removal of dyes.

In light of a comprehensive literature review on effective adsorbents for dyes removal from aqueous media, zeolites have been recognized as the most promising candidates for this purpose due to their high ion exchange capacity and excellent adsorption performance. This family of aluminosilicate minerals features a microporous structure, well-defined crystallinity, and a large specific surface area. Additionally, zeolites are cost-effective, environmentally friendly, and abundantly available in exploitable deposits [24–30]. On the other hand, among the various types of photocatalysts, TiO_2 is one of the most effective for degrading organic substances, particularly dye molecules, from aqueous solutions [31]. Moreover, it is less toxic, more corrosion-resistant, and more cost-effective than other photocatalysts [32].

In addition to the favorable properties of zeolites as adsorbents for dye removal mentioned above, incorporating zeolites as a support for TiO_2 can yield a composite with photocatalytic

performance far superior to that of unsupported TiO_2 nanoparticles. As is well known, zeolites exhibit amphoteric characteristics, with the framework's aluminum ions and charge-balancing cations acting as Lewis acids, while the framework's oxygens−especially those adjacent to aluminum−serve as Lewis bases [33]. Consequently, the zeolitic matrix can play a crucial role in regulating photo-induced charge transfer reactions. Furthermore, the strong electric field within the zeolite framework significantly contributes to delaying the back electron transfer reaction, which is responsible for the low quantum efficiency observed in most photocatalytic processes [34].

Considering all these factors, this thesis presents a composite of TiO_2 nanoparticles supported on an LTA-type zeolite, designed as a versatile adsorbent/photocatalyst for removing dye model molecules from aqueous solutions.

After the general introduction, this thesis is structured into two sections and six chapters, including **three full-length articles**.

- Section I. Literature review
  - Chapter I. Dyes and textile effluents
  - Chapter II. Liquid-phase adsorption
  - Chapter III. Adsorption-photocatalysis synergy for dye removal
- Section II. Investigation of the adsorption performance of zeolite and its synergistic effect with the TiO_2 photocatalyst for textile dye removal
  - Chapter IV. Zeolite waste characterization and use as low-cost, ecofriendly, and sustainable material for Malachite Green and Methylene Blue dyes removal: Box-Behnken design, kinetics, and thermodynamics
  - Chapter V. Adsorption performance of zeolite for the removal of Congo Red dye: Factorial design experiments, kinetic, and equilibrium
  - Chapter VI. Synthesis of a TiO_2/zeolite composite: Evaluation of adsorption-photodegradation synergy for the removal of Malachite Green

Finally, a general conclusion.

Section I. Literature review

Chapter I. Dyes and textile effluents

1. Introduction

Most dye substances contain chromophores and auxochromes in their structures. Chromophores are responsible for imparting color, while auxochromes enhance the dye's color. The term 'auxochrome' originates from the Greek words 'auxo' and 'chrome,' meaning 'enhance' and 'color,' respectively. Chromophores are the key chemical units in dye molecules that absorb and reflect specific wavelengths of light when exposed to the visible spectrum [35,36].

Dyes can be divided into two main categories according to their origin: natural and synthetic. Natural dyes are extracted either from plants such as indigofera, Jack fruits, heather, turmeric, saffron, and others [37] or animal sources such as cochineal, kermes, lac insect, etc. [38]. In contrast, synthetic dyes are unsaturated polyaromatic compounds produced through chemical synthesis. Before the mid-19th century, only natural dyes were available. The development of synthetic dyes was driven by the increasing demand for colors that were intense, long-lasting, and could be produced quickly and cost-effectively. Currently, more than 700,000 tons of synthetic dyes are produced each year, covering about 10,000 structurally distinct colors [4]. This category of dyes finds extensive application in the textile, printing, tanning, and paper industries. Additionally, some are employed in the cosmetics and pharmaceutical industries, as well as in food processing [39]. These compounds include azo, direct, acid, basic, reactive, disperse, mordant, and sulfide dyes (Fig I.1) [40].

Currently, the textile sector utilizes both natural fibers such as wool, cotton, and silk, and synthetic fibers, including polyamides, polyolefins, acrylics, and polyesters [41]. For colouring various materials made from different fibers, an average of 50-90 g of dyestuff and approximately 100-150 liters of water is required to color just 1 kg of fabric [5]. Textile manufacturing is a complex process comprising several stages to produce a variety of fabric materials, including sizing, desizing, scouring, bleaching, mercerization, dyeing and printing, and finishing [42]. Each stage of the process involves the use of a wide variety of chemicals, including strong acids and alkalis, chlorinated inorganic compounds, sodium hypochlorite, organic substances such as dyes, bleaching agents, finishing chemicals, starches, thickeners, surfactants, wetting and dispersing agents, and metal salts [43]. On the other hand, regarding environmental impact, the textile industry is estimated to consume more water than any other industry globally, with practically all discharged wastewater being heavily polluted. According to previous research, more than 10,000 tons of dyes are used worldwide each year to produce 40 million tons of textiles, leading to the discharge of 3,600 tons of highly concentrated dye

waste into natural water sources [3]. Moreover, other studies indicate that the textile industry accounts for approximately 17-20% of all industrial effluents [6]], with nearly 80% of these effluents being released untreated into the environment [7]. In light of these and other data, textile effluents are considered to be the primary sources of dye pollution in the hydrosphere.

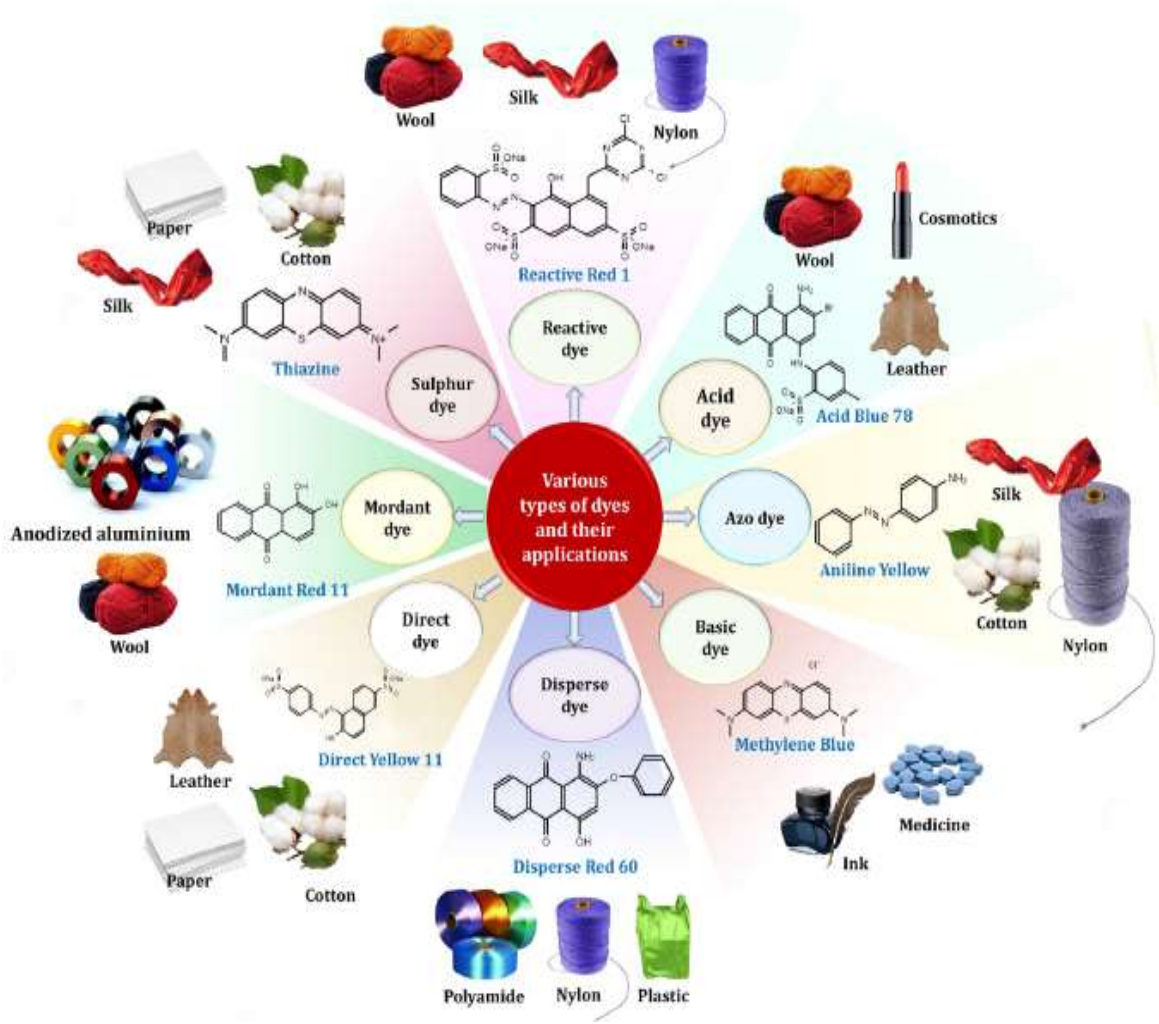

Fig I.1. Different categories of dyes and their suitability for diverse industrial applications [40].

2. Textile dye classification

Dyes are typically classified into various categories. In the textile industry, the most commonly used types include basic, acid, direct, disperse, mordant, reactive, vat, sulfur, and azoic dyes. Among these, acid, direct, and reactive dyes represent the three primary subcategories of anionic dyes [44]. Disperse dyes do not ionize in aqueous medium and are therefore referred to as nonionic dyes. The major basic dyes are categorized into two major groups: azo basic and reactive dyes due to nitrogen, which has free electron pair interact with the p-orbital system delocalized [45].

- **Acid dyes**: These compounds contain sulfonic acid functional groups, which enhance their solubility in water.
- **Basic dyes:** These are also water-soluble, positively charged compounds that exhibit a high affinity for substrates in low-concentration acidic dye baths.
- **Direct dyes**: These are typically salts of azo dyes and anionic substance. They exhibit high solubility in water and can be used directly in alkaline dye baths without the need for a mordant. This allows them to be immediately applied to cellulosic fibers without requiring additional elements such as copper or chromium.

Table I.1 illustrates the classification of various dyes according to their charge and chemical nature.

Table I.1. Dyes categorized according to their nature and ionic charge [45].

Dye class		**Applications**	**Examples**
Cationic		Silk, cotton, wool, tannin mordanted, ink, and medicine	Methylene Blue, Crystal Violet, Malachite Green, and Safranin
Anionic	Acid	Nylon, wool, modified polyesters, polyacrylonitrile, ink, medicine	Acid Red18 and Acid Red88
	Direct	Leather, nylon, paper, rayon and cotton	Copper Blue2R, Brilliant Blue, and Congo Red
	Reactive	Cotton, nylon, wool, and other cellulosic	Reactive Black5 and Reactive Orange16
Disperse		Acrylic fibers, nylon, polyester, cellulose, and cellulose acetate	Disperse Orange37 and Disperse Red1
Vat		Rayon, wool, and cotton	Vat Range1, Vat Violet13, and Vat Red10
Sulfur		Leather, paper, cotton and rayon, wood, and silk	Sulfur Brilliant Green and Sulfur Black1
Solvent		Oils, plastics, gasoline, lubricants and waxes	Solvent Red1, Solvent Red24, and solvent Red111

3. Typical properties of textile wastewater

Untreated wastewater discharged by textile industries typically contains a complex mixture of synthetic dyes, toxic metals, and various organic and inorganic contaminants. These effluents are characterized by high levels of color, biochemical oxygen demand, chemical oxygen demand, total suspended solids, total dissolved solids, toxic metals (such as Cr, Cd, Cu, Pb, and Zn), emulsifiers, as well as variations in pH and temperature [8,35]. The typical properties of textile effluents, as reported in various references, are summarized in Table I.2. As can be seen, these characteristics exhibit variability across different literature sources. As noted by Yaseen & Scholz (2019) [8], defining typical textile wastewater is challenging, as its characteristics largely depend on the type of fibers used and the specific unit processes involved in production.

4. Environmental and human health effects of textile effluents

The discharge of untreated textile wastewater into aquatic ecosystems negatively impacts aquatic flora and fauna and poses risks to human health. These severe ecological effects include undesirable color and odor in the receiving water body, reduced dissolved oxygen levels, blocked sunlight penetration, and inhibited photosynthetic reactions, ultimately leading to severe ecosystem disruption [53]. Fish and other aquatic organisms are significant sources of protein; however, their consumption may lead to health issues such as convulsions, fever, and arterial hypertension due to the accumulation of dyes in their tissues [54]. Suspended solids in textile effluent can block the flow of water through fish gills, impairing gas exchange and potentially leading to reduced growth rates or death [40]. The high concentrations of mineral salts and the presence of toxic metals, even at ppm levels, in textile effluents are harmful to soil quality. As a result, plant growth is negatively affected, limiting seed germination and inhibiting seedling development [55]. Microalgae play a crucial role in aquatic ecosystems as primary producers, providing both economic and ecological benefits. However, dye contamination impairs their growth and disturbs the trophic transfer of energy and nutrients throughout the aquatic food chain [56].

Textile dyes, known for their high toxicity and potential carcinogenicity, have been linked to a variety of diseases in both humans and animals. These dyes can lead to conditions ranging from dermatitis to issues with the immune and nervous systems [57]. The substitution of enzymatic cofactors, which renders the enzymes inactive, may be the underlying cause of these health problems [58].

Table I.2. Typical composition and properties of textile effluents.

Sources / Parameters	Eswaramoorthi et al. [46]	Kalra et al. [47]	Hussein [48]	Ghaly et al. [49]	Elango et al. [50]	Abu Bakar et al. [51]	Bidu et al. [52]
Temperature (°C)	35-45	35-45	33-45	35-45	30	30.13-32.7	28.9- 52.8
pH	6-10	6-10	5.5-10.5	6-10	8.66	6.27-8.80	7.5-12.3
Coulour (pt-Co)		50-2500		50-2500	5200	69-205	231-4,090
BOD (mg/L)	300-500	100-4000	100-4000	80-6000	970	7.1-85	125-550
COD (mg/L)	1000-1500	150-10,000	150-10,000	150-12,000	3080	55-294	480-3,750
TDS (mg/L)	8000-12,000	1800-6000	1500-6000	2900-3100	242,220	1250-3610	2,680-10,160
TSS (mg/L)	200-400	100-5000	100-5000	15-8000	7116	17-140	65-2,435
Turbidity (NTU)					81.5	5.89-26.6	9.4-450.0
Chlorides (mg/L)	3000-6000	1000-6000	200-6000		42,487		
Sulphates (mg/L)	600-1000		500-700	600-1000			
Zinc (mg/L)	< 10		3-6	< 10		0.488-2.220	
Copper (mg/L)	< 10		2-6	< 10		0.059-0.174	
Chromium (mg/L)			2-5				

Other studies have shown that textile dyes can interfere with the function of human serum albumin by binding to it, leading to conformational changes or even precipitation [59]. Moreover, toxic metals commonly found in these effluents, can damage various organs by generating reactive oxygen species (ROS) through the NADPH oxidase pathway. The overproduction of ROS contributes to oxidative stress, which in turn leads to endothelial dysfunction [11].

5. Various technologies and approaches used for treating textile effluents

Given the previous discussions regarding the typical effluents produced by the textile industry and their impact on both the environment and human health, these liquid wastes demand careful management and control. This involves enforcing environmental regulations to monitor pollution and developing technological solutions for their remediation. To address this, various methods have been proposed for treating dye-containing effluents, including ion-exchange resin [12], coagulation-flocculation [13], electrochemical [14], adsorption [15], biodegradation [16], ozonation [17], photocatalysis [18], fenton oxidation [19], and membrane separation [20]. However, these techniques have their limitations, including being unsuitable for all types of dyes, generating high sludge production, requiring high energy consumption, transfer contaminants, facing issues related to environmental conditions, having a short lifespan, exhibiting slow kinetics, producing by-products, and being economically undesirable [21,22]. Among all these techniques, adsorption may offer the most viable solution, as it presents several advantages that outweigh its few drawbacks. The main benefits of this process include its simplicity, eco-friendliness, ability to treat effluents with high pollutant loads, effectiveness in removing various organic and inorganic contaminants, high process stability, low cost, and the potential for multiple reuses of the adsorbent after regeneration [23]. The main limitation of this method is that, during effluent treatment, pollutants are transferred from the liquid phase to the solid phase without undergoing degradation. On the other side, photocatalysis is recognized as a treatment technology effective in degrading organic pollutants. However, its major drawback is that it is primarily applicable to effluents with low concentrations of contaminants, and the degradation reactions occur at relatively slow kinetics. A hybrid process combining adsorption and photocatalysis, working synergistically within a single unit operation, may represent one of the most promising solutions for purifying dye effluents. The core of this hybrid process is a composite material, consisting of a powerful adsorbent that serves as a support for a suitable semiconductor deposited on its surface. Using this innovative technology, several goals can be achieved concurrently in the treatment of this

type of effluents: (i) simultaneous removal of organic pollutants (dyes) and mineral contaminants, such as toxic metals, (ii) photodegradation of dye molecules, (iii) minimize the risk of photocatalyst-poisoning, as intermediate products of photocatalytic reactions can attach to the adsorbent's surface, (iv) enhanced photocatalyst performance by increasing its contact surface with the liquid phase, and (v) improved adsorption capacity of the composite for dyes compared to pure adsorption, as dye molecules adsorbed on the composite surface can be continuously destroyed by the catalyst sites, shifting the adsorption-desorption equilibrium in favor of greater dye adsorption.

In this context, the present thesis aims to develop a versatile and sustainable composite using a simple method, designed to function simultaneously and efficiently as both an adsorbent and a photocatalyst for effective dye removal. Zeolites have proven to be among the most promising candidates for this purpose due to their high ion-exchange capacity and exceptional adsorption performance. Additionally, this family of aluminosilicate minerals possesses a microporous structure with well-defined crystallinity and a large specific surface area. Moreover, they are cost-effective, environmentally sustainable, and obtained from abundant, readily accessible natural deposits [24–30]. On the other hand, among the various types of photocatalysts, TiO_2 is regarded as one of the most effective for removing organic pollutants, particularly dye molecules, from aqueous solutions [31]. Additionally, it is less toxic, corrosion-resistant, and more cost-effective compared to other photocatalysts [32].

In addition to the suitable properties of zeolites as adsorbent, incorporating zeolites as a support for TiO_2 can result in a composite with significantly improved photocatalytic performance compared to unsupported TiO_2 nanoparticles.

For all these reasons, this thesis aims to develop a composite material consisting of TiO_2 nanoparticles supported by an LTA-type zeolite, which can function as a versatile adsorbent and photocatalyst for dye removal from aqueous solutions.

Chapter II. Liquid-phase adsorption

1. Introduction

The adsorption phenomenon is one of the oldest techniques for removing contaminants from gas and liquid phases, based on interaction between adsorbate species and the active adsorption sites of the adsorbent surface [60]. However, adsorption continues to be a widely used technology for wastewater depollution, owing to its excellent removal efficiency and the absence of by-product formation in the treated solution.

This chapter explores adsorption theory, emphasizing the primary kinetic and isothermal models relevant to the process. It offers a detailed methodology for the accurate calculation of thermodynamic parameters for liquid-phase adsorption, utilizing various equilibrium constants associated with adsorption isotherms. In addition, it offers a summary of recent research on various adsorbents, with a particular focus on zeolite, used in water treatment, especially for dye removal.

2. Adsorption process

2.1. General

The adsorption phenomenon involves the removal of contaminants from the system's bulk phase by attaching them to the surface's active sites of an adsorbent. Adsorption processes are generally classified into physisorption, which is driven by weak van der Waals forces, and chemisorption, where covalent bonding occurs. Furthermore, adsorption can also take place via electrostatic attraction [61]. On the other hand, physisorption is characterized by relatively low enthalpy changes, typically ranging between 20 and 40 kJ/mol, and causes minimal disruption to the electronic structures of the species involved. In contrast, chemisorption is highly exothermic, with enthalpy changes typically ranging between 180 and 240 kJ/mol. It also induces significant changes in the electronic structures of both the contaminant molecules and the solid surface [62]. The release of adsorbed compounds from the adsorbent surface, triggered by external constraints, is known as desorption.

In batch adsorption studies, the quantities of adsorbate adsorbed onto the adsorbent surface at equilibrium, q_e (mg/g), and at a given time t, q_t (mg/g), are commonly determined using mass balance equations, as shown below [15].

$$q_e = \frac{(C_0 - C_e)\,V}{m} \qquad (1)$$

$$q_t = \frac{(C_0 - C_t)\, V}{m} \qquad (2)$$

here, C_0 (mg/L), C_e (mg/L), and C_t (mg/L) represent the adsorbate concentrations at the initial time, at equilibrium, and at a given time *t*, respectively; *m* (g) is the mass of the adsorbent, and *V* (L) is the volume of the solution. Thus, the *m*/*V* ratio is referred to as the adsorbent dose.

2.2. Factors Influencing dyes adsorption

In addition to the intrinsic properties of the adsorbate and adsorbent, dye adsorption is significantly influenced by several operational factors, such as solution pH, adsorbent dose, adsorbate concentration, contact time, temperature, and agitation speed, among others [63]. These factors undoubtedly govern the adsorption kinetics and the efficiency of dye molecule interactions with the active sites on the adsorbent. As a result, researchers highlight the importance of optimizing and controlling these environmental parameters to design and develop scalable dye removal processes for industrial applications.

2.2.1. Impact of solution pH

The solution's pH is a key factor in most dye adsorption methods [10], as it directly affects the ionization state of the dye species and the electrical charge on the adsorbent, ultimately influencing both the adsorption rate and capacity. Under acidic conditions, the adsorbent surface tends to acquire a positive charge, which decreases the adsorption of cationic dyes while enhancing the uptake of anionic dyes. Conversely, under alkaline conditions, the adsorbent surface acquires a negative charge, increasing the attraction and adsorption of cationic dyes. However, in such conditions, electrostatic repulsion limits the uptake of anionic dyes [64]. On the other hand, when the solution pH is below the pH_{PZC} (point of zero charge of the adsorbent), the adsorbent surface carries a positive charge, whereas at pH values higher than pH_{PZC}, it becomes negatively charged [65]. This parameter is critical in determining the adsorption behavior of ionic species in aqueous solutions [15].

2.2.2. Impact of initial concentration

The concentration of dye molecules in the solution has a significant impact on the adsorption process. Generally, the initial dye concentration serves as a key driving force, facilitating the transfer of adsorbate species from the bulk solution to the adsorbent surface. As the initial concentration increases, the driving force for adsorption becomes stronger. However,

at higher dye concentrations, increased molecular competition may limit access to the available surface sites [66].

2.2.3. Impact of adsorbent dose

The amount of adsorbent is a critical parameter that affects adsorption performance. Generally, the dye removal percentage increases with higher adsorbent dosages, as a result of the greater availability of active adsorption sites. Evaluating the impact of the adsorbent quantity is essential to determine the minimum amount required for effective dye removal, ensuring the process remains economically feasible and cost-efficient [67].

2.2.4. Impact of temperature

Another important parameter that influences physicochemical processes is temperature. An increase in dye adsorption at higher temperatures indicates a temperature-dependent (endothermic) removal process, likely due to the enhanced mobility of guest molecules. Conversely, a decrease in removal efficiency at elevated temperatures, characteristic of an exothermic process, suggests that the interaction between adsorbate species and the adsorbent surface weakens as the temperature increases, resulting in reduced adsorption efficiency [45].

2.3. Adsorption kinetics

Contact time generally plays a crucial role in determining (i) the true adsorption equilibrium, (ii) the adsorption rate, and (iii) the activation energy of the adsorption process. The equilibrium time and adsorption rate are strongly influenced by the properties of the adsorbent , the nature of the adsorbate, and, in particular, experimental conditions (such as temperature, pH, agitation speed, concentrations of adsorbate and adsorbent, solution ionic strength, adsorbent granulometry, etc) [68].

Kinetic studies are crucial in adsorption research as they offer valuable insights into the uptake mechanism. Identifying the most suitable kinetic model is the primary approach for predicting the optimal adsorption kinetics.

Under nonequilibrium conditions, adsorption kinetics data are commonly interpreted using pseudo-first-order (PFO) and pseudo-second-order (PSO) kinetic models, with one often considered to be more suitable than the other based on better goodness-of-fit criteria. PFO equation, also referred as the Lagergren model, is usually written as:

$$\frac{dq_t}{dt} = k_1 (q_e - q_t) \qquad (3)$$

where k_1 (min^{-1}) is the PFO rate constant.

The PFO rate equation aligns well with the concept of a linear driving force [69]. By integrating Equation (3) under the boundary conditions (q_t = 0 et t = 0 and $q_t = q_t$ at $t = t$), the following nonlinear expression is obtained:

$$q_t = q_t (1 - e^{-k_1 t}) \qquad (4)$$

Originally proposed by Blanchard et al. [70], the PSO rate equation has also been extensively utilized for analyzing adsorption kinetics data [71]. Its corresponding kinetic model is expressed as:

$$\frac{dq_t}{dt} = k_2(q_e - q_t)^2 \qquad (5)$$

By applying the same boundary conditions mentioned earlier, the resulting equation is as follows:

$$q_t = \frac{k_2 \, q_e^2 \, t}{1 + k_2 q_e t} \qquad (6)$$

where k_2 (g/mg min) denotes the PSO rate constant.

The initial adsorption rate h_0 [(mg/g)/min] can be obtained when t tends toward zero [72] as shown in Equation (7):

$$h_0 = k_2 q_e^2 \qquad (7)$$

The potential influence of intraparticle diffusion resistance on the adsorption process can be evaluated using the intraparticle diffusion (IPD) model, as described in Equation (8) [73].

$$q_t = k_{id} \, t^{0.5} + C \qquad (8)$$

k_{id} (mg/g $min^{0.5}$) is the IPD rate constant and C (mg/g) is a constant that reflects the boundary layer thickness. Higher values of C indicate a stronger influence of boundary layer resistance on the adsorption process [74].

2.4. Adsorption isotherms

The literature commonly describes two standard methods for deriving adsorption isotherms in batch adsorption studies. The first method involves determining the adsorption isotherm at different initial adsorbate concentrations while keeping experimental conditions constant, such as contact time, adsorbent dose, temperature, agitation speed, etc. The second method evaluates the adsorption isotherm by varying the adsorbent dose while maintaining all other experimental conditions constant [68].

An adsorption isotherm illustrates the relationship between the quantity of adsorbate retained by the adsorbent (q_e) and the equilibrium concentration of the adsorbate in the bulk solution (C_e) at a constant temperature. Parameters derived from adsorption isotherms provide valuable insights into solid surface characteristics, the mode of adsorbent–adsorbate interactions, and the most probable adsorption mechanisms. Several equations describe adsorption equilibrium, with the Langmuir equation being the most widely used and extensively studied. Other models, including the Freundlich and Temkin isotherms, have also been widely examined in the literature.

The theoretical Langmuir equation, introduced by Langmuir in 1918 and initially applied to gas adsorption on solid surfaces, was derived based on the following assumptions [75]:

i. Adsorption is reversible;
ii. The adsorbent surface contains a fixed number of accessible sites, all of which possess equal adsorption energy;
iii. Adsorption at a site is limited to a single adsorbate molecule, preventing any further adsorption at that site;
iv. Adsorbate species do not interact with each other.

The Langmuir isotherm model is expressed in Eq. 9.

$$q_e = \frac{q_{max}\ K_L\ C_e}{1 + \ K_L\ C_e} \qquad (9)$$

where K_L (L/mg) and q_{max} (mg/g) represent the Langmuir constant and the maximum adsorption capacity, respectively, assuming monolayer adsorption on the adsorbent surface.

The separation factor (R_L; dimensionless), as defined by Webber and Chakravorti [76], is given by the following expression [74]:

$$R_L = \frac{1}{1 + K_L\, C_0} \qquad (10)$$

The value of R_L provides insight into the nature of adsorption, as outlined below: favorable ($0 < R_L < 1$), unfavorable ($R_L > 1$), linear ($R_L = 1$), or irreversible ($R_L = 0$).

The Freundlich isotherm [77] is an empirical model that accommodates multilayer adsorption and accounts for the non-uniform distribution of adsorption energies and affinities on heterogeneous surfaces [78]. It remains widely used today in the analysis of heterogeneous systems and is expressed as:

$$q_e = K_F C_e^{1/n} \qquad (11)$$

here K_F [(mg/g)/(mg/L)$^{1/n}$] is the Freundlich constant, and 1/n [dimensionless; $0 < n < 10$] is the intensity parameter, reflecting the heterogeneity of the adsorbent surface or the adsorption driving force. When *n* exceeds 10, the adsorption isotherm resembles a rectangular isotherm, approaching an irreversible adsorption behavior [79].

The Temkin isotherm equation is frequently employed to characterize adsorption equilibrium. Originally proposed by Temkin and Pyzhev, this model is based on the assumption that the heat of adsorption, which is influenced by temperature, decreases linearly with increasing coverage of the adsorbent surface [69]. The characteristic equation of this isotherm is as follows:

$$q_e = \frac{R\, T}{b_t}\, ln(a_t\, C_e) \qquad (12)$$

where *R* is the universal gas constant, *T* denotes the absolute temperature, b_t is a constant related to the heat of adsorption, and a_t is the Temkin isotherm constant.

2.5. Adsorption thermodynamics

Investigating the thermodynamics of adsorption is essential for evaluating the nature of the adsorption mechanism, whether physical or chemical. Thermodynamic parameters can be determined in accordance with the fundamental laws of thermodynamics by applying the expressions outlined blow [75]:

$$\Delta G^0 = -R\, T\, lnK_C \qquad (13)$$

After rearranging, Eq. 13 becomes:

$$K_C = e^{-\frac{\Delta G^0}{RT}} \qquad (14)$$

The relationship between ΔH^0, ΔS^0, and ΔG^0 is given as:

$$\Delta G^0 = \Delta H^0 - T\,\Delta S^0 \qquad (15)$$

The van′t Hoff equation, a widely recognized relationship, is derived by substituting Eq. 13 into Eq. 15.

$$lnK_C = \frac{-\Delta H^0}{R}\frac{1}{T} + \frac{\Delta S^0}{R} \qquad (16)$$

From Equation (13), the Gibbs free energy change (ΔG^0) can be directly calculated, while from Equation (16), the plot of ln K_C versus 1/T allows the determination of the enthalpy change (ΔH^0) and entropy change (ΔS^0) from the slope and intercept, respectively.

In accordance with the guidelines of the International Union of Pure and Applied Chemistry (IUPAC) [80], the standard units for T, R, and ΔG^0 are K, J/ (mol K), and J/mol, respectively. Therefore, the equilibrium constant K_C in Equation (13) and (14) must be dimensionless. These thermodynamic estimates provide insights into the nature and mechanism of adsorption (physisorption or chemisorption). A positive ΔH^0 value indicates an endothermic adsorption process, while a negative ΔH^0 signifies an exothermic process. A low ΔS^0 value typically indicates minimal entropy change during adsorption, whereas a positive ΔS^0 suggest greater randomness at the solid-liquid interface [81].

It is crucial to note that the accurate estimation of ΔG^0, ΔH^0, and ΔS^0 depends on the precise determination of K_C (dimensionless). According to prominent literature, these thermodynamic parameters can be accurately calculated from K_C values derived from adsorption isotherm constants (e.g., K_L, K_F, etc.). However, several factors need to be carefully considered to ensure the accuracy of the calculation method, which can be summarized as follows: (i) K_C must be dimensionless; (ii) all temperatures involved in the calculations must be reported in kelvin; (iii) the determination coefficient (R^2) of the Equation (16) should be high; (iv) in adsorption equilibrium studies, the adsorbate concentration range must be explicitly specified as either high or low [75].

In this section, we provide a detailed discussion on the derivation of K_C from isotherm models, specifically the Langmuir and Freundlich models, due to their extensive use in the literature.

2.5.1. Relationship between the Langmuir constant and the equilibrium constant

In his insightful article, Liu [81] poses a fundamental but rarely addressed question in adsorption research: Is it reasonable to use Langmuir's constant to calculate ΔG^0 using Equation (13)? To explore this, he presents an analysis based on the principles of chemical equilibrium and physical chemistry.

According to Langmuir [82], the adsorption process can be represented by the following scheme:

$$S + A \leftrightarrow SA \qquad (17)$$

here, S denotes free solute species, A represents vacant active sites on the adsorbent surface, and SA corresponds to the occupied active sites. Based on Eq. 17, the equilibrium constant (K_C) is defined as:

$$K_C = \frac{a_{SA}}{a_S\, a_A} \qquad (18)$$

where a_{SA}, a_S, and a_A represent the activities of the occupied sites, the solute in solution, and the vacant sites on the adsorbent, respectively.

It is reasonable to assume that a_{SA} and a_A are equal. Therefore, Equation (18) becomes:

$$K_C = \frac{\theta_e}{(1-\theta_e)\, a_e} \qquad (19)$$

here, θ_e denotes the fraction of the adsorbent surface covered at equilibrium, and a_e represents the equilibrium activity of the adsorbate in the bulk solution. In chemical terms, the activity of a substance is expressed as a function of its molar concentration (C_e) using the following relation:

$$a_e = \gamma_{adsorbate}\, \frac{C_e}{C^0_{adsorbate}} \qquad (20)$$

In equation 20, $\gamma_{adsorbate}$ (dimensionless) and $C^0_{adsorbate}$ (mol/L) represent the activity coefficient of the adsorbate and its standard concentration, respectively.

Substituting Equation 20 into Equation 19 yields:

$$K_C = \frac{\theta_e\, C^0_{adsorbate}}{(1-\theta_e)\, \gamma_{adsorbate}\, C_e} \qquad (21)$$

In adsorption studies, θ_e is defined as:

$$\theta_e = \frac{q_e}{q_{max}} \qquad (22)$$

Inserting Eq. 22 into the Langmuir isotherm equation (Eq. 9) yields

$$\theta_e = \frac{K_L C_e}{1 + K_L C_e} \qquad (23)$$

from which, K_L can be derived as:

$$K_L = \frac{\theta_e}{(1 - \theta_e)\, C_e} \qquad (24)$$

The comparison of Eq. (21) and Eq. (24) shows that

$$K_C = \frac{K_L\, C^0_{adsorbate}}{\gamma_{adsorbate}} \qquad (25)$$

Although $\gamma_{adsorbate}$ is typically calculated using the Debey-Hückel law, it is assumed to be unity for neutral adsorbates or those with weak charges (e.g., organic compounds), as well as for charged adsorbates (e.g., multivalent ions) in dilute solutions [81]. On the other hand, in nearly all studies on solid-liquid adsorption, the concentration of $C^0_{adsorbate}$ is commonly chosen as 1 mol/L [83,84]. Therefore, K_C will be directly equal to K_L of Langmuir model if K_L is expressed in units of L/mol (Eq. (25)). However, in the literature, K_L is commonly expressed in unit of L/mg, as the units used in adsorption isotherms are q_e (mg/g) versus C_e (mg/L). In some studies, K_L is also expressed in L/mmol when q_e (mmol/g) versus C_e (mmol/L) is used.

To ensure accurate thermodynamic parameter calculation, Tran et al. [85] recommended the following conversions to derive the correct value of K_C from K_L (expressed in various commonly used unites), as shown below:

$$K_C = K_L \times 10^3 \times M_w \times \frac{C^0_{adsorbate}}{\gamma_{adsorbate}} \qquad \{q_e(mg/g)\ and\ C_e\ in\ (mg/L)\} \qquad (26)$$

$$K_C = K_L \times 10^3 \times \frac{C^0_{adsorbate}}{\gamma_{adsorbate}} \qquad \{q_e(mmol/g)\ and\ C_e\ in\ (mmol/L)\} \qquad (27)$$

$$K_C = K_L \times \frac{C^0_{adsorbate}}{\gamma_{adsorbate}} \qquad \{q_e(mol/kg)\ and\ C_e\ in\ (mol/L)\} \qquad (28)$$

where M_w is the molar weight of the adsorbate molecule in g/mol.

2.5.2. Relationship between the Freundlich constant and the equilibrium constant

The accurate value of K_C can be derived from the Freundlich constant K_F as follows [75]:

$$K_C = \frac{K_F\,\rho}{1000}\left(\frac{10^6}{\rho}\right)^{\left(1-\frac{1}{n}\right)} \qquad (29)$$

here K_F is expressed in [(mg/g)/(mg/L)$^{1/n}$], and ρ represents the density of pure water, assumed to be 1.0 g/mL.

When K_F is expressed in [(mmol/g)/(mmol/L)$^{1/n}$], the conversion between the two unit systems of K_F can obtained using the following relationship [79]:

$$K_F\left[\left(\frac{mg}{g}\right)\Big/\left(\frac{mg}{L}\right)^{\frac{1}{n}}\right] = K_F\left[\left(\frac{mmol}{g}\right)\Big/\left(\frac{mmol}{L}\right)^{\frac{1}{n}}\right] M_w{}^{\left(1-\frac{1}{n}\right)} \qquad (30)$$

The exponent 1/n remain unaffected regardless of the units used to express substrate concentration and adsorption capacity in the isotherm.

2.6. Various adsorbents for dye removal

2.6.1. Activated carbon

Of the many adsorbents materials suggested, activated carbon remains the most commonly used for wastewater depollution [86,87]. Due to its high adsorption capacity across a wide range of dyes compounds, it is a more favorable option compared to other costly treatment technologies [86]. However, activated carbon has several limitations, including a higher cost compared to other adsorbents, difficulty in regeneration, lack of selectivity, and limited effectiveness towards certain categories of dyes [87]. These drawbacks have prompted researchers to explore alternative low-cost adsorbents, with some of the most notable examples discussed below.

2.6.2. Low-cost adsorbents for efficient dye removal

Cost is a key factor in comparing adsorbent materials. An adsorbent is typically considered ‘low-cost’ if it requires minimal processing, is naturally abundant, or is sourced from industrial waste or by-products with little to no remaining economic value. A variety of

waste materials from industrial and agricultural sources, as well as natural substances and biosorbents, offer promising low-cost alternatives. Many of these materials have been studied and recommended for use in dye removal applications.

2.6.2.1. Industrial by-products

In the literature [88–91], fly ash, metal hydroxide sludge, red mud, biosolids, and waste slurry are considered low-cost industrial by-products with potential for use as adsorbents in dye removal.

2.6.2.2. Agricultural solid wastes

Numerous studies have demonstrated the effectiveness of various agricultural solid waste as adsorbent for removing both organic and inorganic contaminants, including dyes. The use of these materials for dye removal, as well as the adsorption capacities of different agriculture by-products, has been extensively investigated in the literature [67,87].

2.6.2.3. Biosorbents and microbial biomass

Biosorption refers to the capacity of biomass to remove pollutants from wastewater. This process involves a range of biosorbents, including bacteria, yeast, fungi, mold, and algae. The adsorption capability is influenced by several mechanisms, including ion exchange, surface adsorption, coordination complexation, microprecipitation, etc [92,93]. Biosorption has been widely explored for the removal of dye components from dilute aqueous solutions using inactive or dead biomass [94–97]. Although biosorption offer promising solutions for treating dye effluents, they have several limitations. The sorption process is typically slow, highly dependent on pH, and difficult to implement in column treatments due to clogging issues.

2.6.2.4. Inorganic materials for dye removal

2.6.2.4.1. Clay minerals

Natural clay minerals have been used as adsorbents for many years due to their abundance, high adsorption capacity, and ion-exchange potential. Additionally, their layered structure makes them ideal host materials for adsorbates [86]. Although, clay minerals exhibit a strong affinity for both anionic and cationic dyes [98–101], the adsorption process is primarily governed by ion-exchange, making the adsorption capacity highly dependent on the solution's pH [87].

2.6.2.4.2. Zeolites

The study of zeolite chemistry dates back to 1756, when Axel Fredrik Cronstedt discovered the mineral stilbite ($NaCa_2Al_5Si_{13}O_{36}.14H_2O$). He coined the term 'zeolite'—derived from the Greek words *zeo* (to boil) and *lithos* (stone)—to describe this group of minerals, referring to their characteristic behavior as 'boiling stones' [102].

Zeolites are minerals classified as aluminosilicates with a well-defined crystalline structure. Their primary components are aluminum (Al), silicon (Si), and oxygen (O), arranged in tetrahedral configurations of SiO_4 and AlO_4, which define the different types of zeolites. In these structures, the central aluminum or silicon atom forms covalent bonds with four oxygen atoms, and the formula TO_4 is commonly used to represent the central atom [T] and its surrounding oxygen atoms [O] [103]. Figure II.1 illustrates examples of the structural units along with the pore or cage size for three zeolitic frameworks: zeolite A, sodalite, and faujasite. Additionally, Figure II.2 provides a detailed depiction of the framework structure of zeolite A (LTA). Each type of zeolite is classified based on the number of rings (R) and their arrangement. The structures of zeolites A, sodalite, and faujasite are composed of 4R and 6R primary building units (PBUs), which consist of rings containing four and six tetrahedral TO_4 units, respectively. In the structural models, the T elements within the framework are positioned at the intersections of the edges, while the oxygen atoms occupy the midpoints of those edges [103]. As of July 2014, The Structure Commission of the International Zeolite Association (IZA-SC) had assigned codes to 2018 zeolite frameworks [104,105].

Zeolites are classified into two main types: natural and synthetic. Natural zeolites form over millions of years from volcanic ash or marine salts. In contrast, synthetic zeolites are produced through hydrothermal treatment at temperatures ranging from 90 to 250°C under alkaline conditions [107]. Zeolite minerals are classified into three categories according to their Si/Al molar ratio: (i) high-silica zeolites with a Si/Al greater than 5, (ii) intermediate-silica zeolites with a Si/Al between 2 and 5, and (iii) low-silica zeolites with a Si/Al less than 2 [107,108]. Siliceous zeolites, with a higher silicon content, act as organophilic, non-polar adsorbents, whereas aluminous zeolites, which contain more aluminum, function as highly effective desiccants [109].

Zeolites possess various cavity structures that contribute to their highly porous nature. Their three-dimensional framework carries a negative charge, generated by Al-tetrahedra $[AlO_4]^-$, which is balanced by extraframework cations such as Na^+, K^+, Ca^{+2}, or Mg^{+2}. These cations can be readily exchangeable with other cations from the surrounding medium [10,15].

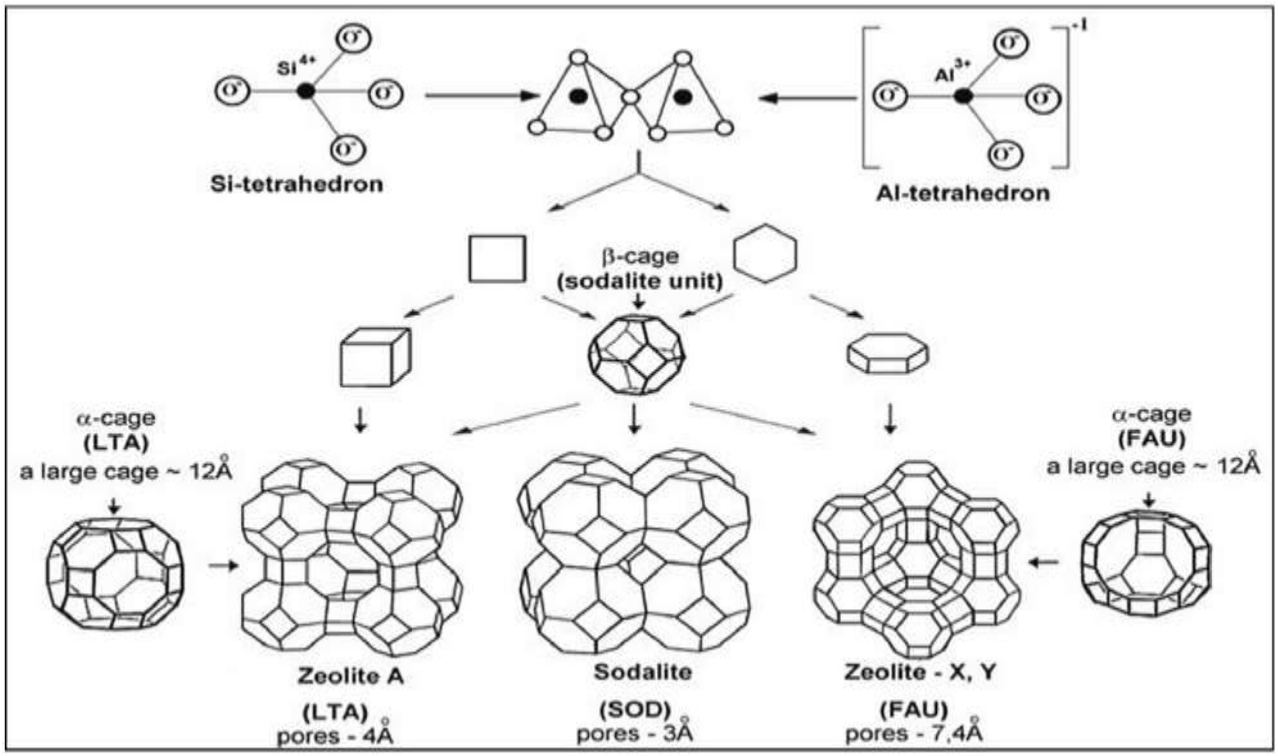

Fig II.1. Examples of zeolite structural units: A (LTA), sodalite (SOD), and faujasite (FAU) [103].

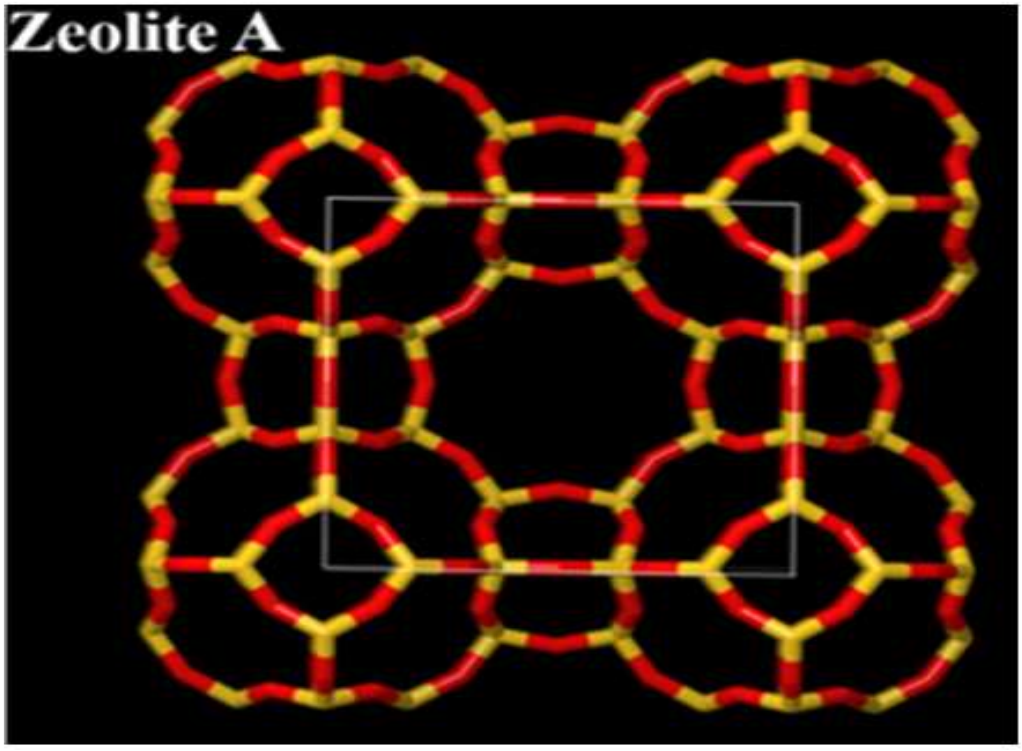

Fig II.2. Framework structure of zeolite A (LTA): Al and/or Si atoms indicated in yellow, oxygen atoms shown in red [106].

Zeolites are highly effective adsorbents due to their exceptional physicochemical and adsorptive properties, including uniform nanosized pores and channels, high surface area, superior ion-exchange capacity, selectivity, eco-friendliness, and excellent thermal and chemical stability. These attributes stem directly from their distinctive structural characteristics [110,111]. Furthermore, Shamsudin et al. [112] provided a summary of the cost per kilogram of commonly used adsorbent materials (Table II.1), confirming that zeolites are among the most cost-effective options. Recent years have seen extensive studies on zeolites, focusing on their effectiveness in removing various contaminants, including phenols, heavy metal ions, and dyes. Numerous studies have investigated their adsorption properties, highlighting their potential for environmental applications [113–124].

Table II.1. Cost of different sorbents [112].

Adsorbent material	**Cost (US$/kg)**
Activated carbon	20-22
Chitosan	15.43
Chitin	5-20
Calcium carbonate	145
Zinc Oxide	0.23-0.28
Zeolites	0.03-0.07
Bentonite	0.005-0.46

Chapter III. Adsorption-photocatalysis synergy for dye removal

1. Introduction

The term *photocatalysis* originates from Greek, combining the prefix *photo-* meaning "light", and *catalysis*, derived from *katalyo*, meaning to "break apart" or to "decompose" [125]. Photocatalysis is a process in which light activates a material, enabling it to accelerate chemical reactions without itself undergoing any permanent chemical transformation. The primary difference between traditional thermal catalysts and photosensitive catalysts lies in their activation mechanisms: thermal catalysts are activated by heat, whereas photosensitive catalysts are activated by light (photons) [126,127]. Photocatalytic reactions can take place in either homogeneous or heterogeneous systems; however, greater attention is given to heterogeneous photocatalysis due to their broad range of applications, from environmental remediation to energy production [128]. In heterogeneous catalysis, a solid semiconductor photocatalyst interacts with reactant molecules or ions present in the liquid or gaseous phase. Among the most widely used semiconductors, titanium dioxide (TiO_2)-based materials are distinguished by their exceptional photodegradation performance. Their popularity is attributed to their high quantum efficiency, resistance to photocorrosion, excellent physical and chemical stability, water insolubility, low cost, and environmentally friendly nature. TiO_2 has a bandgap energy of approximately 3.2 eV, requiring UV light with a wavelength of 385 nm or shorter to achieve photoexcitation [129]. The photocatalytic process involves several key steps: transport of pollutants to the catalyst surface, surface adsorption, chemical reactions within the adsorbed phase, desorption of reaction products, and their subsequent transfer to the gas and/or liquid phase [129]. Photocatalysis is a rapidly emerging technology that offers innovative solutions to industrial challenges, particularly in the degradation of contaminants in aqueous media, on solid surfaces, and within gaseous effluents. A diverse array of materials has been employed in the synthesis of active photocatalysts, including zeolites, clays, metal-organic frameworks, polymers, carbon-based materials, metal nanoparticles (NPs), and various other hybrid or composite structures [129].

2. Bibliometric analysis

Bibliometric analysis constitutes a fundamental methodological approach for investigating scholarly activity within the field of information science and for identifying emerging trends in research topics. The findings of a bibliometric study can help researchers make informed decisions about potential research areas, identify prospective academic collaborators, and select

the most suitable institutions for pursuing academic degrees or research partnerships. Bibliometric analysis can be performed using tools such as VOSviewer, Gephi, SciMAT, CiteSpace, HistCite, and R [130–132]. In this section, a bibliometric analysis was conducted using VOSviewer (version 1.6.20) to analyze data retrieved from the Scopus database, focusing on research related to the adsorption and photodegradation of zeolite materials. VOSviewer is a specialized software tool developed for constructing and visualizing bibliometric networks, representing entities such as journals, authors, or individual publications. These networks are created based on various relationships, including citation links, co-citation, bibliographic coupling, co-authorship, or the co-occurrence derived from the key terms found in the literature [133]. The Scopus database used in this study was queried using the following keyword search: [TITLE-ABS-KEY (zeolite OR zeolites) AND TITLE-ABS-KEY (adsorption OR desorption) AND TITLE-ABS-KEY (photocatalysis OR photodegradation)]. The research covered the period from 1992 to 2024, with data collection carried out on December 26, 2024. In total, 475 documents from global sources were extracted, analyzed, and mapped. This collection includes 15 book chapters, 52 reviews, 378 articles, 3 conference reviews, 25 conference papers, 1 editorial, and 1 retracted paper. As illustrated in Figure III.1, the number of publications grew slowly during the initial period (1992-2000), with no more than two documents published per year. From 2001 to 2019, the publication count fluctuated between 4 and 31 papers per year. However, a progressive increase was observed from 2020 to 2024, peaking at 58 publications in 2023. Table III.1 presents a clear overview of the global distribution of publication output, offering insights into trends in international scientific research activity. Several countries including China, Japan, India, the United States, Iran, South Korea, Mexico, Canada, France, and Spain have made significant contributions to research on the adsorption and photodegradation of zeolite materials. This highlights the global interest in the adsorption and photodegradation of zeolite materials as a major area of research. Additionally, 475 results were analyzed to identify co-occurring keywords, with a minimum threshold of five co- occurrences required for inclusion in Fig III.2. In the visualization, different research domains are represented by clusters of distinct colors. The size of each circle represents the frequency of keyword co-occurrences, where larger circles denote higher frequencies and stronger relationships. The distance between two circles illustrates the relationship between the corresponding keywords. The analysis reveals that most studies have focused on TiO_2-based photocatalysts, with aromatic compounds and antibiotics being the primary pollutants of interest. In conclusion, adsorption and photodegradation related to zeolite materials are strongly interconnected keywords.

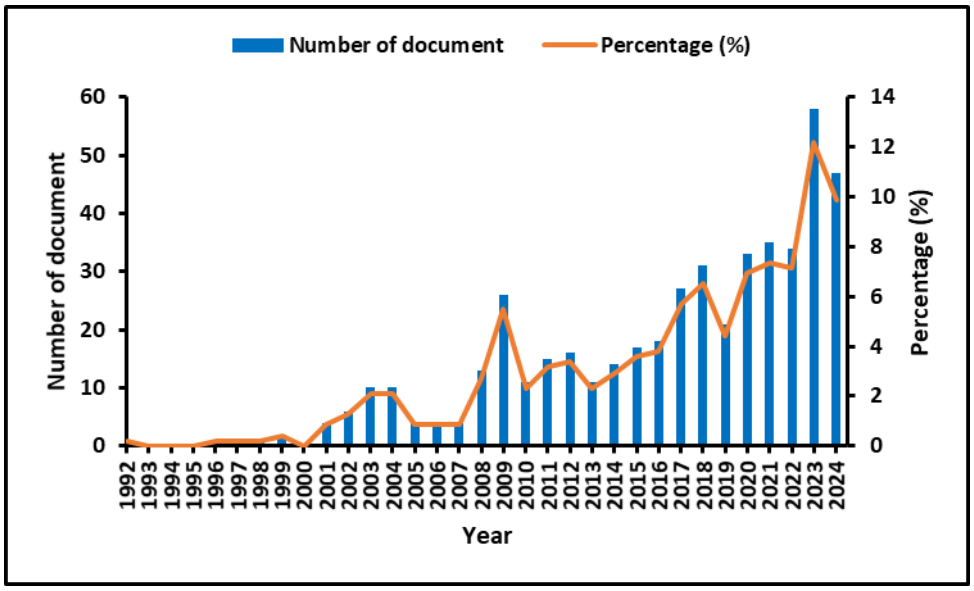

Fig III.1. Publication trend analysis of adsorption and photodegradation of zeolite materials.

Table III.1. The top ten countries ranked by research publication output.

Country	Publication count
China	149
India	58
Japan	49
United States	31
Iran	22
South Korea	19
Mexico	18
Canada	17
France	17
Spain	16

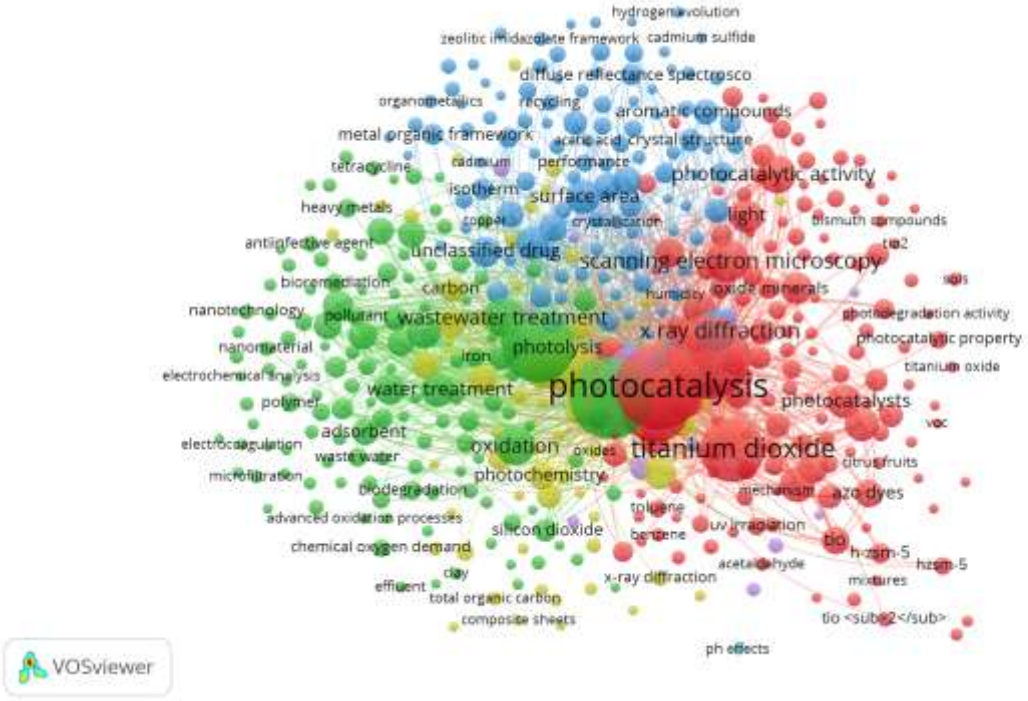

Fig III.2. Network visualization of keyword co-occurrence.

3. Photocatalysis

Photocatalysis refers to chemical reactions driven by light in the presence of a semiconductor. This material, which absorbs light and facilitates these reactions, is called a photocatalyst. Upon exposure to light, the photocatalyst generates an electron-hole pair, which initiates the photocatalytic process. Photocatalytic reactions can be divided into two types depending on the physical states of the reactants. When the semiconductor and reactants are in the same phase, the process is referred to as homogeneous photocatalysis. Conversely, when the photocatalyst and reactants exist in different phases, the reaction is called heterogeneous photocatalysis [134]. Based on the band gap (E_g), defined as the energy difference between the valence band (V_B) and the conduction band (C_B), materials are categorized into three main classes: (i) metals or conductors with E_g less than 1.0 eV, (ii) semiconductors with E_g ranging from 1.5 to 3.0 eV, and (iii) insulators with E_g greater than 5.0 eV (Fig III.3).

Upon irradiation with light of appropriate wavelength and sufficient energy, a photocatalyst absorbs a photon, promoting an excited electron (e^-) from the valence band to the conduction band and leaving behind a hole (h^+) in the valence band. Consequently, an electron-hole (e^-/h^+) pair is generated. In this excited state, the electron contributes to the reduction of an electron acceptor, while the hole promotes the oxidation of electron donor molecules. The

importance of the photocatalysis process lies in its unique ability to simultaneously create both oxidative and reductive environments.

The behavior of the excited electron and hole is determined by the alignment of the semiconductor's conduction and valence band positions with the redox potentials of the target molecule. Consequently, the interaction between the semiconductor and the substrate can proceed through four distinct pathways [134].

i. The substrate undergoes reduction when its redox level is lower than the conduction band of the photocatalyst.
ii. Oxidation of the substrate occurs when its redox level is higher than the valence band of the photocatalyst.
iii. Simultaneous reduction and oxidation of the substrate can occur when its redox level fall between the conduction and valence band of the photocatalyst.
iv. Neither oxidation nor reduction can occur when the substrate's redox level is positioned above the conduction band and below the valence band of the photocatalyst.

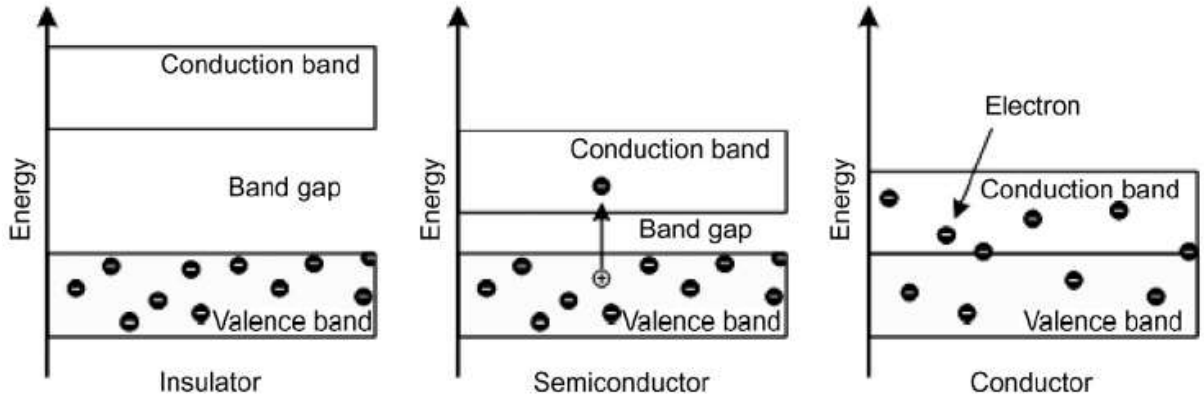

Fig III.3. Various types of materials [134].

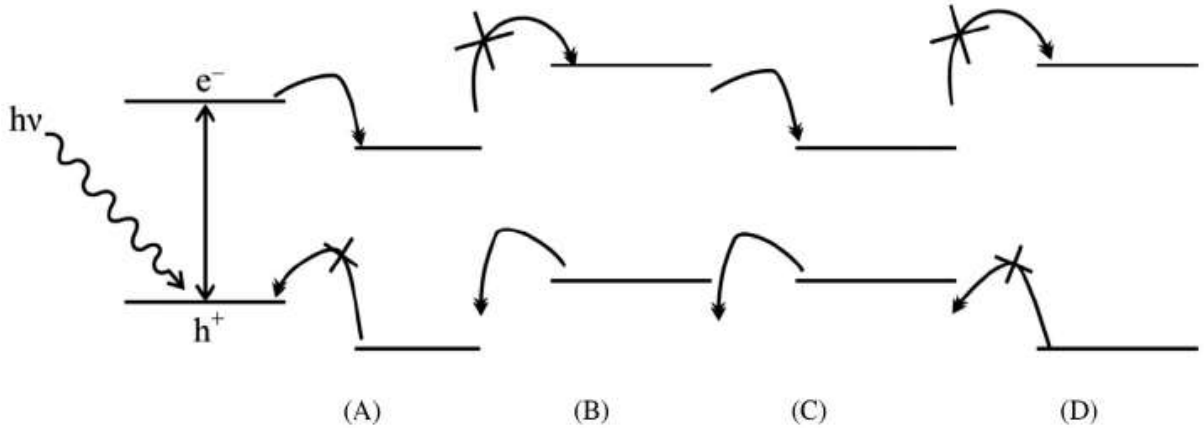

Fig III.4. The possible reaction outcomes include: Reduction (A), Oxidation (B), Redox reaction (C), and No reaction (D) [134].

3.1. Photocatalysis in water treatment

Heterogeneous photocatalysis using metal oxides facilitates the degradation or mineralization of pollutants in water through reactions with active oxygen species generated on the surface of photoactivated catalysts. Both organic and inorganic pollutants present in water solution, whether dissolved or suspended, can also directly interact with the electron-hole (Fig III.4). Photocatalytic reactions in water solutions may lead to partial or complete mineralization of organic substances, water detoxification, metal deposition, hydrogen transfer, dehydrogenation, and other related processes [135].

3.2. The immobilization of photocatalysts

TiO_2 is one of the most widely used photocatalysts in water treatment reactors. Historically, extensive research has been conducted on slurry systems containing fine powdered TiO_2 suspensions. However, the post-treatment removal of suspended titania particles remains a time-consuming and expensive process [18,136]. Immobilizing titania on a carrier offers the advantage of easier recovery. Practically, photocatalysts have been deposited onto a wide variety of surfaces, including silica gel, glass, polymers, ceramics, zeolites, metals, clays, activated carbon, fibers, cellulose, magnetic particles, alumina, and others [137]. When zeolites are used as a support for TiO_2, they form a composite that exhibits significantly improved photocatalytic performance compared to unsupported TiO_2 nanoparticles. This enhancement is attributed to the increased active surface area of the supported catalyst and the amphoteric properties of zeolites. The aluminum ions within the framework and the charge-balancing cations function as Lewis acids, while the oxygen atoms, particularly those adjacent to aluminum, act Lewis bases [33]. Consequently, the zeolitic matrix plays a crucial role in regulating photo-induced charge transfer reactions [138]. Moreover, the strong electric field within the zeolite framework can notably impede the back electron transfer reaction, a key factor limiting quantum efficiency in many photocatalytic reactions [34]. Fig III.5 [18] presents SEM micrographs of both the pure zeolite and the TiO_2-supported zeolite materials.

From a practical perspective, an ideal support for photocatalyst must meet several key criteria [137]:

i. It should ensure strong adhesion between the photocatalyst and the support.
ii. It should retain high photocatalytic activity of the material after the loading operation.
iii. It should possess a high specific surface area.

iv. It should demonstrate a strong adsorption affinity for the contaminants.

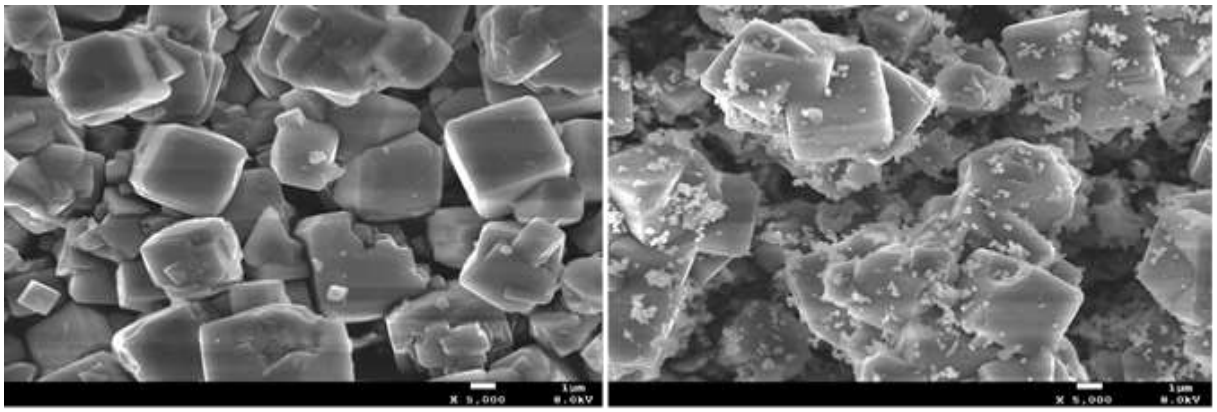

(a) (b)

Fig III.5. SEM micrographs images of zeolite (LTA) (a) and TiO_2-supported zeolite (10% wt.%) (b) [18].

3.3. Photocatalytic reactors for wastewater treatment

Photocatalytic reactors used in wastewater treatment are generally categorized into two main types based on the physical state of the photocatalyst: (i) slurry reactors, in which fine photocatalyst particles are suspended in the liquid phase, and (ii) immobilized systems, where the photocatalyst is fixed onto an inert support [139]. The light source in a photocatalytic reactor can be positioned either internally or externally, with sunlight commonly used as an external irradiation source. A major difference between slurry-type and immobilized photocatalytic reactors is the requirement for post-treatment: slurry reactors necessitate a separation step to recover the photocatalyst particles, while immobilized systems facilitate continuous operation without the need for such step.

3.4. Impact of process conditions on photocatalytic activity

3.4.1. Photocatalyst dose

The amount of photocatalyst employed in a photocatalytic wastewater treatment system directly influences the reaction rate. In heterogeneous photocatalysis, the photodegradation rate generally increases with increasing catalyst dosage. Therefore, identifying the optimal catalyst dose is essential to avoid excessive material use and to maximize photon absorption efficiency [140]. When the photocatalyst dose exceeds the saturation threshold, light absorption efficiency typically decreases. This reduction is mainly due to light scattering effect, which limits the exposure of active photocatalyst surfaces to irradiation and consequently lowers the overall photocatalytic efficiency [141]. When the photocatalyst dose exceeds the saturation threshold,

light absorption efficiency typically decreases. This reduction is mainly due to light scattering effect, which limits the exposure of active photocatalyst surfaces to irradiation and consequently lowers the overall photocatalytic efficiency [141]. As shown in Fig. III.6(a), the reaction rate (r) increases proportionally with the photocatalyst mass (m) until it reaches a plateau, indicating that the photocatalytic system has absorbed the maximum number of available photons. Numerous studies have investigated the effect of titania dosage on the efficiency of the photocatalytic process [18,140,142–146]. However, direct comparisons among these findings are difficult due to variations in reactor geometry, radiation flux, light intensity, and the wavelengths used. It has been observed that the optimal catalyst loading for effective photodegradation differs across studies and is largely influenced by the dimensions of the photoreactor.

3.4.2. Wavelength

The variation in reaction rate with respect to wavelength aligns with the photocatalyst's absorption spectrum and is directly related to its bandgap energy (Fig III.6(b)) [135]. In the case of TiO_2, effective photonic activation of commercial Degussa P-25, which contains approximately 70-80% anatase and 20-30% rutile, requires light with a wavelength shorter than 380 nm [147]. On the other hand, rutile TiO_2 has a bandgap of approximately 3.02 eV, whereas anatase TiO_2 possesses a slightly higher bandgap of about 3.2 eV [140]. Ultraviolet (UV) irradiation is classified into three categories based on wavelength: (i) UV-A, ranging from 315 to 400 nm, (ii) UV-B, spanning 280 to 315 nm, and (iii) UV-C, covering 100 to 280 nm [148].

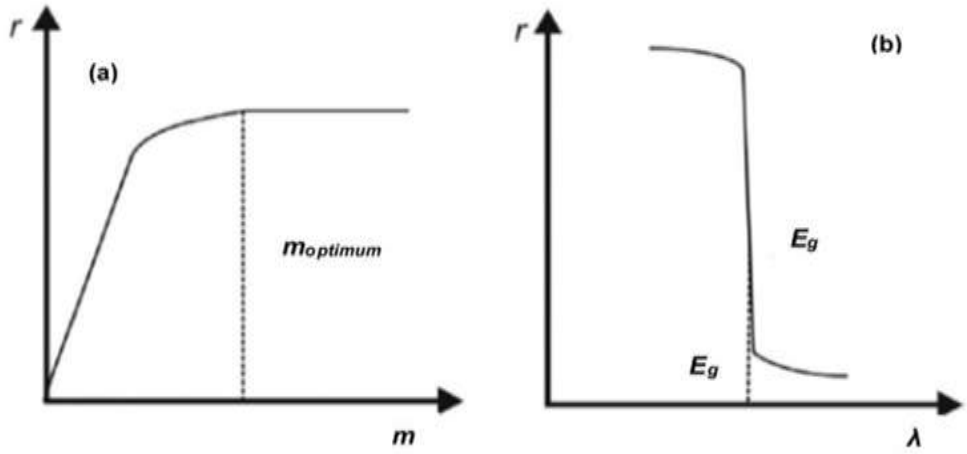

Fig III.6. Influence of (a) catalyst mass (m) and (b) wavelength (λ) on the photocatalysis rate (r) [137].

3.4.3. Solution pH

The performance of photocatalytic wastewater treatment is significantly affected by the medium's pH, which impacts the surface charge of photocatalyst particles, their tendency to aggregate, and the alignment of conduction and valence band energy levels [141]. In acidic environments, the functional groups on the photocatalyst surface are prone to protonation, whereas in alkaline conditions, they tend to undergo deprotonation. The point of zero charge, abbreviated as pH_{PZC} is the pH at which the photocatalyst surface carries no net electrical charge. Its value varies depending on the specific photocatalytic material. When the operating pH is below the pH_{PZC}, the photocatalyst surface becomes positively charged, enhancing electrostatic attraction toward negatively charged pollutants. Conversely, at pH levels above the pH_{PZC}, the surface acquires a negative charge, favoring the adsorption of positively charged contaminants [149]. Electrostatic interactions between the photocatalyst surface and charged organic substances can significantly enhance their adsorption [149].
Equations 31 and 32 represent the protonation and deprotonation reactions occurring on the TiO_2 surface as a function of the solution's pH [141].

$$in\ the\ case\ that\ pH\ < pH_{PZC}: TiOH + H_{aq}^{+} \leftrightarrow TiOH_2^{+} \qquad (31)$$

$$and\ at\ pH\ > pH_{PZC}: TiOH + OH_{aq}^{-} \leftrightarrow TiO^{-} + H_2O \qquad (32)$$

3.4.4. Dissolved oxygen

In photocatalytic reactions, dissolved oxygen plays an essential role by capturing excited conduction-band electrons, effectively acting as an electron scavenger and minimizing electron-hole recombination [141]. Oxidation and reduction reactions occur at separate sites on the photocatalyst surface, ensuring that oxygen molecules do not interfere with the adsorption of target compounds [150]. Additionally, dissolved oxygen facilitates the generation of reactive oxygen species, stabilizes radical intermediates, and enhances both mineralization and direct photocatalytic processes.

3.4.5. Temperature

Elevating the reaction temperature improves photocatalytic activity. However, temperatures above 80°C typically lead to increased charge carrier recombination and reduced adsorption of organic substances on the catalyst surface. Conversely, temperatures below 80°C enhance the sorption of organic species. Nevertheless, further decreasing the temperature to

0°C raises the activation energy, thereby slowing the reaction rate. As a result, the optimal temperature range for the photodegradation of organic compounds is indicated to be between 20°C and 80°C [136,140,141,150].

3.4.6. Pollutants and their concentrations

Elevated pollutant concentrations in water may saturate the photocatalyst surface, which diminishes photocatalytic efficiency and can ultimately lead to catalyst deactivation [151]. Organic molecules that exhibit strong binding to the photocatalyst surface are more prone to direct oxidation. Consequently, the photodegradation of aromatic compounds is heavily influenced by the characteristics of their substituent groups. Organic substances with electron-withdrawing groups, such as nitrobenzene and benzoic acid, generally exhibit stronger adsorption onto the photocatalyst surface, rendering them more susceptible to direct oxidation than those bearing electron-donating groups [152].

3.4.7. Luminosity

Light intensity is a key parameter influencing the photodegradation of organic compounds. Fujishima et al. [153] noted that the initiation of titania photocatalytic reaction rates is not significantly affected by light intensity. Even at a low intensity, such as 1 mW/cm^2, the surface reaction can be effectively induced. Overall, the apparent rate constant for photodegradation tends to rise with increasing UV irradiation, as the greater photon influx boosts interaction with the photocatalyst and promotes the generation of hydroxyl radicals [154]. At low illumination intensities (0-20 mW/cm^2), the degradation rate follows first-order kinetics with respect to light intensity. As the intensity increases to moderate levels, the reaction rate becomes proportional to the square root of the intensity, mainly due to the competing effects of charge carrier (electro-hole pair) separation and recombination [155]. At very high illumination intensities, however, the reaction rate becomes independent of light intensity [156].

3.5. TiO_2 photocatalysis mechanism

Heterogeneous photocatalysis using UV/TiO_2 systems is a widely adopted technique for air and wastewater purification. The process is initiated when a photoexcited electron (e^-) is promoted from the filled valence band (V_B) to the empty conduction band (C_B) of the semiconductor photocatalyst. This excitation takes place when the energy of the absorbed photon (hν) equals or exceeds the bandgap energy (E_g) of the semiconductor—typically around 3.0 eV for rutile

and 3.2 eV for anatase phases of titania [141]. This transition leaves behind a hole (h^+) in the valence band, resulting in the formation of an electron-hole pair (e^-/h^+), as shown in Fig III.7 and described in step 1 of Table III.2. The photodegradation of the pollutant (P) in water solution using a titania photocatalyst under UV light has been comprehensively outlined through a sequence of oxidative-reductive chain reactions (steps 2-10, Table III.2) [140,141,157,158]. During steps 2-8, photogenerated electrons and holes are separated and become trapped at the reductive and oxidative sites on the titania surface, initiating a chain of reactions that produce reactive species such as $OH^{\bullet}$, $O_2^{\bullet-}$, and H_2O_2. The pollutant (P) is then degraded either through direct oxidation by the highly reactive photogenerated hole (step 9) or via interactions with these reactive species (step 10), ultimately forming CO_2 and H_2O as final products. The overall photodegradation reaction of pollutant P under UV-irradiated TiO_2 can be summarized in step 11 (Table III.2).

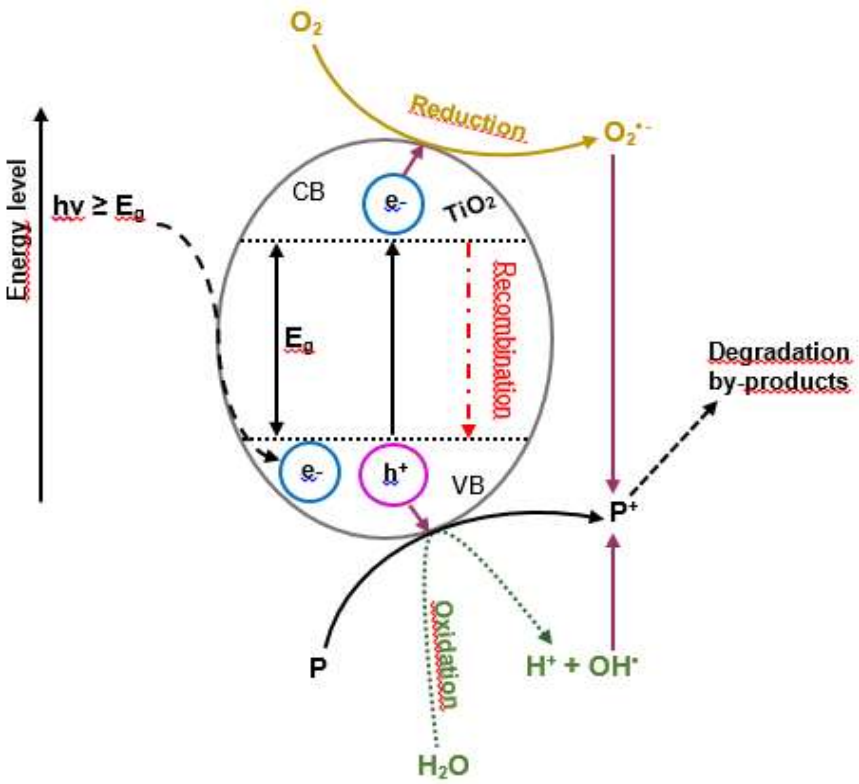

Fig III.7. Mechanism of photo-induced (e^-/h^+) pair generation in a TiO_2 photocatalyst particle in the presence of a contaminant (P) in water [141].

Table III.2. Photodegradation mechanism [157].

$TiO_2 \xrightarrow{h\nu} TiO_2^{\bullet}\ (e_{CB}^- + h_{VB}^+)$ …… (1)
$h_{VB}^+ + H_2O \longrightarrow H^+ + OH^{\bullet}$ …… (2)
$e_{CB}^- + O_2 \longrightarrow O_2^{\bullet -}$ …… (3)
$O_2^{\bullet -} + H_2O \longrightarrow HO_2^{\bullet} + OH^-$ …… (4)
$O_2^{\bullet -} + HO_2^{\bullet} + H^+ \longrightarrow O_2 + H_2O_2$ …… (5)
$H^+ + 2e_{C\,B}^- + O_2 \longrightarrow H_2O_2$ …… (6)
$2H_2O + 2h_{VB}^+ \longrightarrow 2H_2O_2 + 2H^+$ …… (7)
$H_2O_2 + e_{CB}^- \rightarrow OH^- + OH^{\bullet}$ …… (8)
$h_{VB}^+ + P \rightarrow intermediate\ products \rightarrow CO_2 + H_2O$ …… (9)
$OH^{\bullet} + P \rightarrow intermediate\ products \rightarrow CO_2 + H_2O$ …… (10)
$P + O_2 \xrightarrow{h\nu, TiO_2} CO_2 + H_2O$ …… (11)

3.6. Photodegradation kinetics and modelling

Kinetic studies on the photodegradation rates of water pollutants are essential for scaling up the process. The proper application of kinetic models to interpret experimental data enables the design and optimization of photoreactor systems with sufficient processing capacity and minimal unilluminated reactor volume [141].

3.6.1. Langmuir-Hinshelwood (L-H) model

Since the L-H model depends on surface area, the reaction rate generally increases with longer illumination times as the concentration of target molecules in solution decreases and more active surface sites become available [141]. Initially designed to quantitatively describe gas-solid kinetic reactions [159], the L-H model was later adapted for application in solid-liquid systems [160]. This equation is given as [161–165]:

$$r = -\frac{dC_t}{dt} = \frac{kKC_t}{1 + KC_t} \qquad (33)$$

In this expression, *k* [mg/(min L)] is the true rate constant, accounting for various parameters such as catalyst mass, effective photon flux, oxygen availability, and more, while *K* (L/mg) represents the adsorption constant, and C_t (mg/L) denotes the contaminant concentration at irradiation time *t* (min). Integration of this equation results in the following expression:

$$ln\left(\frac{C_0}{C_t}\right) + K(C_0 - C_t) = kKt \qquad (34)$$

where C_0 (mg/L) represents the initial concentration of the organic pollutant.
From Eq. (33), the reaction order varies between 0 and 1, with two limiting cases to consider. For concentrated solutions, where the term $K \times C_t$ is much greater than 1, the reaction rate follows zero-order kinetics, and Eq. (34) simplifies to:

$$C_0 - C_t = kt \qquad (35)$$

In the case of highly diluted solutions, the term $K \times C_t$ becomes much less than 1, allowing the denominator of Eq. (33) to be neglected. Under these conditions, the reaction approximates apparent first-order kinetics, allowing Eq. (32) to be simplified as follows:

$$\ln\left(\frac{C_t}{C_0}\right) = -kKt = -k_{ap}t \qquad (36)$$

where k_{ap} (min^{-1}) is the apparent rate constant for a first-order reaction, defined as the product of *k* and *K*.

3.7. Synergistic interaction of adsorption and photodegradation in removing organic pollutants from water

The schematic mechanism shown in Eq. (37) illustrates the key steps involved the removal of organic pollutants (OP) through a combined adsorption-photodegradation process. Zeolite-supported photocatalyst materials (ZSPM) feature a large specific surface area, a porous matrix, and a well-defined crystalline structure derived from the zeolite adsorbent, along with a high density of functional groups. These characteristics facilitate the exposure of additional active sites and improve adsorption performance through mechanisms including hydrogen bonding, electrostatic interactions, and pore filling between the surface of the zeolite-based photocatalyst and organic pollutant molecules. The adsorption process promotes the transfer of organic pollutants from the liquid to the solid phase, enhancing surface reactions at the interface of the zeolitic materials. Simultaneously, the photodegradation process generates reactive free radicals that effectively oxidize the adsorbed pollutants on the surface of the impregnated photocatalyst, breaking them down into smaller molecules such as CO_2 and H_2O, and thereby regenerating the occupied active sites [166]. As a result, the adsorption-desorption equilibrium shifts toward the adsorption reaction, significantly enhancing the adsorption capacity [18]. In

conclusion, the adsorption and photodegradation processes exhibit a synergistic interaction, enhancing the overall efficiency of organic pollutant removal.

$$OP \underset{desorption}{\overset{adsorption}{\rightleftharpoons}} OP - ZSPM \xrightarrow{Photodegradation} CO_2 + H_2O \qquad (37)$$

3.7.1. Modified Elovich kinetic model for simulating the combined adsorption-photodegradation process

Recently, several studies have explored the kinetics of pollutant removal in the liquid phase through a combined adsorption-photodegradation process [18,167–173]. The findings of these studies revealed that the modified Elovich kinetic model, evaluated under various operating conditions and for different pollutants, exhibited high accuracy in simulating kinetic data. The heterogeneous model (modified Elovich) is controlled by multiple processes, most notably adsorption and photodegradation. The overall removal rate in this model is expressed as:

$$r = -dC_t/dt = k_e C_0 e^{-\beta(C_0 - C_t)} \qquad (38)$$

where k_e (min^{-1}) denotes the rate constant of the modified Elovich model, and β is a constant inversely related to the removal capacity. An increase in β corresponds to a decrease in the removal rate over time.

References

[1] T. Hussain, A. Wahab, A critical review of the current water conservation practices in textile wet processing, Journal of Cleaner Production 198 (2018) 806–819. https://doi.org/10.1016/j.jclepro.2018.07.051.

[2] A.A. Adesibikan, S.S. Emmanuel, C.O. Olawoyin, P. Ndungu, Cellulosic metallic nanocomposites for photocatalytic degradation of persistent dye pollutants in aquatic bodies: A pragmatic review, Journal of Organometallic Chemistry 1010 (2024) 123087. https://doi.org/10.1016/j.jorganchem.2024.123087.

[3] A. Sahu, J.C. Poler, Removal and degradation of dyes from textile industry wastewater: Benchmarking recent advancements, toxicity assessment and cost analysis of treatment processes, Journal of Environmental Chemical Engineering 12 (2024) 113754. https://doi.org/10.1016/j.jece.2024.113754.

[4] J. Sharma, S. Sharma, V. Soni, Classification and impact of synthetic textile dyes on Aquatic Flora: A review, Regional Studies in Marine Science 45 (2021) 101802. https://doi.org/10.1016/j.rsma.2021.101802.

[5] S.P. Bera, S.K. Tank, Microbial degradation of Procion Red by Pseudomonas stutzeri, Sci Rep 11 (2021) 3075. https://doi.org/10.1038/s41598-021-82494-9.

[6] B. Yan, Y. Dai, L. Xin, M. Li, H. Zhang, H. Long, X. Gao, Research progress in the degradation of printing and dyeing wastewater using chitosan based composite photocatalytic materials, International Journal of Biological Macromolecules 263 (2024) 130082. https://doi.org/10.1016/j.ijbiomac.2024.130082.

[7] B. Lellis, C.Z. Fávaro-Polonio, J.A. Pamphile, J.C. Polonio, Effects of textile dyes on health and the environment and bioremediation potential of living organisms, Biotechnology Research and Innovation 3 (2019) 275–290. https://doi.org/10.1016/j.biori.2019.09.001.

[8] D.A. Yaseen, M. Scholz, Textile dye wastewater characteristics and constituents of synthetic effluents: a critical review, Int. J. Environ. Sci. Technol. 16 (2019) 1193–1226. https://doi.org/10.1007/s13762-018-2130-z.

[9] N. Kumar, A. Pandey, Rosy, Y.C. Sharma, A review on sustainable mesoporous activated carbon as adsorbent for efficient removal of hazardous dyes from industrial wastewater, Journal of Water Process Engineering 54 (2023) 104054. https://doi.org/10.1016/j.jwpe.2023.104054.

[10] A. Imessaoudene, S. Cheikh, A. Hadadi, N. Hamri, J.-C. Bollinger, A. Amrane, H. Tahraoui, A. Manseri, L. Mouni, Adsorption Performance of Zeolite for the Removal of

Congo Red Dye: Factorial Design Experiments, Kinetic, and Equilibrium Studies, Separations 10 (2023) 57. https://doi.org/10.3390/separations10010057.

[11] S. Dutta, S. Adhikary, S. Bhattacharya, D. Roy, S. Chatterjee, A. Chakraborty, D. Banerjee, A. Ganguly, S. Nanda, P. Rajak, Contamination of textile dyes in aquatic environment: Adverse impacts on aquatic ecosystem and human health, and its management using bioremediation, Journal of Environmental Management 353 (2024) 120103. https://doi.org/10.1016/j.jenvman.2024.120103.

[12] J. Wu, Q. Li, W. Li, Y. Li, G. Wang, A. Li, H. Li, Efficient removal of acid dyes using permanent magnetic resin and its preliminary investigation for advanced treatment of dyeing effluents, Journal of Cleaner Production 251 (2020) 119694. https://doi.org/10.1016/j.jclepro.2019.119694.

[13] A. Hadadi, A. Imessaoudene, J.-C. Bollinger, S. Cheikh, A.A. Assadi, A. Amrane, M. Kebir, L. Mouni, Parametrical Study for the Effective Removal of Mordant Black 11 from Synthetic Solutions: Moringa oleifera Seeds' Extracts Versus Alum, Water 14 (2022) 4109. https://doi.org/10.3390/w14244109.

[14] E. Chatzisymeon, N.P. Xekoukoulotakis, A. Coz, N. Kalogerakis, D. Mantzavinos, Electrochemical treatment of textile dyes and dyehouse effluents, Journal of Hazardous Materials 137 (2006) 998–1007. https://doi.org/10.1016/j.jhazmat.2006.03.032.

[15] A. Imessaoudene, S. Cheikh, J.-C. Bollinger, L. Belkhiri, A. Tiri, A. Bouzaza, A. El Jery, A. Assadi, A. Amrane, L. Mouni, Zeolite Waste Characterization and Use as Low-Cost, Ecofriendly, and Sustainable Material for Malachite Green and Methylene Blue Dyes Removal: Box–Behnken Design, Kinetics, and Thermodynamics, Applied Sciences 12 (2022) 7587. https://doi.org/10.3390/app12157587.

[16] Y. Mittal, S. Dash, P. Srivastava, P.M. Mishra, T.M. Aminabhavi, A.K. Yadav, Azo dye containing wastewater treatment in earthen membrane based unplanted two chambered constructed wetlands-microbial fuel cells: A new design for enhanced performance, Chemical Engineering Journal 427 (2022) 131856. https://doi.org/10.1016/j.cej.2021.131856.

[17] A. Muniyasamy, G. Sivaporul, A. Gopinath, R. Lakshmanan, A. Altaee, A. Achary, P. Velayudhaperumal Chellam, Process development for the degradation of textile azo dyes (mono-, di-, poly-) by advanced oxidation process - Ozonation: Experimental & partial derivative modelling approach, Journal of Environmental Management 265 (2020) 110397. https://doi.org/10.1016/j.jenvman.2020.110397.

[18] A. Imessaoudene, O. Mechraoui, B. Aberkane, A. Benabbas, A. Manseri, Y. Moussaoui, J.-C. Bollinger, A. Amrane, A. Zoukel, L. Mouni, Synthesis of a TiO2/zeolite composite: Evaluation of adsorption-photodegradation synergy for the removal of Malachite Green, Nano-Structures & Nano-Objects 38 (2024) 101191. https://doi.org/10.1016/j.nanoso.2024.101191.

[19] J. Shin, S. Bae, K. Chon, Fenton oxidation of synthetic food dyes by Fe-embedded coffee biochar catalysts prepared at different pyrolysis temperatures: A mechanism study, Chemical Engineering Journal 421 (2021) 129943. https://doi.org/10.1016/j.cej.2021.129943.

[20] H. Zeng, Z. Yu, L. Shao, X. Li, M. Zhu, Y. Liu, X. Feng, X. Zhu, A novel strategy for enhancing the performance of membranes for dyes separation: Embedding PAA@UiO-66-NH2 between graphene oxide sheets, Chemical Engineering Journal 403 (2021) 126281. https://doi.org/10.1016/j.cej.2020.126281.

[21] C.D. Raman, S. Kanmani, Textile dye degradation using nano zero valent iron: A review, Journal of Environmental Management 177 (2016) 341–355. https://doi.org/10.1016/j.jenvman.2016.04.034.

[22] M. Ahmadian, H. Derakhshankhah, M. Jaymand, Biosorptive removal of organic dyes using natural gums-based materials: A comprehensive review, Journal of Industrial and Engineering Chemistry 124 (2023) 102–131. https://doi.org/10.1016/j.jiec.2023.05.002.

[23] V.K. Gupta, R. Kumar, A. Nayak, T.A. Saleh, M.A. Barakat, Adsorptive removal of dyes from aqueous solution onto carbon nanotubes: A review, Advances in Colloid and Interface Science 193–194 (2013) 24–34. https://doi.org/10.1016/j.cis.2013.03.003.

[24] S. Wang, Y. Peng, Natural zeolites as effective adsorbents in water and wastewater treatment, Chemical Engineering Journal 156 (2010) 11–24. https://doi.org/10.1016/j.cej.2009.10.029.

[25] N.A. Hernández-Beltrán, M.T. Olguín, A. Rosas-Aburto, Effect of acid phosphate media on the stability of clinoptilolite-rich tuff, J Incl Phenom Macrocycl Chem 61 (2008) 93–100. https://doi.org/10.1007/s10847-007-9399-8.

[26] I. Humelnicu, A. Băiceanu, M.-E. Ignat, V. Dulman, The removal of Basic Blue 41 textile dye from aqueous solution by adsorption onto natural zeolitic tuff: Kinetics and thermodynamics, Process Safety and Environmental Protection 105 (2017) 274–287. https://doi.org/10.1016/j.psep.2016.11.016.

[27] S. Kesraoui-Ouki, C.R. Cheeseman, R. Perry, Natural zeolite utilisation in pollution control: A review of applications to metals' effluents, J of Chemical Tech & Biotech 59 (1994) 121–126. https://doi.org/10.1002/jctb.280590202.

[28] L.T.V. Da Silva, A.D.L. De Freitas, T. De Gois Martins, A.M. De Morais França, A.R. Loiola, R.F. Do Nascimento, Comparative study on the performance of two synthetic zeolite 4A on the removal of heavy metals from aqueous solution—effect of coal fly ash as Al and Si source, Desalination and Water Treatment 310 (2023) 157–166. https://doi.org/10.5004/dwt.2023.29948.

[29] B. Senthil Rathi, P. Senthil Kumar, J. Natanya Ida Susana, J. Francia Virgin, R. Dharani, S. Sanjay, G. Rangasamy, Recent research progress on the removal of heavy metals from wastewater using modified zeolites: A critical review, Desalination and Water Treatment 319 (2024) 100573. https://doi.org/10.1016/j.dwt.2024.100573.

[30] N. Finish, P. Ramos, E.J.C. Borojovich, O. Zeiri, Y. Amar, M. Gottlieb, Zeolite performance in removal of multicomponent heavy metal contamination from wastewater, Journal of Hazardous Materials 457 (2023) 131784. https://doi.org/10.1016/j.jhazmat.2023.131784.

[31] D. Chen, Y. Cheng, N. Zhou, P. Chen, Y. Wang, K. Li, S. Huo, P. Cheng, P. Peng, R. Zhang, L. Wang, H. Liu, Y. Liu, R. Ruan, Photocatalytic degradation of organic pollutants using TiO2-based photocatalysts: A review, Journal of Cleaner Production 268 (2020) 121725. https://doi.org/10.1016/j.jclepro.2020.121725.

[32] A.Y. Shan, T.I.Mohd. Ghazi, S.A. Rashid, Immobilisation of titanium dioxide onto supporting materials in heterogeneous photocatalysis: A review, Applied Catalysis A: General 389 (2010) 1–8. https://doi.org/10.1016/j.apcata.2010.08.053.

[33] N. Dubey, S.S. Rayalu, Nitin.K. Labhsetwar, R.R. Naidu, R.V. Chatti, S. Devotta, Photocatalytic properties of zeolite-based materials for the photoreduction of methyl orange, Applied Catalysis A: General 303 (2006) 152–157. https://doi.org/10.1016/j.apcata.2006.01.043.

[34] S. Sankararaman, K.B. Yoon, T. Yabe, J.K. Kochi, Control of back electron transfer from charge-transfer ion pairs by zeolite supercages, J. Am. Chem. Soc. 113 (1991) 1419–1421. https://doi.org/10.1021/ja00004a057.

[35] S. Das, L. Cherwoo, R. Singh, Decoding dye degradation: Microbial remediation of textile industry effluents, Biotechnology Notes 4 (2023) 64–76. https://doi.org/10.1016/j.biotno.2023.10.001.

[36] M.D. Khan, A. Singh, M.Z. Khan, S. Tabraiz, J. Sheikh, Current perspectives, recent advancements, and efficiencies of various dye-containing wastewater treatment technologies, Journal of Water Process Engineering 53 (2023) 103579. https://doi.org/10.1016/j.jwpe.2023.103579.

[37] E.O. Alegbe, T.O. Uthman, A review of history, properties, classification, applications and challenges of natural and synthetic dyes, Heliyon 10 (2024) e33646. https://doi.org/10.1016/j.heliyon.2024.e33646.

[38] A. AlAshkar, A. Hassabo, Recent Use of Natural Animal Dyes in Various Field, J.Text.Color. Pol. Sci. 0 (2021) 0–0. https://doi.org/10.21608/jtcps.2021.79791.1067.

[39] A. Tkaczyk, K. Mitrowska, A. Posyniak, Synthetic organic dyes as contaminants of the aquatic environment and their implications for ecosystems: A review, Science of The Total Environment 717 (2020) 137222. https://doi.org/10.1016/j.scitotenv.2020.137222.

[40] R. Al-Tohamy, S.S. Ali, F. Li, K.M. Okasha, Y.A.-G. Mahmoud, T. Elsamahy, H. Jiao, Y. Fu, J. Sun, A critical review on the treatment of dye-containing wastewater: Ecotoxicological and health concerns of textile dyes and possible remediation approaches for environmental safety, Ecotoxicology and Environmental Safety 231 (2022) 113160. https://doi.org/10.1016/j.ecoenv.2021.113160.

[41] B.L. Deopura, N.V. Padaki, Synthetic Textile Fibres, in: Textiles and Fashion, Elsevier, 2015: pp. 97–114. https://doi.org/10.1016/B978-1-84569-931-4.00005-2.

[42] R. Kishor, D. Purchase, G.D. Saratale, R.G. Saratale, L.F.R. Ferreira, M. Bilal, R. Chandra, R.N. Bharagava, Ecotoxicological and health concerns of persistent coloring pollutants of textile industry wastewater and treatment approaches for environmental safety, Journal of Environmental Chemical Engineering 9 (2021) 105012. https://doi.org/10.1016/j.jece.2020.105012.

[43] S. Paul, S. Chavan, S. Khambe, Studies on characterization of textile industrial waste water in Solapur city, International Journal of Chemical Sciences 10 (2012).

[44] T. Robinson, G. McMullan, R. Marchant, P. Nigam, Remediation of dyes in textile effluent: a critical review on current treatment technologies with a proposed alternative, Bioresource Technology 77 (2001) 247–255. https://doi.org/10.1016/S0960-8524(00)00080-8.

[45] P. Pourhakkak, M. Taghizadeh, A. Taghizadeh, M. Ghaedi, Adsorbent, in: Interface Science and Technology, Elsevier, 2021: pp. 71–210. https://doi.org/10.1016/B978-0-12-818805-7.00009-6.

[46] S. Eswaramoorthi, K. Dhanapal, D. Chauhan, Advances in textile wastewater treatment: the case for UV-Ozonation and membrane bioreactor for common effluent treatment plants in Tirupur, Tamil Nadu, India, Environmental Technology Awareness Series (2008).

[47] S. Kalra, S. Mohan, A. Sinha, G. Singh, Advanced oxidation processes for treatment of textile and dye wastewater: a review, In: 2nd International Conference on Environmental Science and Development IPCBEE 4 IACSIT Press, Singapore (2011).

[48] F.H. Hussein, Chemical Properties of Treated Textile Dyeing Wastewater, Asian J. Chem. 25 (2013) 9393–9400. https://doi.org/10.14233/ajchem.2013.15909A.

[49] A. Ghaly, R. Ananthashankar, M. Alhattab, V. Ramakrishnan, Production, Characterization and Treatment of Textile Effluents: A Critical Review, Journal of Chemical Engineering & Process Technology (2014) 1–18.

[50] G. Elango, G. Rathika, S. Elango, Physico-Chemical Parameters of Textile Dyeing Effluent and Its Impacts with Casestudy, International Journal of Research in Chemistry and Environment (2017) 17–24.

[51] N. Abu Bakar, N. Othman, Z.M. Yunus, Z. Daud, N. Salsabila Norisman, M. Haziq Hisham, Physico-Chemical Water Quality Parameters Analysis on Textile, IOP Conf. Ser.: Earth Environ. Sci. 498 (2020) 012077. https://doi.org/10.1088/1755-1315/498/1/012077.

[52] J.M. Bidu, B. Van Der Bruggen, M.J. Rwiza, K.N. Njau, Current status of textile wastewater management practices and effluent characteristics in Tanzania, Water Science and Technology 83 (2021) 2363–2376. https://doi.org/10.2166/wst.2021.133.

[53] H.H. Sornaly, S. Ahmed, K.F. Titin, M.N. Islam, A. Parvin, M.A. Islam, H.M. Faruquee, K.K. Biswas, R. Islam, D.K. Paul, S.K. Biswas, The utility of bioremediation approach over physicochemical methods to detoxify dyes discharges from textile effluents: A comprehensive review study, Sustainable Chemistry and Pharmacy 39 (2024) 101538. https://doi.org/10.1016/j.scp.2024.101538.

[54] W.U. Khan, S. Ahmed, Y. Dhoble, S. Madhav, A critical review of hazardous waste generation from textile industries and associated ecological impacts, Journal of the Indian Chemical Society 100 (2023) 100829. https://doi.org/10.1016/j.jics.2022.100829.

[55] M.A.S. Jiku, A. Singha, M. Faruquee, M.A. Rahaman, M.A. Alam, M. Ehsanullah, Toxic wastewater status for irrigation usage at Gazipur and Savar industrial vicinity of Bangladesh, Acta Ecologica Sinica 41 (2021) 358–364. https://doi.org/10.1016/j.chnaes.2021.07.001.

[56] D. Goswami, J. Mukherjee, C. Mondal, B. Bhunia, Bioremediation of azo dye: A review on strategies, toxicity assessment, mechanisms, bottlenecks and prospects, Science of The Total Environment 954 (2024) 176426. https://doi.org/10.1016/j.scitotenv.2024.176426.

[57] H. Tounsadi, Y. Metarfi, M. Taleb, K. El Rhazi, Z. Rais, Impact of chemical substances used in textile industry on the employee's health: Epidemiological study, Ecotoxicology and Environmental Safety 197 (2020) 110594. https://doi.org/10.1016/j.ecoenv.2020.110594.

[58] L. Wu, Y. Xu, X. Lv, X. Chang, X. Ma, X. Tian, X. Shi, X. Li, X. Kong, Impacts of an azo food dye tartrazine uptake on intestinal barrier, oxidative stress, inflammatory response and intestinal microbiome in crucian carp (Carassius auratus), Ecotoxicology and Environmental Safety 223 (2021) 112551. https://doi.org/10.1016/j.ecoenv.2021.112551.

[59] A. Bafana, S.S. Devi, T. Chakrabarti, Azo dyes: past, present and the future, Environ. Rev. 19 (2011) 350–371. https://doi.org/10.1139/a11-018.

[60] N.M. Mahmoodi, M. Taghizadeh, A. Taghizadeh, Activated carbon/metal-organic framework composite as a bio-based novel green adsorbent: Preparation and mathematical pollutant removal modeling, Journal of Molecular Liquids 277 (2019) 310–322. https://doi.org/10.1016/j.molliq.2018.12.050.

[61] M.S. Soffian, F.Z. Abdul Halim, F. Aziz, M. A. Rahman, M.A. Mohamed Amin, D.N. Awang Chee, Carbon-based material derived from biomass waste for wastewater treatment, Environmental Advances 9 (2022) 100259. https://doi.org/10.1016/j.envadv.2022.100259.

[62] S. Lombardo, W. Thielemans, Thermodynamics of adsorption on nanocellulose surfaces, Cellulose 26 (2019) 249–279. https://doi.org/10.1007/s10570-018-02239-2.

[63] N.M. Mahmoodi, M. Oveisi, A. Taghizadeh, M. Taghizadeh, Novel magnetic amine functionalized carbon nanotube/metal-organic framework nanocomposites: From green ultrasound-assisted synthesis to detailed selective pollutant removal modelling from binary systems, Journal of Hazardous Materials 368 (2019) 746–759. https://doi.org/10.1016/j.jhazmat.2019.01.107.

[64] Y. Onal, C. Akmilbasar, D. Eren, C. Sariciozdemir, T. Depci, Adsorption kinetics of malachite green onto activated carbon prepared from Tunçbilek lignite, Journal of Hazardous Materials 128 (2006) 150–157. https://doi.org/10.1016/j.jhazmat.2005.07.055.

[65] A. Ghazali, M. Shirani, A. Semnani, V. Zare-Shahabadi, M. Nekoeinia, Optimization of crystal violet adsorption onto Date palm leaves as a potent biosorbent from aqueous solutions using response surface methodology and ant colony, Journal of Environmental Chemical Engineering 6 (2018) 3942–3950. https://doi.org/10.1016/j.jece.2018.05.043.

[66] Y. Feng, D.D. Dionysiou, Y. Wu, H. Zhou, L. Xue, S. He, L. Yang, Adsorption of dyestuff from aqueous solutions through oxalic acid-modified swede rape straw: Adsorption process and disposal methodology of depleted bioadsorbents, Bioresource Technology 138 (2013) 191–197. https://doi.org/10.1016/j.biortech.2013.03.146.

[67] M.A.M. Salleh, D.K. Mahmoud, W.A.W.A. Karim, A. Idris, Cationic and anionic dye adsorption by agricultural solid wastes: A comprehensive review, Desalination 280 (2011) 1–13. https://doi.org/10.1016/j.desal.2011.07.019.

[68] H.N. Tran, H.C. Nguyen, S.H. Woo, T.V. Nguyen, S. Vigneswaran, A. Hosseini-Bandegharaei, J. Rinklebe, A. Kumar Sarmah, A. Ivanets, G.L. Dotto, T.T. Bui, R.-S. Juang, H.-P. Chao, Removal of various contaminants from water by renewable lignocellulose-derived biosorbents: a comprehensive and critical review, Critical Reviews in Environmental Science and Technology 49 (2019) 2155–2219. https://doi.org/10.1080/10643389.2019.1607442.

[69] Y. Liu, Y.-J. Liu, Biosorption isotherms, kinetics and thermodynamics, Separation and Purification Technology 61 (2008) 229–242. https://doi.org/10.1016/j.seppur.2007.10.002.

[70] G. Blanchard, M. Maunaye, G. Martin, Removal of heavy metals from waters by means of natural zeolites, Water Research 18 (1984) 1501–1507. https://doi.org/10.1016/0043-1354(84)90124-6.

[71] Y.S. Ho, J.C.Y. Ng, G. McKay, KINETICS OF POLLUTANT SORPTION BY BIOSORBENTS: REVIEW, Separation and Purification Methods 29 (2000) 189–232. https://doi.org/10.1081/SPM-100100009.

[72] Y. Ho, Review of second-order models for adsorption systems, Journal of Hazardous Materials 136 (2006) 681–689. https://doi.org/10.1016/j.jhazmat.2005.12.043.

[73] É.C. Lima, M.A. Adebayo, F.M. Machado, Kinetic and Equilibrium Models of Adsorption, in: C.P. Bergmann, F.M. Machado (Eds.), Carbon Nanomaterials as Adsorbents for Environmental and Biological Applications, Springer International Publishing, Cham, 2015: pp. 33–69. https://doi.org/10.1007/978-3-319-18875-1_3.

[74] H.N. Tran, S.-J. You, T.V. Nguyen, H.-P. Chao, Insight into the adsorption mechanism of cationic dye onto biosorbents derived from agricultural wastes, Chemical Engineering Communications 204 (2017) 1020–1036. https://doi.org/10.1080/00986445.2017.1336090.

[75] H.N. Tran, S.-J. You, A. Hosseini-Bandegharaei, H.-P. Chao, Mistakes and inconsistencies regarding adsorption of contaminants from aqueous solutions: A critical review, Water Research 120 (2017) 88–116. https://doi.org/10.1016/j.watres.2017.04.014.

[76] T.W. Weber, R.K. Chakravorti, Pore and solid diffusion models for fixed-bed adsorbers, AIChE Journal 20 (1974) 228–238. https://doi.org/10.1002/aic.690200204.

[77] H. Freundlich, Über die Adsorption in Lösungen, Zeitschrift Für Physikalische Chemie 57U (1907) 385–470. https://doi.org/10.1515/zpch-1907-5723.

[78] K.Y. Foo, B.H. Hameed, Insights into the modeling of adsorption isotherm systems, Chemical Engineering Journal 156 (2010) 2–10. https://doi.org/10.1016/j.cej.2009.09.013.

[79] H.N. Tran, S.-J. You, H.-P. Chao, Thermodynamic parameters of cadmium adsorption onto orange peel calculated from various methods: A comparison study, Journal of Environmental Chemical Engineering 4 (2016) 2671–2682. https://doi.org/10.1016/j.jece.2016.05.009.

[80] X. Zhou, X. Zhou, THE UNIT PROBLEM IN THE THERMODYNAMIC CALCULATION OF ADSORPTION USING THE LANGMUIR EQUATION, Chemical Engineering Communications 201 (2014) 1459–1467. https://doi.org/10.1080/00986445.2013.818541.

[81] Y. Liu, Is the Free Energy Change of Adsorption Correctly Calculated?, J. Chem. Eng. Data 54 (2009) 1981–1985. https://doi.org/10.1021/je800661q.

[82] I. Langmuir, THE ADSORPTION OF GASES ON PLANE SURFACES OF GLASS, MICA AND PLATINUM., J. Am. Chem. Soc. 40 (1918) 1361–1403. https://doi.org/10.1021/ja02242a004.

[83] E.C. Lima, A. Hosseini-Bandegharaei, J.C. Moreno-Piraján, I. Anastopoulos, A critical review of the estimation of the thermodynamic parameters on adsorption equilibria. Wrong use of equilibrium constant in the Van't Hoof equation for calculation of thermodynamic parameters of adsorption, Journal of Molecular Liquids 273 (2019) 425–434. https://doi.org/10.1016/j.molliq.2018.10.048.

[84] S. Salvestrini, V. Leone, P. Iovino, S. Canzano, S. Capasso, Considerations about the correct evaluation of sorption thermodynamic parameters from equilibrium isotherms, The Journal of Chemical Thermodynamics 68 (2014) 310–316. https://doi.org/10.1016/j.jct.2013.09.013.

[85] H.N. Tran, E.C. Lima, R.-S. Juang, J.-C. Bollinger, H.-P. Chao, Thermodynamic parameters of liquid–phase adsorption process calculated from different equilibrium constants related to adsorption isotherms: A comparison study, Journal of Environmental Chemical Engineering 9 (2021) 106674. https://doi.org/10.1016/j.jece.2021.106674.

[86] S. Babel, Low-cost adsorbents for heavy metals uptake from contaminated water: a review, Journal of Hazardous Materials 97 (2003) 219–243. https://doi.org/10.1016/S0304-3894(02)00263-7.

[87] M.T. Yagub, T.K. Sen, S. Afroze, H.M. Ang, Dye and its removal from aqueous solution by adsorption: A review, Advances in Colloid and Interface Science 209 (2014) 172–184. https://doi.org/10.1016/j.cis.2014.04.002.

[88] S. Netpradit, P. Thiravetyan, S. Towprayoon, Application of 'waste' metal hydroxide sludge for adsorption of azo reactive dyes, Water Research 37 (2003) 763–772. https://doi.org/10.1016/S0043-1354(02)00375-5.

[89] B. Acemioğlu, Adsorption of Congo red from aqueous solution onto calcium-rich fly ash, Journal of Colloid and Interface Science 274 (2004) 371–379. https://doi.org/10.1016/j.jcis.2004.03.019.

[90] C. Namasivayam, S. Sumithra, Removal of direct red 12B and methylene blue from water by adsorption onto Fe (III)/Cr (III) hydroxide, an industrial solid waste, Journal of Environmental Management 74 (2005) 207–215. https://doi.org/10.1016/j.jenvman.2004.08.016.

[91] C.-H. Weng, Y.-F. Pan, Adsorption characteristics of methylene blue from aqueous solution by sludge ash, Colloids and Surfaces A: Physicochemical and Engineering Aspects 274 (2006) 154–162. https://doi.org/10.1016/j.colsurfa.2005.08.044.

[92] H.C. Chu, K.M. Chen, Reuse of activated sludge biomass: I. Removal of basic dyes from wastewater by biomass, Process Biochemistry 37 (2002) 595–600. https://doi.org/10.1016/S0032-9592(01)00234-5.

[93] H.C. Chu, K.M. Chen, Reuse of activated sludge biomass: II. The rate processes for the adsorption of basic dyes on biomass, Process Biochemistry 37 (2002) 1129–1134. https://doi.org/10.1016/S0032-9592(01)00326-0.

[94] J.R. Guarín, J.C. Moreno-Pirajan, L. Giraldo, Kinetic Study of the Bioadsorption of Methylene Blue on the Surface of the Biomass Obtained from the Algae *D. antarctica*, Journal of Chemistry 2018 (2018) 1–12. https://doi.org/10.1155/2018/2124845.

[95] G. Crini, Non-conventional low-cost adsorbents for dye removal: A review, Bioresource Technology 97 (2006) 1061–1085. https://doi.org/10.1016/j.biortech.2005.05.001.

[96] T. Lu, Q. Zhang, S. Yao, Efficient decolorization of dye-containing wastewater using mycelial pellets formed of marine-derived Aspergillus niger, Chinese Journal of Chemical Engineering 25 (2017) 330–337. https://doi.org/10.1016/j.cjche.2016.08.010.

[97] Y. Xi, Y. Shen, F. Yang, G. Yang, C. Liu, Z. Zhang, D. Zhu, Removal of azo dye from aqueous solution by a new biosorbent prepared with Aspergillus nidulans cultured in tobacco wastewater, Journal of the Taiwan Institute of Chemical Engineers 44 (2013) 815–820. https://doi.org/10.1016/j.jtice.2013.01.031.

[98] R. Wibulswas, Batch and fixed bed sorption of methylene blue on precursor and QACs modified montmorillonite, Separation and Purification Technology 39 (2004) 3–12. https://doi.org/10.1016/j.seppur.2003.12.018.

[99] M. Auta, B.H. Hameed, Modified mesoporous clay adsorbent for adsorption isotherm and kinetics of methylene blue, Chemical Engineering Journal 198–199 (2012) 219–227. https://doi.org/10.1016/j.cej.2012.05.075.

[100] V. Vimonses, S. Lei, B. Jin, C.W.K. Chow, C. Saint, Kinetic study and equilibrium isotherm analysis of Congo Red adsorption by clay materials, Chemical Engineering Journal 148 (2009) 354–364. https://doi.org/10.1016/j.cej.2008.09.009.

[101] D. Chen, J. Chen, X. Luan, H. Ji, Z. Xia, Characterization of anion–cationic surfactants modified montmorillonite and its application for the removal of methyl orange, Chemical Engineering Journal 171 (2011) 1150–1158. https://doi.org/10.1016/j.cej.2011.05.013.

[102] R.F. De Farias, Zeolites, in: Interface Science and Technology, Elsevier, 2023: pp. 141–144. https://doi.org/10.1016/B978-0-443-18791-9.00004-0.

[103] Y. Dehmani, B. Ba Mohammed, R. Oukhrib, A. Dehbi, T. Lamhasni, Y. Brahmi, A. El-Kordy, D.S.P. Franco, J. Georgin, E.C. Lima, A.A. Alrashdi, N. Tijani, S. Abouarnadasse, Adsorption of various inorganic and organic pollutants by natural and synthetic zeolites: A critical review, Arabian Journal of Chemistry 17 (2024) 105474. https://doi.org/10.1016/j.arabjc.2023.105474.

[104] P. He, Q. Wang, S. Fu, M. Wang, S. Zhao, X. Liu, Y. Jiang, D. Jia, Y. Zhou, Hydrothermal transformation of geopolymers to bulk zeolite structures for efficient hazardous elements adsorption, Science of The Total Environment 767 (2021) 144973. https://doi.org/10.1016/j.scitotenv.2021.144973.

[105] B. Ji, W. Zhang, Adsorption of cerium (III) by zeolites synthesized from kaolinite after rare earth elements (REEs) recovery, Chemosphere 303 (2022) 134941. https://doi.org/10.1016/j.chemosphere.2022.134941.

[106] S. Keerthanan, M. Vithanage, Potential of zeolite as an adsorbent for the removal of trace metal(loids) in wastewater, in: Advanced Materials for Sustainable Environmental Remediation, Elsevier, 2022: pp. 339–359. https://doi.org/10.1016/B978-0-323-90485-8.00022-9.

[107] N.S. Samanta, P.P. Das, P. Mondal, M. Changmai, M.K. Purkait, Critical review on the synthesis and advancement of industrial and biomass waste-based zeolites and their applications in gas adsorption and biomedical studies, Journal of the Indian Chemical Society 99 (2022) 100761. https://doi.org/10.1016/j.jics.2022.100761.

[108] E. Cataldo, L. Salvi, F. Paoli, M. Fucile, G. Masciandaro, D. Manzi, C.M. Masini, G.B. Mattii, Application of Zeolites in Agriculture and Other Potential Uses: A Review, Agronomy 11 (2021) 1547. https://doi.org/10.3390/agronomy11081547.

[109] R.M. Barrer, Expanded clay minerals: a major class of molecular sieves, Journal of Inclusion Phenomena 4 (1986) 109–119. https://doi.org/10.1007/BF00655925.

[110] S. Liu, M. Lim, R. Amal, TiO2-coated natural zeolite: Rapid humic acid adsorption and effective photocatalytic regeneration, Chemical Engineering Science 105 (2014) 46–52. https://doi.org/10.1016/j.ces.2013.10.041.

[111] A. Nezamzadeh-Ejhieh, E. Shahriari, Photocatalytic decolorization of methyl green using Fe(II)-o-phenanthroline as supported onto zeolite Y, Journal of Industrial and Engineering Chemistry 20 (2014) 2719–2726. https://doi.org/10.1016/j.jiec.2013.10.060.

[112] M.S. Shamsudin, S.F. Azha, M. Shahadat, S. Ismail, Cellulose/bentonite-zeolite composite adsorbent material coating for treatment of N-based antiseptic cationic dye from water, Journal of Water Process Engineering 29 (2019) 100764. https://doi.org/10.1016/j.jwpe.2019.02.004.

[113] E. Salah Elbanna, A.A. Farghali, M.H. Khedr, M. Taha, Nano clinoptilolite zeolite as a sustainable adsorbent for dyes removal: Adsorption and computational mechanistic studies, Journal of Molecular Liquids 409 (2024) 125538. https://doi.org/10.1016/j.molliq.2024.125538.

[114] H. Mittal, R. Babu, A.A. Dabbawala, S. Stephen, S.M. Alhassan, Zeolite-Y incorporated karaya gum hydrogel composites for highly effective removal of cationic dyes, Colloids and Surfaces A: Physicochemical and Engineering Aspects 586 (2020) 124161. https://doi.org/10.1016/j.colsurfa.2019.124161.

[115] M.T. Ritter, M.Á. Lobo-Recio, I. Padilla, M.E. Nagel-Hassemer, M. Romero, A. López-Delgado, Adsorption of Safranine-T dye using a waste-based zeolite: Optimization, kinetic and isothermal study, Journal of Industrial and Engineering Chemistry 136 (2024) 177–187. https://doi.org/10.1016/j.jiec.2024.02.005.

[116] V. Sodha, H. Koshti, R. Gaur, R. Bandyopadhyay, S. Shahabuddin, Investigation on the adsorption of cationic dyes and heavy metal ions on zeolite HY from aqueous solution,

Materials Today: Proceedings (2024) S2214785323053361. https://doi.org/10.1016/j.matpr.2023.12.048.

[117] R.H. Khudhur, N.S. Ali, E.H. Khader, N.S. Abbood, I.K. Salih, T.M. Albayati, Adsorption of anionic azo dye from aqueous wastewater using zeolite NaX as an efficient adsorbents, Desalination and Water Treatment 306 (2023) 245–252. https://doi.org/10.5004/dwt.2023.29861.

[118] M.E.S. Pedebos, D.M. Druzian, L.R. Oviedo, Y.P.M. Ruiz, A. Galembeck, G. Pavoski, D.C.R. Espinosa, W.L. Da Silva, Removal of Rhodamine B dye by adsorption onto an eco-friendly zeolite and machine learning modeling, Journal of Photochemistry and Photobiology A: Chemistry 449 (2024) 115404. https://doi.org/10.1016/j.jphotochem.2023.115404.

[119] M. Das, S. Dasgupta, M.A. Klunk, S.X. Juceli Siqueira, F. Chemale Junior, P.R. Wander, Study involving removal of azo dye Direct Orange 34 by adsorption in zeolite–clay system, Can. J. Chem. 98 (2020) 609–615. https://doi.org/10.1139/cjc-2020-0142.

[120] B. Senthil Rathi, P. Senthil Kumar, J. Natanya Ida Susana, J. Francia Virgin, R. Dharani, S. Sanjay, G. Rangasamy, Recent research progress on the removal of heavy metals from wastewater using modified zeolites: A critical review, Desalination and Water Treatment 319 (2024) 100573. https://doi.org/10.1016/j.dwt.2024.100573.

[121] M.K. Tufail, M. Ifrahim, M. Rashid, I. Ul Haq, R. Asghar, U.T. Uthappa, M. Selvaraj, M. Kurkuri, Chemistry of zeolites and zeolite based composite membranes as a cutting-edge candidate for removal of organic dyes & heavy metal ions: Progress and future directions, Separation and Purification Technology 354 (2025) 128739. https://doi.org/10.1016/j.seppur.2024.128739.

[122] N. Finish, P. Ramos, E.J.C. Borojovich, O. Zeiri, Y. Amar, M. Gottlieb, Zeolite performance in removal of multicomponent heavy metal contamination from wastewater, Journal of Hazardous Materials 457 (2023) 131784. https://doi.org/10.1016/j.jhazmat.2023.131784.

[123] B. Ba Mohammed, K. Yamni, N. Tijani, A.A. Alrashdi, H. Zouihri, Y. Dehmani, I.-M. Chung, S.-H. Kim, H. Lgaz, Adsorptive removal of phenol using faujasite-type Y zeolite: Adsorption isotherms, kinetics and grand canonical Monte Carlo simulation studies, Journal of Molecular Liquids 296 (2019) 111997. https://doi.org/10.1016/j.molliq.2019.111997.

[124] A. El-Kordy, Y. Dehmani, M. Douma, A. Bouazizi, H. El Moustansiri, S. El Abbadi, N. Tijani, Experimental study of phenol removal from aqueous solution by adsorption onto

synthesized Faujasite-type Y zeolite, Desalination and Water Treatment 277 (2022) 144–154. https://doi.org/10.5004/dwt.2022.28958.

[125] Mu. Naushad, S. Rajendran, F. Gracia, eds., Advanced Nanostructured Materials for Environmental Remediation, Springer International Publishing, Cham, 2019. https://doi.org/10.1007/978-3-030-04477-0.

[126] M. Ghoussoub, M. Xia, P.N. Duchesne, D. Segal, G. Ozin, Principles of photothermal gas-phase heterogeneous CO_2 catalysis, Energy Environ. Sci. 12 (2019) 1122–1142. https://doi.org/10.1039/C8EE02790K.

[127] N.M. Mahmoodi, J. Abdi, M. Taghizadeh, A. Taghizadeh, B. Hayati, A.A. Shekarchi, M. Vossoughi, Activated carbon/metal-organic framework nanocomposite: Preparation and photocatalytic dye degradation mathematical modeling from wastewater by least squares support vector machine, Journal of Environmental Management 233 (2019) 660–672. https://doi.org/10.1016/j.jenvman.2018.12.026.

[128] M.K. Yazdi, V. Vatanpour, A. Taghizadeh, M. Taghizadeh, M.R. Ganjali, M.T. Munir, S. Habibzadeh, M.R. Saeb, M. Ghaedi, Hydrogel membranes: A review, Materials Science and Engineering: C 114 (2020) 111023. https://doi.org/10.1016/j.msec.2020.111023.

[129] F. Sadeghfar, Z. Zalipour, M. Taghizadeh, A. Taghizadeh, M. Ghaedi, Photodegradation processes, in: Interface Science and Technology, Elsevier, 2021: pp. 55–124. https://doi.org/10.1016/B978-0-12-818806-4.00013-9.

[130] M. Liu, J. He, D. Liu, M. Hou, Y. Ma, Bibliometric and visualized analysis of dynamic balance and brain function using web of science and CiteSpace from 1995 to 2022, Heliyon 10 (2024) e24300. https://doi.org/10.1016/j.heliyon.2024.e24300.

[131] M. Nazari, A. Asgary, I.M. Nezami, S. Ghayourisales, From resistance to resilience: A comprehensive bibliometric analysis of carbon pricing public acceptance, Energy Research & Social Science 107 (2024) 103340. https://doi.org/10.1016/j.erss.2023.103340.

[132] F. Azizoğlu, B. Terzi, Research topics on pressure injury prevention and measurement tools from 1997 to 2023: A bibliometric analysis using VOSviewer, Intensive and Critical Care Nursing 80 (2024) 103557. https://doi.org/10.1016/j.iccn.2023.103557.

[133] H.S. Kusuma, D.E. Christa Jaya, N. Illiyanasafa, K.L. Ikawati, E. Kurniasari, H. Darmokoesoemo, A.N. Amenaghawon, A critical review and bibliometric analysis of methylene blue adsorption using leaves, Chemosphere 356 (2024) 141867. https://doi.org/10.1016/j.chemosphere.2024.141867.

[134] R. Ameta, M.S. Solanki, S. Benjamin, S.C. Ameta, Photocatalysis, in: Advanced Oxidation Processes for Waste Water Treatment, Elsevier, 2018: pp. 135–175. https://doi.org/10.1016/B978-0-12-810499-6.00006-1.

[135] J.-M. Herrmann, Heterogeneous photocatalysis: fundamentals and applications to the removal of various types of aqueous pollutants, Catalysis Today 53 (1999) 115–129. https://doi.org/10.1016/S0920-5861(99)00107-8.

[136] J.A. Byrne, B.R. Eggins, N.M.D. Brown, B. McKinney, M. Rouse, Immobilisation of TiO2 powder for the treatment of polluted water, Applied Catalysis B: Environmental 17 (1998) 25–36. https://doi.org/10.1016/S0926-3373(97)00101-X.

[137] B. Bajorowicz, M.P. Kobylański, A. Malankowska, P. Mazierski, J. Nadolna, A. Pieczyńska, A. Zaleska-Medynska, Application of metal oxide-based photocatalysis, in: Metal Oxide-Based Photocatalysis, Elsevier, 2018: pp. 211–340. https://doi.org/10.1016/B978-0-12-811634-0.00004-4.

[138] R. Chatti, S.S. Rayalu, N. Dubey, N. Labhsetwar, S. Devotta, Solar-based photoreduction of methyl orange using zeolite supported photocatalytic materials, Solar Energy Materials and Solar Cells 91 (2007) 180–190. https://doi.org/10.1016/j.solmat.2006.08.009.

[139] R.L. Pozzo, J.L. Giombi, M.A. Baltanás, A.E. Cassano, The performance in a fluidized bed reactor of photocatalysts immobilized onto inert supports, Catalysis Today 62 (2000) 175–187. https://doi.org/10.1016/S0920-5861(00)00419-3.

[140] U.I. Gaya, A.H. Abdullah, Heterogeneous photocatalytic degradation of organic contaminants over titanium dioxide: A review of fundamentals, progress and problems, Journal of Photochemistry and Photobiology C: Photochemistry Reviews 9 (2008) 1–12. https://doi.org/10.1016/j.jphotochemrev.2007.12.003.

[141] M.N. Chong, B. Jin, C.W.K. Chow, C. Saint, Recent developments in photocatalytic water treatment technology: A review, Water Research 44 (2010) 2997–3027. https://doi.org/10.1016/j.watres.2010.02.039.

[142] K. Całus-Makowska, A. Grosser, A. Grobelak, H. Białek, E. Siedlecka, Kinetic study of the simultaneous removal of ibuprofen, carbamazepine, sulfamethoxazole, and diclofenac from water using biochar and activated carbon adsorption, and TiO2 photocatalysis, Desalination and Water Treatment 320 (2024) 100817. https://doi.org/10.1016/j.dwt.2024.100817.

[143] M.N. Chong, S. Lei, B. Jin, C. Saint, C.W.K. Chow, Optimisation of an annular photoreactor process for degradation of Congo Red using a newly synthesized titania

impregnated kaolinite nano-photocatalyst, Separation and Purification Technology 67 (2009) 355–363. https://doi.org/10.1016/j.seppur.2009.04.001.

[144] S.S. Chin, K. Chiang, A.G. Fane, The stability of polymeric membranes in a TiO2 photocatalysis process, Journal of Membrane Science 275 (2006) 202–211. https://doi.org/10.1016/j.memsci.2005.09.033.

[145] H. Esfandian, S. Mirzaei, A.S. Chari, R.A. Ghadi, I.H. Moqadam, Photocatalytic degradation of chlorpyrifos pesticide in aqueous solution using Cu-doped TiO2/GO photocatalysis vicinity of UV and visible light, Materials Science and Engineering: B 305 (2024) 117385. https://doi.org/10.1016/j.mseb.2024.117385.

[146] T.M. Le, T.D. Nguyen, Enhancement of visible-light photocatalysis of TiO2 via nanocomposite incorporating with Fe(III) species, Results in Engineering 23 (2024) 102500. https://doi.org/10.1016/j.rineng.2024.102500.

[147] D. Bahnemann, Photocatalytic water treatment: solar energy applications, Solar Energy 77 (2004) 445–459. https://doi.org/10.1016/j.solener.2004.03.031.

[148] A.-G. Rincón, C. Pulgarin, Use of coaxial photocatalytic reactor (CAPHORE) in the TiO2 photo-assisted treatment of mixed E. coli and Bacillus sp. and bacterial community present in wastewater, Catalysis Today 101 (2005) 331–344. https://doi.org/10.1016/j.cattod.2005.03.022.

[149] S. Cheikh, A. Imessaoudene, J.-C. Bollinger, A. Manseri, A. Bouzaza, A. Hadadi, N. Hamri, A. Amrane, L. Mouni, Adsorption behavior and mechanisms of the emerging antibiotic pollutant norfloxacin on eco-friendly and low-cost hydroxyapatite: Integrated experimental and response surface methodology optimized adsorption process, Journal of Molecular Liquids 392 (2023) 123424. https://doi.org/10.1016/j.molliq.2023.123424.

[150] S. Malato, P. Fernández-Ibáñez, M.I. Maldonado, J. Blanco, W. Gernjak, Decontamination and disinfection of water by solar photocatalysis: Recent overview and trends, Catalysis Today 147 (2009) 1–59. https://doi.org/10.1016/j.cattod.2009.06.018.

[151] M. Saquib, TiO2-mediated photocatalytic degradation of a triphenylmethane dye (gentian violet), in aqueous suspensions, Dyes and Pigments 56 (2003) 37–49. https://doi.org/10.1016/S0143-7208(02)00101-8.

[152] M. Umar, H. Abdul, Photocatalytic Degradation of Organic Pollutants in Water, in: M.N. Rashed (Ed.), Organic Pollutants - Monitoring, Risk and Treatment, InTech, 2013. https://doi.org/10.5772/53699.

[153] A. Fujishima, T.N. Rao, D.A. Tryk, Titanium dioxide photocatalysis, Journal of Photochemistry and Photobiology C: Photochemistry Reviews 1 (2000) 1–21. https://doi.org/10.1016/S1389-5567(00)00002-2.

[154] N. Bouanimba, R. Zouaghi, N. Laid, T. Sehili, Factors influencing the photocatalytic decolorization of Bromophenol blue in aqueous solution with different types of TiO2 as photocatalysts, Desalination 275 (2011) 224–230. https://doi.org/10.1016/j.desal.2011.03.005.

[155] E. Vulliet, J.-M. Chovelon, C. Guillard, J.-M. Herrmann, Factors influencing the photocatalytic degradation of sulfonylurea herbicides by TiO2 aqueous suspension, Journal of Photochemistry and Photobiology A: Chemistry 159 (2003) 71–79. https://doi.org/10.1016/S1010-6030(03)00108-4.

[156] K.M. Lee, C.W. Lai, K.S. Ngai, J.C. Juan, Recent developments of zinc oxide based photocatalyst in water treatment technology: A review, Water Research 88 (2016) 428–448. https://doi.org/10.1016/j.watres.2015.09.045.

[157] Z. Pan, E.A. Stemmler, H.J. Cho, W. Fan, L.A. LeBlanc, H.H. Patterson, A. Amirbahman, Photocatalytic degradation of 17α-ethinylestradiol (EE2) in the presence of TiO2-doped zeolite, Journal of Hazardous Materials 279 (2014) 17–25. https://doi.org/10.1016/j.jhazmat.2014.06.040.

[158] S. Cheikh, A. Imessaoudene, J.-C. Bollinger, A. Hadadi, A. Manseri, A. Bouzaza, A. Assadi, A. Amrane, M. Zamouche, A. El Jery, L. Mouni, Complete Elimination of the Ciprofloxacin Antibiotic from Water by the Combination of Adsorption–Photocatalysis Process Using Natural Hydroxyapatite and TiO2, Catalysts 13 (2023) 336. https://doi.org/10.3390/catal13020336.

[159] C.N. Satterfield, D.H. Cortez, Mass Transfer Characteristics of Woven-Wire Screen Catalysts, Ind. Eng. Chem. Fund. 9 (1970) 613–620. https://doi.org/10.1021/i160036a015.

[160] D.F. Ollis, Contaminant degradation in water, Environ. Sci. Technol. 19 (1985) 480–484. https://doi.org/10.1021/es00136a002.

[161] A. Fernández, G. Lassaletta, V.M. Jiménez, A. Justo, A.R. González-Elipe, J.-M. Herrmann, H. Tahiri, Y. Ait-Ichou, Preparation and characterization of TiO2 photocatalysts supported on various rigid supports (glass, quartz and stainless steel). Comparative studies of photocatalytic activity in water purification, Applied Catalysis B: Environmental 7 (1995) 49–63. https://doi.org/10.1016/0926-3373(95)00026-7.

[162] J.P.S. Valente, P.M. Padilha, A.O. Florentino, Studies on the adsorption and kinetics of photodegradation of a model compound for heterogeneous photocatalysis onto TiO2, Chemosphere 64 (2006) 1128–1133. https://doi.org/10.1016/j.chemosphere.2005.11.050.

[163] Y.-S. Cho, T.T.H. Nguyen, H.H. Nguyen, Q.H. Tran, Modeling and experimental study of hollow cylindrical catalysts for prediction of transient behaviors of suspension photoreaction systems by Langmuir-Hinshelwood kinetics, Catalysis Today 425 (2024) 114345. https://doi.org/10.1016/j.cattod.2023.114345.

[164] Y.-S. Cho, H.H. Nguyen, T.T.H. Nguyen, Modeling of slurry-type photocatalytic reactors containing core-shell particles for predicting transient behaviours based on Langmuir-Hinshelwood kinetics, Catalysis Today 411–412 (2023) 113909. https://doi.org/10.1016/j.cattod.2022.09.015.

[165] A. Mahmood, X. Wang, X. Xie, J. Sun, Degradation behavior of mixed and isolated aromatic ring containing VOCs: Langmuir-Hinshelwood kinetics, photodegradation, in-situ FTIR and DFT studies, Journal of Environmental Chemical Engineering 9 (2021) 105069. https://doi.org/10.1016/j.jece.2021.105069.

[166] Y. Huang, Y. Luo, Z. Liu, X. Xie, M. Xue, B. Gao, Engineering carbon materials for organic pollutant removal via adsorption and photodegradation: A review, Separation and Purification Technology 359 (2025) 130872. https://doi.org/10.1016/j.seppur.2024.130872.

[167] X. Wei, X. Wang, Y. Pu, A. Liu, C. Chen, W. Zou, Y. Zheng, J. Huang, Y. Zhang, Y. Yang, Mu. Naushad, B. Gao, L. Dong, Facile ball-milling synthesis of CeO2/g-C3N4 Z-scheme heterojunction for synergistic adsorption and photodegradation of methylene blue: Characteristics, kinetics, models, and mechanisms, Chemical Engineering Journal 420 (2021) 127719. https://doi.org/10.1016/j.cej.2020.127719.

[168] Y. Luo, X. Wei, B. Gao, W. Zou, Y. Zheng, Y. Yang, Y. Zhang, Q. Tong, L. Dong, Synergistic adsorption-photocatalysis processes of graphitic carbon nitrate (g-C3N4) for contaminant removal: Kinetics, models, and mechanisms, Chemical Engineering Journal 375 (2019) 122019. https://doi.org/10.1016/j.cej.2019.122019.

[169] Y. Luo, Y. Han, M. Xue, Y. Xie, Z. Yin, C. Xie, X. Li, Y. Zheng, J. Huang, Y. Zhang, Y. Yang, B. Gao, Ball-milled bismuth oxybromide/biochar composites with enhanced removal of reactive red owing to the synergy between adsorption and photodegradation, Journal of Environmental Management 308 (2022) 114652. https://doi.org/10.1016/j.jenvman.2022.114652.

[170] Y. Luo, A. Zheng, M. Xue, Y. Xie, S. Yu, Z. Yin, C. Xie, Z. Hong, W. Tan, W. Zou, L. Dong, B. Gao, Ball-milled Bi2MoO6/biochar composites for synergistic adsorption and photodegradation of methylene blue: Kinetics and mechanisms, Industrial Crops and Products 186 (2022) 115229. https://doi.org/10.1016/j.indcrop.2022.115229.

[171] Y. Luo, Y. Han, Y. Hua, M. Xue, S. Yu, L. Zhang, Z. Yin, X. Li, X. Ma, H. Wu, T. Liu, Y. Shen, B. Gao, Step scheme nickel-aluminium layered double hydroxides/biochar heterostructure photocatalyst for synergistic adsorption and photodegradation of tetracycline, Chemosphere 309 (2022) 136802. https://doi.org/10.1016/j.chemosphere.2022.136802.

[172] D. Ning, J. Li, Y. Lan, H.Y. Sohn, J. Yang, C. Chen, Z. Chu, X. Mao, Molten salt synthesis of Z-scheme CeO2/C3N4 photocatalysts with excellent properties for removal of organic pollutants: Characterization, kinetics and mechanisms, Journal of Rare Earths 41 (2023) 1153–1162. https://doi.org/10.1016/j.jre.2022.07.021.

[173] F. Yu, F. Tian, H. Zou, Z. Ye, C. Peng, J. Huang, Y. Zheng, Y. Zhang, Y. Yang, X. Wei, B. Gao, ZnO/biochar nanocomposites via solvent free ball milling for enhanced adsorption and photocatalytic degradation of methylene blue, Journal of Hazardous Materials 415 (2021) 125511. https://doi.org/10.1016/j.jhazmat.2021.125511.

Section II. Investigation of the adsorption performance of zeolite and its synergistic effect with the TiO_2 photocatalyst for textile dye removal

Chapter IV: Zeolite Waste Characterization and Use as Low-Cost, Ecofiendly, and Sustainable Material for Malachite Green and Methylene Blue Dyes Removal: Box-Behnken Design, Kinetics, and Thermodynamics

The findings of this study have been published in the journal "*Applied sciences*"

Ali Imessaoudene, Sabrina Cheikh, Jean-Claude Bollinger, Lazhar Belkhir, Ammar Tiri, Abedelkrim Bouzaza, Atef El Jery, Aymen Assadi, Abdeltif Amrane and Lotfi Mouni. Zeolite Waste Characterization and Use as Low-Cost, Ecofiendly, and Sustainable Material for Malachite Green and Methylene Blue Dyes Removal: Box-Behnken Design, Kinetics, and Thermodynamics. *Appl.Sci*. **2022**, 12, *7587*.
https://doi.org/10.3390/app12157587

Introduction

In this chapter, the adsorption performance of zeolite for cationic dyes was investigated, using Malachite Green and Methylene Blue as model molecules. Adopting the "treating waste with waste" approach, LTA-type zeolite waste, generated by the natural gas dehydration units at the TFT complex (Sonatrach), was employed after undergoing an appropriate regeneration treatment and is referred to here as 4AZW. The main conclusions of this study are as follows: After thorough characterization, the 4AZW material exhibited minimal loss in its crystalline structure, which provides a significant advantage. However, a key limitation of this adsorbent is its relatively low maximum adsorption capacity, which is 9.95 mg/g for Methylene Blue and 45.64 mg/g for Malachite Green.

Chapter IV: Zeolite Waste Characterization and Use as Low-Cost, Ecofiendly, and Sustainable Material for Malachite Green and Methylene Blue Dyes Removal: Box-Behnken Design, Kinetics, and Thermodynamics

Abstract: This study investigated the potential of 4A zeolite, named 4AZW in this work, generated by natural gas dehydration units as solid waste after several treatment cycles, as a low-cost adsorbent to separately remove two cationic dyes, methylene blue (MB) and malachite green (MG), from an aqueous solution within a batch process. The adsorbent material was characterized by N_2 gas adsorption–desorption, X-ray fluorescence spectrometry, X-ray diffraction, FT-IR spectroscopy, and the determination of its cation exchange capacity and point of zero charge. The influence of key operating parameters, such as the pH, adsorbent dosage, ionic strength, contact time, initial dye concentration, and temperature, was investigated. Three independent variables acting on MB adsorption performance were selected from the Box–Behnken design (BBD) and for process modeling and optimization. An analysis of variance (ANOVA), an F-test, and p-values were used to analyze the main and interaction effects. The experimental data were satisfyingly fitted with quadratic regression with adjusted $R^2 = 0.9961$. The pseudo-second-order kinetic model described the adsorption of the dyes on 4AZW. The equilibrium data were well-fitted by the Langmuir model for each adsorption system (MB-4AZW and MG-4AZW) with maximum adsorption capacity (q_{max}) values of 9.95 and 45.64 mg/g, respectively, at 25°C. Thermodynamics studies showed that both adsorption systems are spontaneous and endothermic.

Keywords: 4A zeolite reuse; dye removal; adsorption kinetics; isotherms; response surface methodology

1. Introduction

Fossil fuels have always been the primary source of the global energy supply. Algeria has an important energy potential: It holds the tenth largest gas reserve in the world and the third largest oil reserves in Africa [1]. Among all fossil fuel energy sources, natural gas (NG) is the cleanest and is a safe source when transported, stored, and used [2]. The chemical composition of the crude NG found in oil and gas reservoirs is composed of methane (as a major component), and in smaller quantities, ethane, propane, and butane, among other gaseous hydrocarbons. It also contains undesirable compounds such as water vapor, carbon dioxide, nitrogen, and hydrogen sulfide [3,4]. In industrial use, natural gas is subjected to different cleaning processes to meet product quality standards. Two main standards can be distinguished: Liquid natural gas

(LNG) and pipeline gas [5]. The water vapor contained in NG must be removed from the gas stream for the following reasons: Reducing the heating value of the produced gas, condensation of the water in the pipelines, and the risk of corrosion [2].

Extensive literature is available on common gas dehydration systems including glycol absorption, zeolite adsorption, and refrigeration-based systems [6]. Among these processes, adsorption on zeolite, especially the Temperature Swing Adsorption (TSA) system, is the most frequently used industrially for technical and energetic considerations [7]. The simplest configuration for the application of a TSA system to obtain a continuous flow of produced gas is the fixed double-bed system, with one operating in adsorption mode and the second in desorption mode (regeneration) [5]. Due to the higher capacity of water adsorption and selectivity, as well as its regeneration potential for several cycles of adsorption, the 4A zeolite adsorbent is widely used for the fine drying of NG in the TSA system [5,7].

Zeolites [8] are crystalline microporous aluminosilicates with a three-dimensional framework structure bearing AlO_4 and SiO_4 tetrahedra. These are linked to each other by sharing all of the oxygen to form interconnected cages and channels [9] with the characteristics of high ion exchange capacity and excellent selectivity (size, charge, and shape) and porosity on the surface [10]. Zeolites present a high potential for the purification of gases, especially those containing moisture [11]. 4A zeolite belongs to the LTA-type, with a pore size of 0.4 nm and a Si/Al ratio of approximately 1. This low Si/Al ratio, owing to the high aluminum content, makes the material highly hydrophilic [12]. The dehydration unit in the gas plant TFT of the Sonatrach company in Algeria generates important amounts of 4A zeolites after using the material in several adsorption and regeneration cycles, which reduces its adsorptive capacity with respect to the desired product quality during the dehydration operation. Under such a situation, the adsorbent is treated as solid waste to be disposed of in the technical landfill center near the plant site. The reuse of this adsorbent in wastewater treatment can be a possible way to valorize it by increasing its lifetime before it is considered waste. Several studies have applied natural and synthetic zeolites [13-18], as well as other eco-friendly materials [19], in waste water treatment.

In the present paper, batch experiments were carried out to separately remove methylene blue (MB) or malachite green (MG), two very popular and toxic cationic dyes [20,21], by the adsorption technique using 4A zeolite solid waste from the gas dehydration unit of TFT plant (Sonatrach company). This adsorbent material is named ′4A zeolite waste′ (4AZW) here. The characterization of the 4AZW sample was performed by BET surface area analysis, X-ray diffraction, and FT-IR analysis. The influence of temperature, pH, amount of adsorbent, contact

time, and initial MB or MG concentrations on the removal rate of those dyes were studied under shaken conditions. Different classical kinetic models were used to interpret the adsorption of each dye on 4AZW. Experimental equilibrium data were fitted with Freundlich and Langmuir isotherm equations to determine the best-fitting model. Additionally, in this work, it has been established that pH, the initial concentration, and the amount of adsorbent interacted and ultimately affected MB removal efficiency by the response surface methodology (RSM). This approach is a statistical application on the basis of fitting empirical models to a set of data obtained from several experiments: It is considered one of the most multivariate techniques used in process optimization [22,23]. By collectively optimizing all the affecting parameters, RSM can eliminate the limitations of single factor-at-a-time experiments [24,25]. This global investigation allowed for the study of new kinds of Zeolites.

This study on the investigation of the potential of 4AZW for the removal of two basic cationic dyes, MB and MG, from aqueous solutions under batch experimental conditions shows that wastewater treatment with this kind of zeolite constitutes an economical and efficient way to eliminate aqueous pollutants, which clearly meets the main aims of the UN Sustainable Development Goals (UN SDGs).

2. Materials and Methods

2.1. Materials

The 4AZW used in this study was obtained from the gas dehydration unit of the TFT plant (Sonatrach company, Algeria). This material was received as a binder-containing zeolite in the form of cylindrical pellets. After crushing, 100 g of the raw sample with a particle size lower than 100 µm was dried at 110°C for two hours and then dispersed in 1 L of deionized water and mixed for 24 h to eliminate all water-soluble impurities. After solid-liquid separation by filtration under a vacuum with Whatman® paper filter grade 40 (particle retention 8 µm), the obtained residue was calcined at 450°C for 2 h to eliminate all the organic compounds possibly retained during its initial use in the dehydration of the gas and finally kept in a desiccator until tested.

Two cationic dyes were selected for this study: Methylene blue (MB) and Malachite green (MG), obtained from Biochem Chemopharma (France). The maximum absorbance wavelengths of MB (664 nm) and MG (620 nm) were determined with a double beam UV-vis spectrometer (Specord 200 plus).

2.2. Characterization of 4AZW

The physicochemical properties of the solid material were determined using standard analytical techniques. To obtain the specific surface area and pore structure of the material, the Nitrogen adsorption-desorption isotherms at 77 K were measured with an automated gas adsorption analyzer ASAP2000 (Micromeritics, Norcross, GA) with ±5% accuracy. The total contents of chemical components were determined by X-ray fluorescence spectrometry (XRF) using a Philips PW-2400 X-ray spectrophotometer with Rh and Au excitation tubes. The X-ray diffraction (XRD) analysis of the samples was carried out via a powder X-ray diffractometer (Bruker AXS) in the angular range of 2-60° in steps of 2θ with a scan rate of 0.025 °/s. For Fourier-Transform Infrared spectroscopy (FT-IR, Bruker ALPHA), the spectrum was recorded in the 400-4000 cm^{-1} range.

The pH of 4AZW was measured as follows: A 1:2 (w:v) 4AZW: distilled water suspension was shaken for 24 h at 30°C, then filtered, and the pH of the filtrate was determined by a pH-meter [26]. The cation exchange capacity (CEC) of 4AZW was determined by the $BaCl_2$-triethanolamine procedure [27]. To determine the point of zero charge (pH_{PZC}) of the material, the ′drift method′ was applied [28]: 0.2 g of adsorbent was added to 40 mL of the 0.1 mol/L NaCl solution at different initial pH values (pH_i) in the range of 3 to 12, and agitated for 24 h at room temperature; the final pH (pH_f) values of solutions were then measured, and ΔpH is plotted vs. pH_i.

2.3. Adsorption Methodology

Batch adsorption experiments on the 4AZW adsorbent were conducted with either MB or MG aqueous solutions. A stock solution of MB or MG (1000 mg/L) was prepared by dissolving an accurately weighed quantity (1.0 g) of solid dye in 1 L of deionized water; the solutions for adsorption tests were diluted from the stock solution to the desired concentration.

One hundred milliliters of the dye solution at various concentrations were placed in 250 mL PE flasks with 0.1 g of the adsorbent and shaken (Labwit ZWY-304) at a speed of 200 rpm. The experiments were carried out at different pH (from 3 to 12) and temperature (from 25 to 50°C) values. The initial pH of the solution was adjusted to the desired value by using either HCl or NaOH solutions (0.1 mol/L). Kinetics of adsorption was determined by analyzing the dye uptake at different time intervals. From the kinetic experiments, a time contact equal to 110 min was fixed for all following isotherm experiments in order to reach a steady-state or pseudo-equilibrium. Solid and solution were separated using a 0.22 μm cellulose acetate membrane

filter, then the concentration of MB or MG in the supernatant was determined by a double-beam UV/vis spectrophotometer (SPECORD 200 plus). Kinetics of adsorption was determined by analyzing the dye uptake at different time intervals.

Each experiment was carried out in triplicate and all calculations were conducted with their average values; the maximum difference between the three values was less than 3% of the mean. The adsorbed amount of MB or MG at equilibrium was calculated by the straightforward equation:

$$q_e = \frac{(C_0 - C_e).V}{m} \qquad (1)$$

where q_e (mg/g) is the equilibrium adsorption capacity of dye adsorbed per gram of 4AZW, C_0 and C_e are the initial and equilibrium concentrations (mg/L) of MB or MG, respectively, V (L) is the volume of the dye solution, and m (g) is the weight of 4AZW. A linear calibration curve was prepared with MB (R^2 = 0.997) and GM (R^2 = 0.999) for UV/vis quantification.

The adsorption yield (% removal from aqueous solution) of the dye is calculated as:

$$Yield\ (\%) = \frac{(C_0 - C_e).100}{C_0} \qquad (2)$$

2.4. Experimental Design

To better understand the effect of important parameters such as pH, the initial concentration, and the amount of adsorbent, a Box-Behnken design was applied to the removal of MB, here selected as a dye model. In order to obtain the most important independent and influential variables with the minimum number of runs, the response surface methodology (RSM) proceeds by a two-in-one technique, i.e., both mathematical and statistical techniques are used together to obtain a relationship between a response, here defined by the yield removal (Yield (%)) as the dependent variable, and a number of independent variables defined by X_1, X_2, …,X_n. Usually, RSM is combined with factorial design methods such as the Box-Behnken design (BBD), i.e., a second-order multivariate design based on a three-level incomplete factorial design with no axial points [29].

In our case, fifteen experiments were performed with three replicates at the center point to estimate the pure error. Minitab® 17 software was used to apply the BBD model. Experimental data were fitted to a quadratic model using a second-order polynomial model as follows:

$$Yield\ (\%) = \beta_0 + \sum_{i=1}^{n} \beta_i\ .X_i + \sum_{i=1}^{n} \beta_{ii}.X_i^2 + \sum_{i=1}^{n-1} \sum_{j=i+1}^{n} \beta_{ij}.X_i.X_j + \varepsilon \qquad (3)$$

where n, β_0, β_i, X_i and X_j, β_{ii}, β_{ij}, and ε represent the number of variables, a constant term, the coefficients of the linear parameters, the variables, the coefficients of the quadratic parameters, the coefficients of the interaction parameters, and the residual associated with the experiments, respectively. A total of 15 experiments were needed to estimate the removal of MB on 4AZW.

The predicted values for the yield removal of MB were then obtained by applying the quadratic model. The accuracy and fitness of the model were evaluated by an analysis of variance (ANOVA): Various descriptive statistic parameters were used such as the *p*-value, an F-test, degrees of freedom (df), the determination coefficient (R^2), and the adjusted determination coefficient (R^2_{adj}) [30,31]. Moreover, 3D-surface plots also allowed us to describe the effect on the desired response of interaction between two-by-two factors [32].

3. Results and Discussion

3.1. Characterization of Material

The physicochemical properties of the 4AZW sample are presented in Table IV.1. XRF measurement showed that the main chemical components of the 4AZW are SiO_2, Al_2O_3, Na_2O, Fe_2O_3, CaO, and K_2O. The XRD pattern of our sample (Figure IV.1) corresponds well with the crystalline peaks of pure 4A zeolite. The diffraction peaks at 7.18°, 10.17°, 12.46°, 16.11°, 21.66°, 23.99°, 26.10°, 27.11°, 29.94°, 32.54°, and 34.17° are associated with (200), (220), (222), (420), (442), (622), (640), (642), (820), (840), and (664) crystal planes of 4A zeolite, respectively [10,33], indicating that the 4AZW has not undergone a serious loss in its crystalline structure.

Table IV.1. Physicochemical properties of 4AZW.

	Typical parameters	Value
Chemical composition	SiO_2 (%)	55.39 ± 0.88
	Al_2O_3 (%)	27.18 ± 0.64
	Na_2O (%)	4.49 ± 0.52
	K_2O (%)	1.03 ± 0.12
	CaO (%)	3.34 ± 0.41
	P_2O_5(%)	0.79 ± 0.08
	Fe_2O_3 (%)	4.47 ± 0.49
	TiO_2 (%)	0.32 ± 0.04
	MgO (%)	2.99 ± 0.31
	S_{BET} (m^2/g)	35.5 ± 0.3
CEC (meq/100 g)		120 ± 6
pH (1:2 w:v slurry)		11 ± 0.1
pH_{PZC}		10.5 ± 0.1

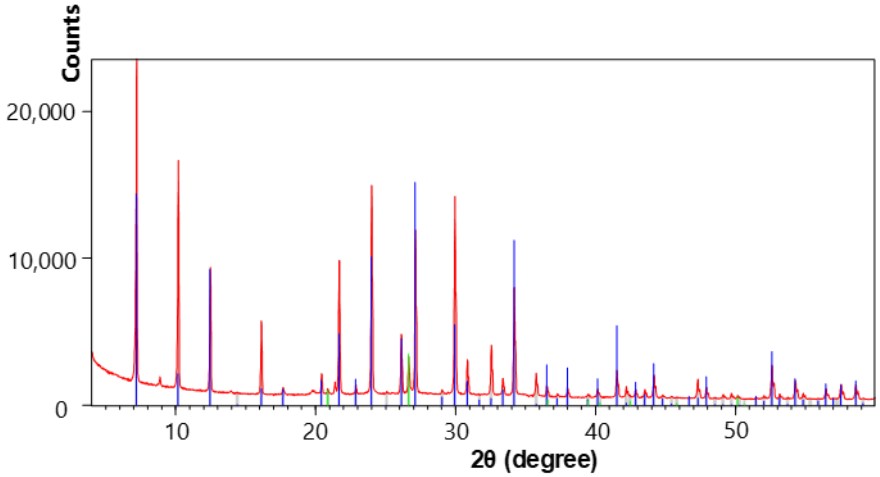

Fig. IV.1. XRD pattern of 4AZW.

As shown in Table IV.1, the cation exchange capacity is 120 meq/100 g. The synthesized material exhibits strong basicity (pH = 11 for the suspension slurry) suggesting the presence of negative charges on the solid surface in an aqueous solution; this is also confirmed by the value of pH_{PZC} = 10.5 (see below). The BET/N_2 specific surface area was 35.5 m^2/g.

From FT-IR spectroscopy (Figure IV.2), the broad band at 3441cm^{-1} and the sharp absorption bond at 1660 cm^{-1} correspond to the stretching and bending vibration bands of H-O-H derived from H_2O present in 4AZW [34]. In addition, there are four distinct absorption

bands at 994, 787, 684, and 464 cm^{-1}, which are assigned to the asymmetric stretching vibrations of bridge bonds T-O-(T) where (T=Si or Al), symmetric stretching vibrations of bridge bonds Si-O-Si, symmetric stretching vibrations of bridge bonds Si-O-Al, and the bending vibrations O-Si-O, respectively [35].

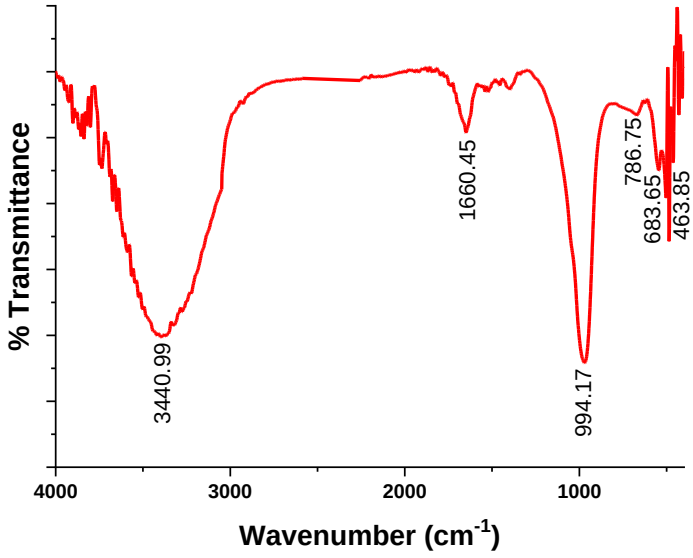

Fig. IV.2. FT-IR spectra of 4AZW.

3.2. Effect of Initial Dye Concentration

Contact time data allow us to select the optimum shaking time to achieve a steady-state of pseudo-equilibrium of the process. The corresponding data for the removal of MB and MG are shown in Figure IV.3, hence the plateau becomes evident.

The q_e values of both MB and MG sharply increased from 10 min to 50 min and balanced beyond 70 min contact time. This can be related to the number of initially vacant surface sites at the beginning. Over time, repulsive forces between the cationic dye molecules adsorbed on the surface of 4AZW and the solution phase make the remaining vacant surface sites more difficult to be occupied; thus, the adsorption slows down and finally levels off. As can be considered obvious, increasing the initial concentration will provide more driving force to overcome the mass transfer resistance between the solid and liquid phases, then the q_e values increase [36].

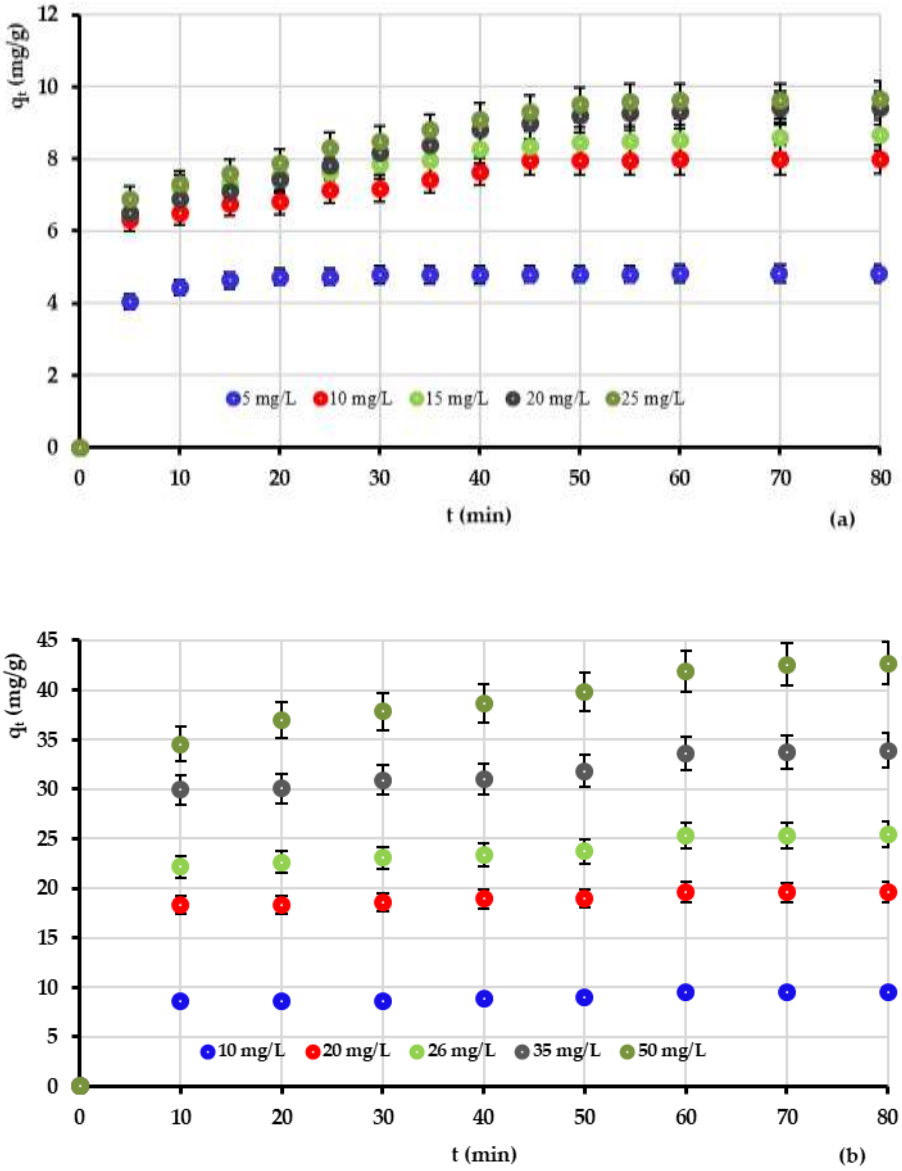

Fig IV.3. Effect of contact time and initial concentration of dyes: (**a**) MB; (**b**) MG on the adsorption capacity of 4AZW (S/L = 1 g/L, T = 25 ± 1°C and unadjusted pH).

3.3. Effect of the Adsorbent Dose

The effect of the mass of adsorbent (0.25 to 3.0 g/L) on the adsorption capacity and the percentage of dye removal showed (Figure IV. 4) that the removal of each dye increased when the adsorbent amount increased, which could be attributed to the greater availability of adsorption sites; after reaching a plateau, one can observe the steady-state of the (pseudo) equilibrium, likely because of the saturation of the available adsorption sites as already reported in several papers [37,38]. For the following investigations, equilibrium was attained with a selected adsorbent dosage of 1 g/L.

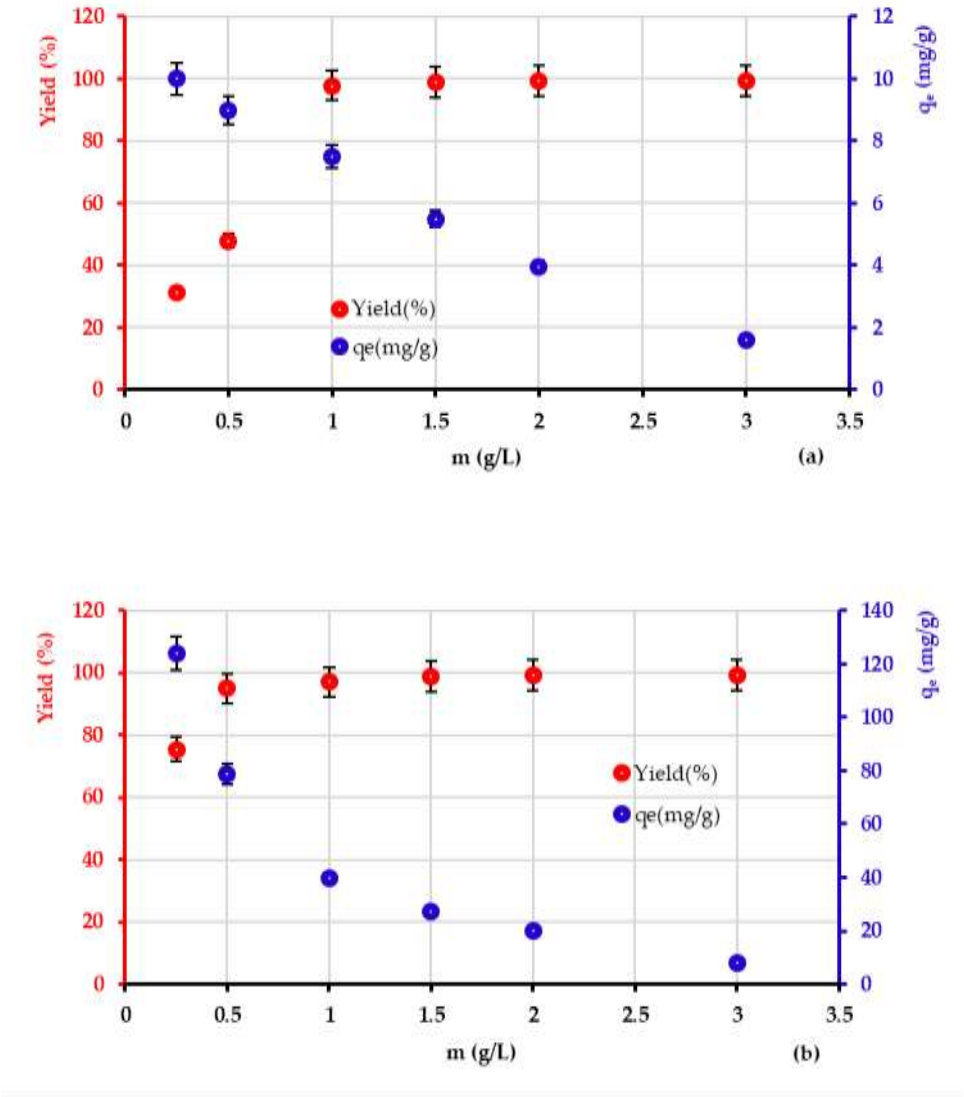

Fig IV.4. Effect of adsorbent dosage on the percentage of removal and amount of dyes adsorbed on 4AZW: (**a**) MB; (**b**) MG (C_0 (MB) = 8 mg/L, C_0 (MG) = 41 mg/L, contact time 70 min, T = 25 ± 1°C and unadjusted pH).

On the other hand, the increase in the adsorbent mass led to a decrease in the amount of dye uptake per gram of adsorbent (q_e). This dropin adsorption capacity is likely due to sites remaining unsaturated during adsorption [39,40] and particle aggregation [41].

3.4. Effect of Ionic Strength

As can be observed from Figure IV.5, the co-existence of sodium cations and dye molecules in the solution decreases the adsorption yield. Furthermore, the increase in the ionic strength is unfavorable to the adsorption efficiency. Because the ionic strength of the solution controls either electrostatic or non-electrostatic interactions between the adsorbate and the

adsorbent surface [42], the electrostatic attraction mechanism for our cationic dyes can be suppressed with the addition of Na^+ ions at a high concentration, due to the competition for the active sites on the adsorbent surface, leading to electrostatic repulsion [43].

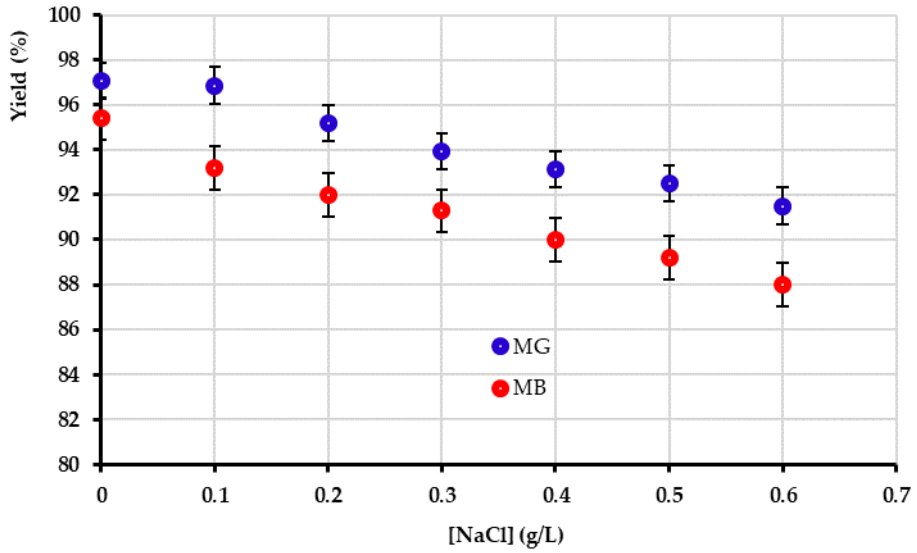

Fig IV.5. Effect of NaCl concentration on the adsorption percentage of MB and MG (C_0 (MB) = 8 mg/L, C_0 (MG) = 41 mg/L, S/L = 1 g/L, contact time 70 min, T = 25 ± 1°C and unadjusted pH).

3.5. Effect of Solution pH

The pH_{PZC} value of 4AZW is 10.5 (Figure IV.6). Then, at pH < pH_{PZC}, the surface of the adsorbent is predominantly positive; while when the solution pH > pH_{PZC}, the adsorbent surface is predominantly negative [44]. The effect of the initial solution's pH (in the range of 3 to 12) on the removal of each dye, at initial concentrations of MB and MG of 11.5 mg/L and 45 mg/L, respectively, at 25°C, is shown in Figure IV.7.

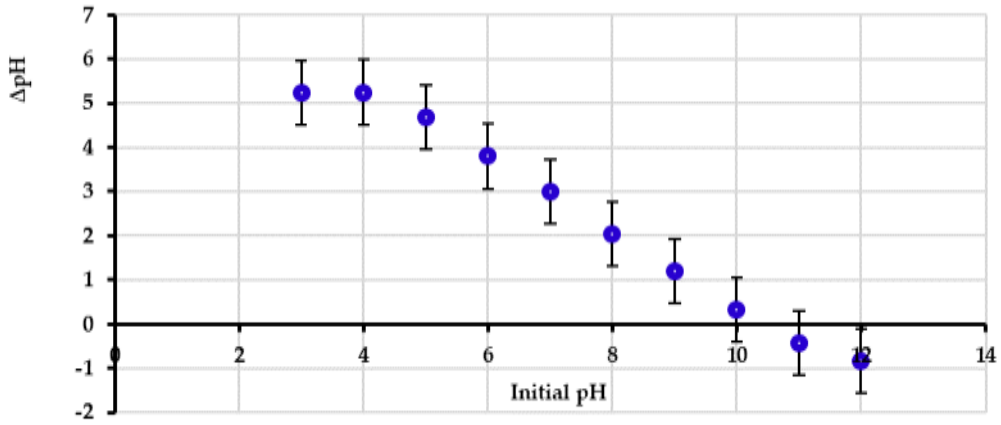

Fig IV.6. The plot of ΔpH vs. initial pH for the determination of 4AZW′s point of zero charge.

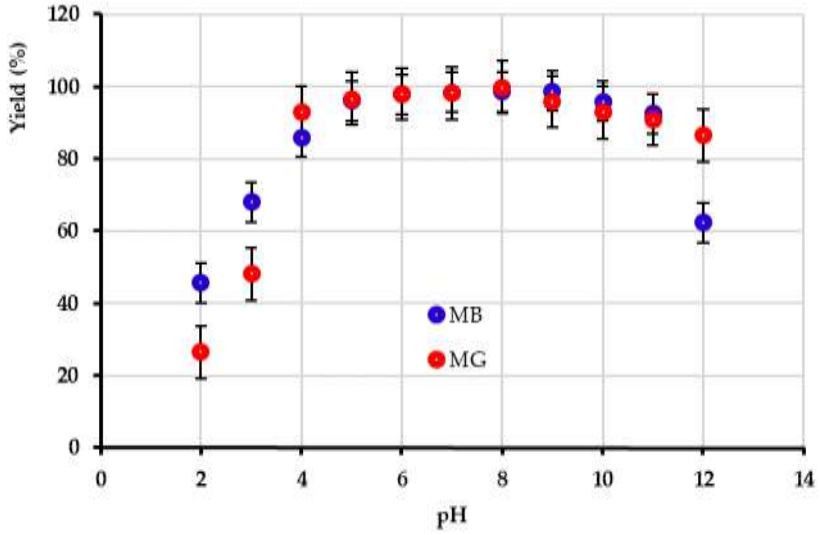

Fig IV.7. Effect of pH on the removal of MB and MG by 4AZWfrom aqueous solution. (C_0 (MB) = 11.5 mg/L, C_0 (MG) = 45 mg/L, S/L = 1 g/L, contact time 70 min, T = 25 ± 1°C).

Generally, for a cationic dye, at a lower pH, the percentage of dye removal will decrease, but it will increase at higher pH values [45]. Although methylene blue has no determinable pKa between pH 0 and 14, it is in the form MB^+ in this aqueous pH range, but several species can be formed according to the redox status of the solution [46]; for malachite green, however, pKa = 6.90 [47]. Then, for MB or MG cations, the protonated form is the predominant species in solutions at pH < pKa, and above this pH value, the dye becomes ever more de-protonated.

The highest adsorption capacities were obtained in the pH range of 5 to 10 for MB with a maximum adsorption efficiency of 99% at pH = 8.5. For MG, a relatively high adsorption

capacity can be kept at pH = 5 to 11 with maximum adsorption of 99.5% at pH = 8 (Figure IV.7). Similar observations have also been reported by other researchers [48–53].

However, a definitive explanation of this point cannot be established on the basis of pH values only, because pH can be influenced, separately or together, by the surface charge of the adsorbent, the degree of ionization of the adsorbate, and the extent of dissociation of functional groups at the adsorbent active sites [44,54]. Lower sorption of dyes obtained at very acidic pH values can be explained through the behavior of the zeolite in acidic and basic mediums, as reported elsewhere [55].

First, zeolite in an acidic medium can easily exchange its M^+ metal cation with protons according to the following reaction:

$$[Z\text{-}OM]_n + H^+_{(aq)} \leftrightarrows [Z\text{-}OH]_n + M^+_{(aq)} \qquad (4)$$

where Z is the Silicon or Aluminum atom at the solid surface and within the zeolite structure. This ion-exchange reaction leads to an increase in the solution pH as observed in Figure IV.7. If the initial H^+ concentration is high, proton adsorption at the neutral surface of the zeolite will take place:

$$[Z\text{-}OH]_n + H^+_{(aq)} \leftrightarrows [ZOH_2^+]_n \qquad (5)$$

The protonation of the zeolite surface (Equation (5)) diminishes the possible dye adsorption due to electrostatic repulsive forces that may occur between the zeolite surface and the cationic dye. On the other hand, in an alkaline medium, hydroxyl ions can de-protonate the surface as follows:

$$[Z\text{-}OH]_n + OH^-_{(aq)} \leftrightarrows [ZO^-]_n + H_2O \qquad (6)$$

Under such conditions, the attraction forces between the negatively charged zeolite surface and the positively charged MB and MG species favor the adsorption. Similar results have been obtained with other inorganic pollutants such as heavy metals in wastewater by using zeolite nano-particles impregnated in polysulfone membranes [14].

3.6. Kinetics Studies

Kinetics models are important before any further investigation intothe mechanism of adsorption; the most popular are [56,57] the Lagergren′s pseudo-first-order and the pseudo-second-order rate equations.

The pseudo-first-order equation is:

$$\frac{dq_t}{dt} = k_1.(q_e - q_t) \quad (7)$$

where q_t (mg/g) is the adsorption capacity at time t (min), k_1 is the rate constant of pseudo-first-order adsorption (min^{-1}), and qe (mg/g) is the equilibrium adsorption capacity. Integrating Equation (7) for boundary conditions (t = 0, q_t = 0 and t = t, q_t = q_t) leads to the nonlinear equation:

$$q_t = q_e.(1 - e^{-k_1.t}) \quad (8)$$

The rate equation for pseudo-second-order kinetics was given as [58]:

$$\frac{dq_t}{dt} = k_2.(q_e - q_t)^2 \quad (9)$$

Integrating Equation (9), using the boundary conditions at t = 0, q_t = 0 and with the amount of dye adsorbed being q_t for any time t, and after rearranging the corresponding rate law, one obtains:

$$q_t = \frac{k_2.q_e^2.t}{1 + k_2.q_e.t} \quad (10)$$

where k_2 (g/mg.min) is the pseudo-second-order rate constant.

The parameters obtained for the pseudo-second-order model are given in Table IV.2. At different dye concentrations, the pseudo-first-order model could not describe the entire range of adsorption time (detailed data not shown) and is limited only to the initial time range, as also described by others [57]. However, the pseudo-second-order data treatment presents higher determination coefficient (R^2) values and lower values for error analysis parameters. Furthermore, the corresponding $q_{e(cal)}$ values are in better agreement with experimental data $q_{e(exp)}$. These results suggested that the pseudo-second-order model can be used to represent our adsorption data kinetics. For each dye, the k_2 value decreases when its concentration increases, and this might be related to higher competition for the adsorption sites when the dye concentration is high [59].

Table IV.2. Parameters for second-order kinetic model for removal of MB and MG dyes by 4AZW at 25°C using nonlinearized model.

Parameters	**MB**				**MG**			
C_0 (mg/L)	5	15	20	25	10	20	35	50
$q_{e(exp)}$ (mg/g)	4.898	8.680	9.501	9.713	9.478	19.564	34.420	42.900
$q_{e(cal)}$ (mg/g)	4.903 ± 0.011	8.688 ± 0.091	9.560 ± 0.140	9.731 ± 0.117	9.503 ± 0.135	19.633 ± 0.153	34.480 ± 0.547	43.480 ± 0.646
k_2 (g/mg.min)	0.198 ± 0.009	0.054 ± 0.007	0.034 ± 0.002	0.030 ± 0.002	0.072 ± 0.022	0.054 ± 0.013	0.015 ± 0.004	0.007 ± 0.001
R^2	0.999	0.989	0.989	0.991	0.991	0.997	0.990	0.992
ARE (%)	0.10	0.09	0.62	0.18	0.26	0.35	0.17	1.35
SD	0.031	0.226	0.246	0.215	0.263	0.307	0.977	0.985

The relative error (ARE) function is a measure of the differences between the experimental amount of adsorbed dye and the value predicted by the model:

$$ARE(\%) = \frac{100}{n}\sum_{i=1}^{n}\frac{\left|q_{e(exp)} - q_{e(cal)}\right|}{q_{e(exp)}} \qquad (11)$$

where n is the number of experiments (here n = 3). The values of ARE (%) for the second-order kinetic model are presented in Table IV.2.

3.7. Adsorption Isotherms

At higher initial dye concentrations, the mass transfer resistance between the solid surface and the solution can be more easily overcome. With an increasing concentration of dye, empty active centers at the adsorbent surface are rapidly filled. Thus, as the initial concentration increased, the adsorption capacity increased [60].

For the optimization of an adsorption process, it is important to establish the most appropriate correlation for the equilibrium curve. Two widely known isotherm models, namely the Langmuir and Freundlich models [56,61], were used in this study to describe the adsorption process of MB and MG onto 4AZW.

The Langmuir model assumes that only one solute species will occupy one active site on the homogeneous surface of the adsorbent, and the corresponding nonlinear equation is:

$$q_e = \frac{K_L . C_e . q_{max}}{1 + K_L . C_e} \quad (12)$$

where C_e is the equilibrium concentration of the adsorbate (mg/L), C_0 is the initial concentration of the adsorbate (mg/L), and qmax (mg/g) and K_L (L/mg) are the maximum adsorption capacity and a constant related to the energy of adsorption, respectively. One can also introduce a separation factor:

$$R_L = \frac{1}{1 + K_L . C_0} \quad (13)$$

This is a useful dimensionless constant: The isotherm is either unfavorable ($R_L > 1$), linear ($R_L = 1$), favorable ($0 < R_L < 1$), or irreversible ($R_L = 0$) [56]. For the adsorption of MB and MG onto 4AZW, all the R_L values are in the range of 0.008 to 0.043 and 0.015 to 0.064, respectively. Then, the adsorption process is favorable.

The Freundlich isotherm is an empirical model assuming a process on heterogeneous adsorption surfaces, and is not restricted to monolayer formation. The corresponding nonlinear equation is:

$$q_e = K_F . C_e^{\frac{1}{n}} \quad (14)$$

where K_F (mg/g)/(mg/L)$^{1/n}$ and n (dimensionless) are constants representing the adsorption capacity and the adsorption intensity, respectively.

The Langmuir and Freundlich models were compared for our experimental results (Figure IV.8). On the basis of R^2 determination coefficients values, the Langmuir model gave high values for both dyes (0.993 and 0.994), while those obtained by the Freundlich model were lower (0.949 and 0.985, see Table IV.3). The Langmuir maximum adsorption capacity (q_{max}) for MB and MG onto 4AZW at 25°C is determined as 9.95 mg/g (0.031 mmol/g) and 45.64 mg/g (0.125 mmol/g), respectively (Table IV.3).

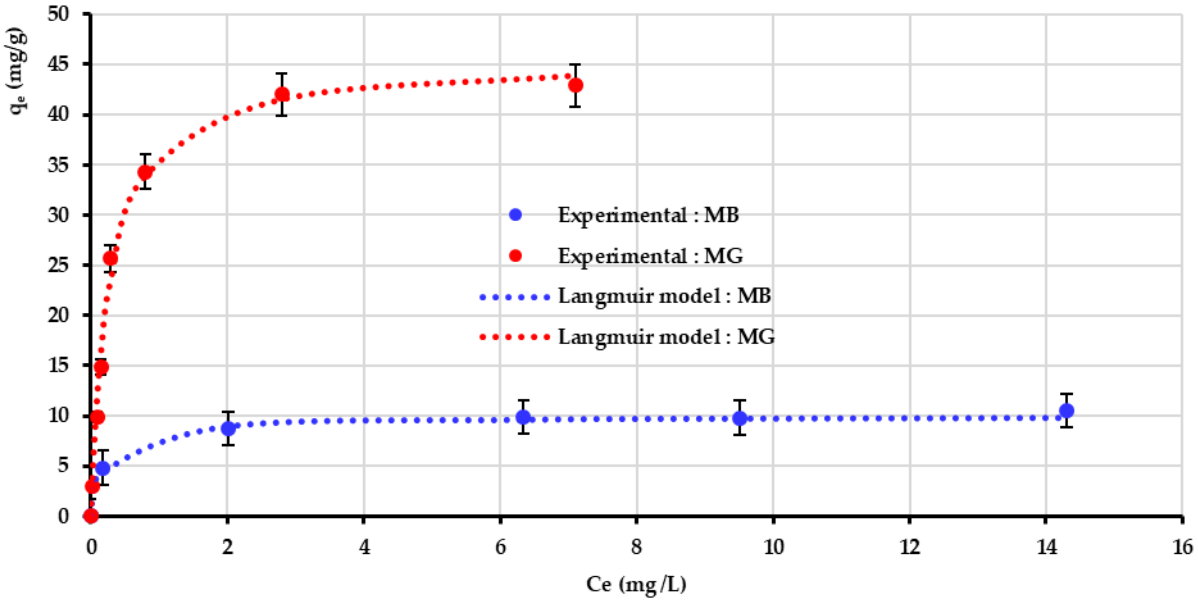

Fig IV.8. The Langmuir adsorption isotherms models for MB and MG adsorption on 4AZW (S/L = 1 g/L, T = 25 ± 1°C and unadjusted pH), as a nonlinear expression.

Table IV.3. Parameters of Langmuir isotherm for removal of MB and MG onto 4AZW at 25°C.

Dye	**Langmuir**				**Freundlich**			
	q_{max} **(mg/g)**	K_L **(L/mg)**	R^2	*SD*	K_F **(mg/g)/(mg/L)$^{1/n}$**	*n*	R^2	*SD*
MB	9.95 ± 0.16	4.45 ± 0.54	0.993	0.241	7.08 ± 0.96	6.29 ± 0.87	0.949	1.026
MG	45.64 ± 1.17	4.34 ± 0.20	0.994	0.315	28.48 ± 0.93	3.67 ± 0.47	0.985	0.594

3.8. Data Analysis by Response Surface Methodology

The optimization of the adsorption of MB on the 4AZW process needs 27 (that is: $(3)^3$) experiences, but it can be reduced to 15 by using a BBD. The experimental design matrix and the predicted values obtained by BBD are compared to experimental data in Table IV.4, and the analysis of variance (ANOVA) allowed us to check the quality of the model (Table IV.5). The relationship between the experimental response (Yield (%)) and the uncoded forms of the three variables is:

$$Yield(\%) = 69.88 - 2.340X_1 + 1406X_2 - 6.50X_3 + 0.0395X_1^2 - 2605X_2^2 + 0.562X_3^2 - 33.64X_1.X_2 - 0.1523X_1.X_3 + 19.7X_2.X_3 \quad (15)$$

Table IV.4. The uncoded Box–Behnken design matrix of experiments for MB removal.

Run	Initial Dye Concentration (X_1) (mg/L)	Amount of Adsorbent (X_2) (g)	pH (X_3)	Yield (%)		
				Observed	Predicted	Residual
1	14	0.0250	4.0	42.46	43.00	-0.54125
2	8	0.0425	4.0	79.79	78.71	1.07375
3	8	0.0600	6.5	93.76	93.69	0.07000
4	8	0.0425	9.0	80.17	80.78	-0.61125
5	20	0.0425	4.0	40.05	39.44	0.61125
6	20	0.0250	6.5	20.34	20.41	-0.07000
7	14	0.0600	4.0	69.57	70.71	-1.14375
8	14	0.0425	6.5	53.15	52.89	0.25667
9	14	0.0250	9.0	39.92	38.77	1.14375
10	20	0.0425	9.0	31.29	32.36	-1.07375
11	14	0.0425	6.5	52.02	52.89	-0.87333
12	14	0.0425	6.5	53.51	52.89	0.61667
13	20	0.0600	6.5	43.31	42.77	0.53250
14	14	0.0600	9.0	70.47	69.93	0.54125
15	8	0.0250	6.5	56.66	57.19	-0.53250

Table IV.5. ANOVA for the fit of the experimental results to response surface model.

Factor	**DF**	**Sum of Squares**	**Mean Square**	***F*-Value**	***p*-Value**
Model	9	5719.41	635.49	395.15	< 0.0001
X_1- Initial concentration	1	3845.21	3845.21	2390.96	< 0.0001
X_2-m	1	1732.54	1732.54	1077.30	< 0.0001
X_3-pH	1	12.55	12.55	7.80	0.038
X_1^2	1	7.47	7.47	4.64	0.084
X_2^2	1	2.35	2.35	1.46	0.281
X_3^2	1	45.48	45.48	28.28	0.003
X_1X_2	1	49.91	49.91	31.04	0.003
X_1X_3	1	20.88	20.88	12.99	0.015
X_2X_3	1	2.96	2.96	1.84	0.233
Residual	5	8.04	1.61		
Lack-of-fit	3	6.83	2.28	3.77	0.217
Pure Error	2	1.21	0.60		

Standard variation error S = 1.268; R^2 = 99.86%; $R^2_{adjusted}$ = 99.61%; $R^2_{predicted}$ = 98.04%.

The model Equation (15) indicates that the initial MB concentration (X_1) had a significant effect ($p < 0.001$, F = 2390) on the yield, followed by the amount of adsorbent m (X_2) and the solution pH (X_3) with a low F = 7.8. The positive coefficients of X_2, ($X_2.X_3$) and quadratic terms (X_1^2, X_3^2) indicated a direct effect on the removal yield of MB. In contrast, the negative terms X_1, X_3, ($X_1.X_2$), ($X_1.X_3$) and the quadratic term (X_2^2) had an inverse effect on MB adsorption. In addition, ANOVA results (Table IV.5) showed that this regression model was very significant with $p < 0.0001$ and F = 395.15. Moreover, regression analysis data indicated that quadratic terms X_1^2, X_2^2, and the interactive term $X_2.X_3$ are not significant at all ($p > 0.05$).

From Table IV.4, the agreement between the yield predicted by Equation (15) and the corresponding experimental data is very strong: The values of the determination coefficient R^2 = 0.9986 and of its adjusted R^2_{adj}= 0.9961 indicate a good correlation between the observed and predicted values of MB removal efficiency. Finally, one can conclude that this experimental design is valid, because the error value is lesser than 5%.

Figure IV.9 illustrates the 3-D response surface plots of the removal efficiency of MB as a function of two independent variables: (a) The initial concentration C_0 and adsorbent dose m, (b) the initial concentration C_0 and pH, and (c) the adsorbent dose m and pH.

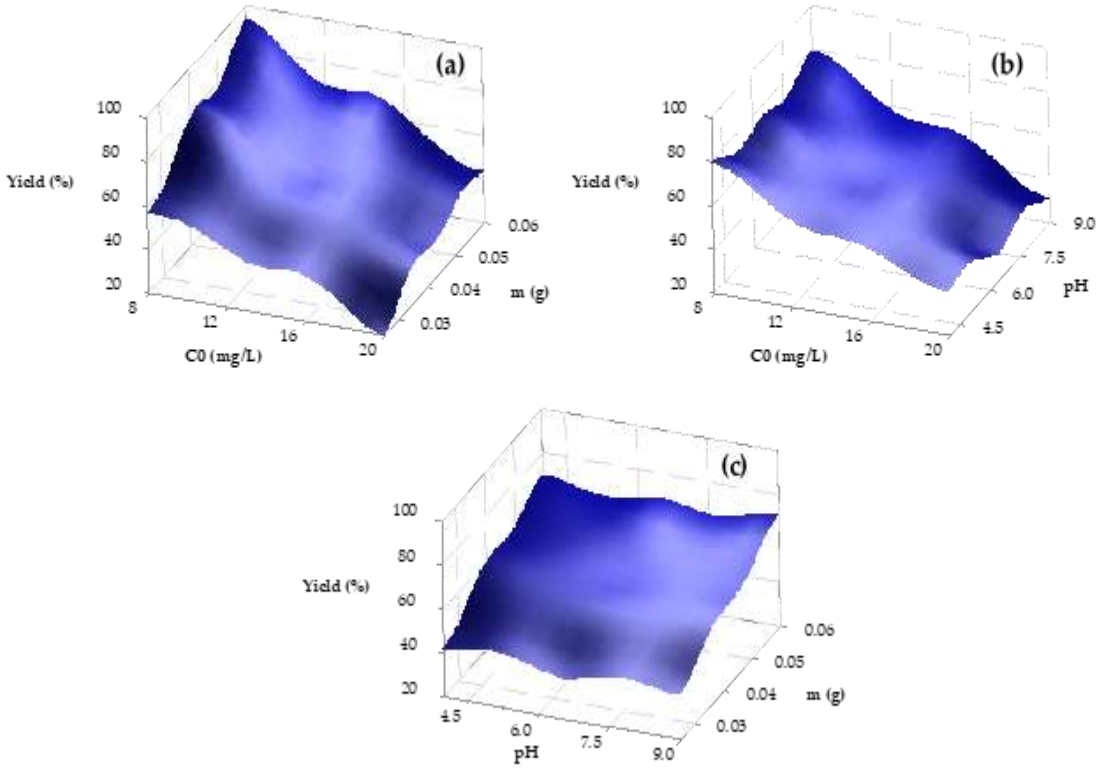

Fig IV.9. 3-D response surface plots for MB removal efficiency (%) onto 4AZW: (**a**) Effect of initial concentration/adsorbent dose; (**b**) effect of initial concentration/pH; (**c**) effect of adsorbent dose/pH.

On the other hand, the optimum values of the variables X_1, X_2, and X_3 were obtained by solving the model Equation (15) with Minitab® 17, to establish the values of variables maximizing the removal yield. Figure IV.10 shows the optimization diagram obtained with the maximum desirability function (i.e., D = 1) for MB yield removal: In separate columns, the response is related to each of the three factors: Red vertical lines indicate the current factor settings, while the horizontal dotted lines show the response for the selected factor levels. In our case, the simulation was adjusted to maximize the adsorption percentage. The statistical sweet spot was determined for a maximal MB removal yield of 99.09% and a desirability of d = 1.0, leading to: C_0 = 8 mg/L, m = 0.06 g, and pH = 9.

Fig IV.10. Diagrammatic optimization of MB removal parameters.

3.9. Thermodynamics Studies

To obtain complementary information on the feasibility of the process, standard thermodynamic parameters were calculated for the adsorption of either MB or MG on 4AZW at temperatures varying from 25 to 50°C: The Gibbs free energy change (ΔG°), enthalpy change (ΔH°), and entropy change (ΔS°).

The Gibbs free energy of adsorption ΔG° is derived from:

$$\Delta G^0 = -R.T.ln(K_L^0) \qquad (16)$$

where R = 8.314 J/mol.K is the universal gas constant, T is the absolute temperature (K), and $K_L°$ is the (dimensionless) ′thermodynamic′ Langmuir constant for the adsorption process. This value is calculated from K_L (L/mg) in the Langmuir model (Equation (12)), after changing all concentrations to molar form and considering the standard state C° = 1 mol/L [61-63]:

$$K_L^0 = K_L(L/mg)\ .1000\ (mg/g)\ .M\ (g/mol)\ .\ C^0\ (mol/L) \qquad (1)$$

where M = 319.85 g/mol or M = 364.91 g/mol are the molar mass of MB or MG, respectively, and the factor 1000 converts g to mg.

The enthalpy (ΔH°) and entropy (ΔS°) parameters were estimated from the classical thermodynamic relationships:

$$K_L^0 = exp\left(\frac{\Delta S^0}{R} - \frac{\Delta H^0}{R.T}\right) \qquad (28)$$

$$\Delta G^0 = \Delta H^0 - T.\Delta S^0 \qquad (39)$$

The non-linear plots (not shown) of the van′t Hoff Equation (18) allowed us to calculate ΔH° (kJ/mol) and ΔS° (J/mol.K). The values of ΔG° (kJ/mol) were again calculated from these values of ΔH° and ΔS° (see Table IV.6).

Table IV.6. Thermodynamic parameters for adsorption of MG and MB onto 4AZW.

Dye	*T* (K)	*SD*	K_L (L/mg)	K_L° (×10^6) (Dimensionless)	Ln K_L°	Δ*G*° (kJ/mol)	Δ*H*° (kJ/mol)	Δ*S*° (J/mol.K)
MB	298	0.241	4.45 ± 0.54	1.42 ± 0.20	14.16 ± 0.14	-35.14 ± 0.37	18.68 ± 1.37	180.64 ± 4.09
	303	0.287	5.24 ± 0.68	1.67 ± 0.25	14.33 ± 0.15	-36.04 ± 0.40		
	313	0.338	6.71 ± 0.75	2.14 ± 0.28	14.57 ± 0.13	-37.85 ± 0.37		
	323	0.359	7.96 ± 0.70	2.54 ± 0.27	14.75 ± 0.11	-39.65 ± 0.31		
MG	298	0.315	4.34 ± 0.20	1.58 ± 0.10	14.27 ± 0.07	-35.41 ± 0.19	25.53 ± 1.12	204.53 ± 3.28
	303	0.214	5.47 ± 0.37	1.99 ± 0.17	14.50 ± 0.09	-36.43 ± 0.24		
	313	0.384	7.20 ± 0.28	2.62 ± 0.15	14.78 ± 0.06	-38.48 ± 0.18		
	323	0.299	9.84 ± 0.44	3.59 ± 0.23	15.09 ± 0.06	-40.52 ± 0.20		

The negative values of ΔG° slightly increase as temperature increases from 298 to 323 K; while they are negative at different temperatures, the adsorption process of MB and MG on 4AZW is favored and spontaneous. These values of ΔG° increased in the order 4AZW-MB < 4AZW-MG indicating that the adsorption was more spontaneous for the 4AZW-MG system than for the 4AZW-MB one [62].

Furthermore, both ΔH° values are positive, the characteristic of an endothermic process; for each dye, ΔH° < 40kJ/mol, suggesting that their adsorption is a physically driven process [64]. With positive ΔS° for both dyes, there is an increase in the randomness of the system due to the desorption of water molecules from the adsorbent surface; similar results have also been reported by other research groups [51,65].

4. Conclusions

This study investigated the potential of 4AZW to remove two basic cationic dyes, MB and MG, from aqueous solutions under batch experimental conditions. It was observed that adsorption depends on the pH, adsorbent dose, contact time, and initial dye concentration. It is interesting to note that the initial solution pH is one of the key parameters in the MB and MG

adsorption performance; the presence of salt in the solution decreased the adsorption by competitive inhibition.

According to kinetic data, the adsorption process could be defined by a pseudo-second-order kinetic model. The Langmuir model aptly represented both systems (4AZW-MB and 4AZW-MG) giving maximum adsorption capacity (q_{max}) values of 9.95 mg/g and 45.64 mg/g, respectively, at 25°C. A thermodynamic study revealed that the adsorption was spontaneous, endothermic, and physical in nature.

The analysis of our results performed by the Box–Behnken Design (BBD) for the adsorption of MB on 4AZW allowed us to define the corresponding optimum conditions: More than 99.09 % MB removal with pH = 9; 4AZW load = 0.06 g in 50 mL; initial MB concentration = 8 mg/L, and 70 min removal time at 25°C.

Thus, the large amounts of 4A zeolite generated as solid waste by the natural gas dehydration units after several treatment cycles of the gas can be efficiently used as an adsorbent for these cationic dyes, without any specific treatment. Although it is well known that zeolite is not a renewable natural resource, its use as an adsorbent has both practical and cost-effective advantages.

Author Contributions: Conceptualization, A.I., S.C. and L.M.; methodology, A.I., S.C., A.A. (Aymen Assadi) and L.M.; software, L.B. and A.T.; validation, J.-C.B., L.B., A.T., A.A. (Abdeltif Amrane), A.E.J. and L.M.; formal analysis, J.-C.B., L.B. and A.T.; investigation, A.I., A.A. (Aymen Assadi), L.B. and L.M.; resources, A.A. (Aymen Assadi) and L.M.; data curation, A.I., S.C.; writing—original draft preparation, A.I., S.C.; writing—review and editing, A.I., A.A. (Aymen Assadi), A.B., A.A.,(Abdeltif Amrane) and L.M.; visualization, A.I., S.C., L.B. and J.-C.B.; supervision, J.-C.B., L.M. and A.A. (Aymen Assadi); project administration, L.M., A.A. (Aymen Assadi), A.E.J.; funding acquisition, A.E.J. All authors have read and agreed to the published version of the manuscript.

Funding: The authors extend their appreciation to the King Khalid University for funding this work through the Large Groups Project under grant number (R.G.P. 2/37/43).

Institutional Review Board Statement: Not applicable.

Informed Consent Statement: Not applicable.

Data Availability Statement: Not applicable.

Acknowledgments: This work was supported by King Khalid University, Abha, Saudi Arabia. The authors extend their appreciation to the Deanship of Scientific Research at King Khalid University for funding this work. The authors thank the University of Bouira (Algeria) for scientific collaboration.

Conflicts of Interest: The authors declare no conflict of interest.

References

1. Abada, Z.; Bouharkat, M. Study of management strategy of energy resources in Algeria. *Energy Rep*. **2018**, *4*, 1-7. https://doi.org/10.1016/j.egyr.2017.09.004.
2. Faramawy, S.; Zaki, T.; Sakr, A.A.E. Natural gas origin, composition, and processing: A review. *J. Nat. Gas Sci. Eng.* **2016**, *34*, 34-54. http://dx.doi.org/10.1016/j.jngse.2016.06.030.
3. Lenhard, L.G.; Andersen, S.M.; Coimbra-Araújo, C.H. Energy-environmental implications of shale gas exploration in Paraná hydrological basin, Brazil. *Renew. Sust. Energy Rev.* **2018**, *90*, 56–69. https://doi.org/10.1016/j.rser.2018.03.042.
4. Santos, K.M.C.; Menezes, T.R.; Oliveira, M.R.; Silva, T.S.L.; Santos, K.S.; Barros, V.A.; Melo, D.C.; Ramos, A.L.; Santana, C.C.; Franceschi, E.; et al. Natural gas dehydration by adsorption using MOFs and silicas: A review. *Sep. Purif. Technol.* **2021**, *276*, 119409. https://doi.org/10.1016/j.seppur.2021.119409.
5. Berg, F.; Pasel, C.; Eckardt, T.; Bathen, D. Temperature Swing Adsorption in natural gas processing: A concise overview. *ChemBioEng Rev.* **2019**, *6*, 59-71. https://doi.org/10.1002/cben.201900005.
6. Bahadori, A.; Vuthaluru, H.B. Simple methodology for sizing of absorbers for TEG (triethylene glycol) gas dehydration systems. *Energy* **2009**, *34*, 1910-1916. https://doi.org/10.1016/j.energy.2009.07.047.
7. Santos, M.G.R.S.; Correia, L.M.S.; de Medeiros, J.L.; de Queiroz, O.; Araújo, F. Natural gas dehydration by molecular sieve in offshore plants: Impact of increasing carbon dioxide content. *Energy Convers. Manag.* **2017**, *149*, 760-773. http://dx.doi.org/10.1016/j.enconman.2017.03.005.
8. Cundy, C.S.; Cox, P.A. The hydrothermal synthesis of zeolites: History and development from the earliest days to the present time. *Chem. Rev.* **2003**, *103*, 663-702. https://doi.org/10.1021/cr020060i.

9. Englert, A.H.; Rubio, J. Characterization and environmental application of a Chilean natural zeolite. *Int. J. Min. Process.* **2005**, *75*, 21-29. https://doi.org/10.1016/j.minpro.2004.01.003.
10. Liu, H.; Zeng, S.; He, M.; He, P.; Jia, L.; Dong, F.; Yang, D.; Gao, J.; Wang, S.; Zhang, T.; et al. Remarkably enhanced activity of 4A zeolite modified Pt/reduced graphene oxide electrocatalyst towards methanol electrooxidation in alkaline medium. *Ionics* **2019**, *25*, 5131-5140. https://doi.org/10.1007/s11581-019-03098-y.
11. Khulbe, K.C.; Matsuura,T.; Feng, C.Y.; Ismail, A.F. Recent development on the effect of water/moisture on the performance of zeolite membrane and MMMs containing zeolite for gas separation; review. *RSC Adv.* **2016**, *6*, 42943-42961. https://doi.org/10.1039/c6ra03007f.
12. Zito, P.F.; Brunetti, A.; Caravella, A.; Drioli, E.; Barbieri, G. Water vapor permeation and its influence on gases through a zeolite-4A membrane. *J. Membr. Sci.* **2019**, *574*, 154–163. https://doi.org/10.1016/j.memsci.2018.12.065.
13. Fertu, D.I.T.; Gavrilescu, M. Application of natural zeolites as sorbents in the clean-up of aqueous streams. *Environ. Eng. Manag. J.* **2012**, *11*, 867-878. http://dx.doi.org/10.30638/eemj.2012.110.
14. Yurekli, Y. Removal of heavy metals in wastewater by using zeolite nano-particles impregnated polysulfone membranes. *J. Hazard. Mater.* **2016**, *309*, 53-64. https://doi.org/10.1016/j.jhazmat.2016.01.064.
15. Ciosek, A.L.; Luk, G.K. Kinetic modelling of the removal of multiple heavy metallic ions from mine waste by natural zeolite sorption. *Water* **2017**, *9*, 482. https://doi.org/10.3390/w9070482.
16. Wang, S.; Peng, Y. Natural zeolites as effective adsorbents in water and wastewater treatment. *Chem. Eng. J.* **2010**, *156*, 11-24. https://doi.org/10.1016/j.cej.2009.10.029.
17. Amin, M.T.; Alazba, A.A.; Manzoor, U. A review of removal of pollutants from water/wastewater using different types of nanomaterials. *Adv. Mater. Sci. Eng.* **2014**, *2014*, 825910. https://doi.org/10.1155/2014/825910.
18. Mateen, F.; Javed, I.; Rafique, U.; Tabassum, N.; Sarfraz, M.; Safi, S.Z.; Yusoff, I.; Ashraf, M.A. New method for the adsorption of organic pollutants using natural zeolite incinerator ash (ZIA) and its application as an environmentally friendly and cost-effective adsorbent. *Desalination Water Treat.* **2016**, *57*, 6230-6238. https://doi.org/10.1080/19443994.2015.1005146.

19. Vítězová, M.; Jančiková, S.; Dordević, D.; Vítěz, T.; Elbl, J.; Hanišáková, N.; Jampílek, J.; Kushkevych, I. The possibility of using spent coffee grounds to improve wastewater treatment due to respiration activity of microorganisms. *Appl. Sci.* **2019**, *9*, 3155. https://doi.org/10.3390/app9153155.
20. Vyavahare, G.D.; Gurav, R.G.; Jadhav, P.P.; Patil, R.R.; Aware, C.B.; Jadhav, J.P. Response surface methodology optimization for sorption of malachite green dye on sugarcane bagasse biochar and evaluating the residual dye for phyto and cytogenotoxicity. *Chemosphere* **2018**, *194*, 306-315. https://doi.org/10.1016/j.chemosphere.2017.11.180.
21. Ahamad, T.; Naushad, M.; Eldesoky, G.E.; Al-Saeedi, S.I.; Nafady, A.; Al-Kadhi, N.S.; Al-Muhtaseb, A.H.; Khan, A.A.; Khan, A. Effective and fast adsorptive removal of toxic cationic dye (MB) from aqueous medium using amino-functionalized magnetic multiwall carbon nanotubes. *J. Mol. Liq.* **2019**, *282*, 154-161. https://doi.org/10.1016/j.molliq.2019.02.128.
22. Tanyol, M. Rapid malachite green removal from aqueous solution by natural zeolite: Process optimization by response surface methodology. *Desalination Water Treat.* **2017**, *65*, 294-303. https://doi.org/10.5004/dwt.2017.20185.
23. Ani, J.U.; Okoro, U.C.; Aneke, L.E.; Onukwuli, O.D.; Obi, I.O.; Akpomie, K.G.; Ofomatah, A.C. Application of response surface methodology for optimization of dissolved solids adsorption by activated coal. *Appl. Water Sci.* **2019**, *9*, 60. https://doi.org/10.1007/s13201-019-0943-7.
24. Mirzabe, G.H.; Keshtkar, A.R. Application of response surface methodology for thorium adsorption on PVA/Fe_3O_4/SiO_2/APTES nanohybrid adsorbent. *J. Ind. Eng. Chem.* **2015**, *26*, 277-285. https://doi.org/10.1016/j.jiec.2014.11.040.
25. Varala, S.; Ravisankar, V.; Al-Ali, M.; Pownceby, M.I.; Parthasarathy, R.; Bhargava, S.K. Process optimization using response surface methodology for the removal of thorium from aqueous solutions using rice-husk. *Chemosphere* **2019**, *237*, 124488. https://doi.org/10.1016/j.chemosphere.2019.124488.
26. Pansu, M.; Gautheyrou, J. *Handbook of Soil Analysis: Mineralogical, Organicand Inorganic Methods*; Springer: Berlin/Heidelberg, Germany; New York, NY, USA, 2006.
27. Primo Yúfera, E.; Carrasco Dorrien, J. *Química Agrícola*, 1st ed.; Alhambra: Madrid, Spain, 1973; Volume 1.

28. Kosmulski, M. *Surface Charging and Points of Zero Charge*; CRC Press: Boca Raton, FL, USA, 2009; ISBN 9781420051889.
29. Ferreira, S.L.C.; Bruns, R.E.; Ferreira, H.S.; Matos, G.D.; David, J.M.; Brandao, G.C.; da Silva, E.G.P.; Portugal, L.A.; Dos Reis, P.S.; Souza, A.S.; et al. Box-Behnken design: An alternative for the optimization of analytical methods. *Anal. Chim. Acta* **2007**, *597*,179-186. https://doi.org/10.1016/j.aca.2007.07.011.
30. Salahshoor, Z.; Shahbazi, A. Modeling and optimization of cationic dye adsorption onto modified SBA-15 by application of response surface methodology. *Desalination Water Treat.* **2016**, *57*, 13615-13631. http://doi.org/10.1080/19443994.2015.1060537.
31. Chowdhury, S.; Saha, P.D. Scale-up of a dye adsorption process using chemically modified rice husk: Optimization using response surface methodology. *Desalination Water Treat.* **2012**, *37*, 331-336. https://doi.org/10.1080/19443994.2012.661289.
32. Mora, B.P.; Bellú, S.; Mangiameli, M.F.; Frascaroli, M.I.; González, J.C. Response surface methodology and optimization of arsenic continuous sorption process from contaminated water using chitosan. *J. Water Process. Eng.* **2019**, *32*, 100913. https://doi.org/10.1016/j.jwpe.2019.100913.
33. Treacy, M.M.J.; Higgins, J.B. *Collection of Simulated XRD Powder Patterns for Zeolites*, 4th ed.; Elsevier: Amsterdam, The Netherlands, 2001; ISBN 978-0-444-53067-7.
34. Ma, B.; Lothenbach, B. Synthesis, characterization, and thermodynamic study of selected Na-based zeolites. *Cem. Concr. Res.* **2020**, *135*, 106111. https://doi.org/10.1016/j.cemconres.2020.106111.
35. Mozgawa, W.; Król, M.; Barczyk, K. FT-IR studies of zeolites from different structural groups. *Chemik* **2011**, *65*, 667-674.
36. Feng, Y.; Dionysiou, D.D.; Wu, Y.; Zhou, H.; Xue, L.; He, S.; Yang, L. Adsorption of dyestuff from aqueous solutions through oxalic acid-modified swede rape straw: Adsorption process and disposal methodology of depleted bioadsorbents. *Bioresour. Technol.* **2013**, *138*, 191-197. https://doi.org/10.1016/j.biortech.2013.03.146.
37. Dallel, R.; Kesraoui, A.; Seffen, M. Biosorption of cationic dye onto "Phragmites australis" fibers: Characterization and mechanism. *J. Environ. Chem. Eng.* **2018**, *6*, 7247-7256. https://doi.org/10.1016/j.jece.2018.10.024.
38. Parlayici, Ş. Alginate-coated perlite beads for the efficient removal of methylene blue, malachite green, and methyl violet from aqueous solutions: Kinetic, thermodynamic, and equilibrium studies. *J. Anal. Sci. Technol.* **2019**, *10*, 4.

https://doi.org/10.1186/s40543-019-0165-5.

39. Kazemi, S.Y.; Biparva, P.; Ashtiani, E. Cerastodermalamarcki shell as a natural, low cost and new adsorbent to removal of dye pollutant from aqueous solutions: Equilibrium and kinetic studies. *Ecol. Eng.* **2016**, *88*, 82-89. https://doi.org/10.1016/j.ecoleng.2015.12.020.
40. Alwared, A.I.; Jaeel, A.J.; Ismail, Z.Z. New application of eco-friendly biosorbent giant reed for removal of reactive dyes from water followed by sustainable path for recycling the dyes-loaded sludge in concrete mixes. *J. Mater. Cycles Waste Manag.* **2020**, *22*, 1036-1046. https://doi.org/10.1007/s10163-020-00998-4.
41. Fungaro, D.A.; Yamaura, M.; Carvalho, T.E.M.; Graciano, J.E.A. Zeolite from fly ash-iron oxide magnetic nanocomposite: Synthesis and application as an adsorbent for removal of contaminants from aqueous solution. In *Zeolites: Synthesis, Chemistry and Applications*; Andreyev, M.K., Zubkov, O.L., Eds.; Nova Science Publishers, Inc.: New York, NY, USA, 2012; pp. 1–34, ISBN 978-1-61942-861-4.
42. Zhang, Y.; Zhu, C.; Liu, F.; Yuan, Y.; Wu, H.; Li, A. Effects of ionic strength on removal of toxic pollutants from aqueous media with multifarious adsorbents: A review. *Sci. Total Environ.* **2019**, *646*, 265-279. https://doi.org/10.1016/j.scitotenv.2018.07.279.
43. Hu, Y.; Guo, T.; Ye, X.; Li, Q.; Guo, M.; Liu, H.; Wu, Z. Dye adsorption by resins: Effect of ionic strength on hydrophobic and electrostatic interactions. *Chem. Eng. J.* **2013**, *228*, 392-397. https://doi.org/10.1016/j.cej.2013.04.116.
44. Stumm, W.; Kummert, R.; Sigg, L. A ligand exchange model for the adsorption of inorganic and organic ligands at hydrous oxide interfaces. *Croat. Chem. Acta* **1980**, *53*, 291-312.
45. Boukhemkhem, A.; Rida, K. Improvement adsorption capacity of methylene blue onto modified Tamazert kaolin.*Adsorpt. Sci. Technol.* **2017**, *35*, 753-773. https://doi.org/10.1177/0263617416684835.
46. Kishore, K.; Guha, S.N.; Mahadevan, J.; Moorthy, P.N.; Mittal, J.P. Redox reactions of methylene blue: A pulse radiolysis study. *Int. J. Radiat. Appl. Instr. Part C Radiat. Phys. Chem.* **1989**, *34*, 721-727. https://doi.org/10.1016/1359-0197(89)90084-2.
47. Srivastava, S.; Sinha, R.; Roy, D. Toxicological effects of malachite green. *Aquat.Toxicol.* **2004**, *66*, 319-329. https://doi.org/10.1016/j.aquatox.2003.09.008.
48. Gupta, V.K.; Mittal, A.; Krishnan, L.; Gajbe, V. Adsorption kinetics and column operations for the removal and recovery of malachite green from wastewater using bottom ash. *Sep. Purif. Technol.* **2004**, *40*, 87-96.

https://doi.org/10.1016/j.seppur.2004.01.008.

49. Baran, E.; Acemioğlu, B. Competitive removal of malachite green and rhodamine B using clinoptilolite in a two-dye system. *Clays Clay Miner.* **2016**, *64*, 299-313. https://doi.org/10.1346/CCMN.2016.0640308.
50. Han, R.; Wang, Y.; Zhao, X.; Wang, Y.; Xie, F.; Cheng, J.; Tang, M. Adsorption of methylene blue by phoenix tree leaf powder in a fixed-bed column: Experiments and prediction of breakthrough curves. *Desalination* **2009**, *245*, 284-297. https://doi.org/10.1016/j.desal.2008.07.013.
51. Rida, K.; Bouraoui, S.; Hadnine, S. Adsorption of methylene blue from aqueous solution by kaolin and zeolite. *Appl. Clay Sci.* **2013**, *83–84*, 99-105. https://doi.org/10.1016/j.clay.2013.08.015.
52. Tamez Uddin, M.D.; Akhtarul Islam, M.D.; Mahmud, S.; Rukanuzzaman, M.D. Adsorptive removal of methylene blue by tea waste. *J Hazard Mater*. **2009**, *164*, 53-60. https://doi.org/10.1016/j.jhazmat.2008.07.131.
53. Mouni, L.; Belkhiri, L.; Bollinger, J.C.; Bouzaza, A.; Assadi, A.; Tirri, A.; Dahmoune, F.; Madani, K.; Remini, H. Removal of Methylene Blue from aqueous solutions by adsorption on Kaolin: Kinetic and equilibrium studies. *Appl. Clay Sci.* **2018**, *153*, 38-45. https://doi.org/10.1016/j.clay.2017.11.034.
54. Nandi, B.K.; Goswami, A.; Purkait, M.K. Removal of cationic dyes from aqueous solutions by kaolin: Kinetic and equilibrium studies. *Appl. Clay Sci.* **2009**, *42*, 583-590. https://doi.org/10.1016/j.clay.2008.03.015.
55. Polatoglu, I.; Cakicioglu-Ozkan, F. Aqueous interactions of zeolitic material in acidic and basic solutions. *Microporous Mesoporous Mater.* **2010**, *132*, 219-225. https://doi.org/10.1016/j.micromeso.2010.03.001.
56. Tran, H.N.; You, S.J.; Hosseini-Bandegharaei, A.; Chao, H.P. Mistakes and inconsistencies regarding adsorption of contaminants from aqueous solutions: A critical review. *Water Res.* **2017**, *120*, 88-116. https://doi.org/10.1016/j.watres.2017.04.014.
57. Lima, E.C.; Sher, F.; Guleria, A.; Saeb, M.R.; Anastopoulos, I.; Tran, H.N.; Hosseini-Bandegharaei, A. Is one performing the treatment data of adsorption kinetics correctly? *J Environ Chem Eng*. **2021**, *9*, 104813. https://doi.org/10.1016/j.jece.2020.104813.
58. Ho, Y.S.; McKay, G. Pseudo-second order model for sorption processes. *Process.Biochem.* **1999**, *34*, 451-465. https://doi.org/10.1016/S0032-9592(98)00112-5.

59. Chen, H.; Zhao, J.; Dai, G. Silkworm exuviae-A new non-conventional and low-cost adsorbent for removal of methylene blue from aqueous solutions. *J. Hazard. Mater*. **2011**, *186*, 1320–1327. https://doi.org/10.1016/j.jhazmat.2010.12.006.
60. Gobi, K.; Mashitah, M.D.; Vadivelu, V.M. Adsorptive removal of Methylene Blue using novel adsorbent from palm oil mill effluent waste activated sludge: Equilibrium, thermodynamics and kinetic studies. *Chem. Eng. J.* **2011**, *171*, 1246-1252. https://doi.org/10.1016/j.cej.2011.05.036.
61. Tran, H.N.; Lima, E.C.; Juang, R.S.; Bollinger, J.C.; Chao, H.P. Thermodynamic parameters of liquid–phase adsorption process calculated from different equilibrium constants related to adsorption isotherms: A comparison study. *J Environ Chem Eng*. **2021**, *9*, 106674. https://doi.org/10.1016/j.jece.2021.106674.
62. Salvestrini, S.; Leone, V.; Iovino, P.; Canzano, S.; Capasso, S. Considerations about the correct evaluation of sorption thermodynamic parameters from equilibrium isotherms. *J Chem Thermodyn*. **2014**, *68*, 310-316. https://doi.org/10.1016/j.jct.2013.09.013.
63. Zhou, X.; Zhou, X. The unit problem in the thermodynamic calculation of adsorption using the langmuir equation. *Chem Eng Commun*. **2014**, *201*, 1459-1467. https://doi.org/10.1080/00986445.2013.818541.
64. Raval, N.P.; Shah, P.U.; Shah, N.K. Malachite green "a cationic dye" and its removal from aqueous solution by adsorption. *Appl Water Sci*. **2017**, *7*, 3407-3445. https://doi.org/10.1007/s13201-016-0512-2.
65. Dahri, M.K.; Kooh, M.R.R.; Lim, L.B.L. Application of Casuarina equisetifolia needle for the removal of methylene blue and malachite green dyes from aqueous solution. *Alex Eng J*. **2015**, *54*, 1253-1263. https://doi.org/10.1016/j.aej.2015.07.005.

Chapter V. Adsorption Performance of Zeolite for the Removal of Congo Red Dye: Factorial Design Experiments, Kinetic, and Equilibrium Studies

The findings of this study have been published in the journal "*Separations*"

Ali Imessaoudene, Sabrina Cheikh, Amina Hadadi, Nadia Hamri, Jean-Claude Bollinger, Abdeltif Amrane, Hichem Tahraoui, Amar Manseri and Lotfi Mouni. Adsorption Performance of Zeolite for the Removal of Congo Red Dye: Factorial Design Experiments, Kinetic, and Equilibrium Studies. *Separations* **2023**, 10, *57*
https://doi.org/10.3390/separations10010057

Introduction

In this chapter, Congo Red was selected as the model molecule to examine the adsorption behavior of LTA-type zeolite toward anionic dyes. A virgin commercial zeolite of this type was utilized with the objective of enhancing the adsorption capacity of these materials. The main conclusions of this study are as follows: (i) the adsorption process occurs at a relatively fast rate, and (ii) the adsorbent exhibits excellent performance in Congo Red removal, achieving up to 98.7% dye removal even at low doses of 0.1 g/L, with an exceptionally high maximum adsorption capacity of up to 666.5 mg/g.

Chapter V. Adsorption Performance of Zeolite for the Removal of Congo Red Dye: Factorial Design Experiments, Kinetic, and Equilibrium Studies

Abstract: In the present research, zeolite is used for the removal of toxic Congo red dye from water solution. The effects of different operating conditions such as hydrogen potential (pH), contact time (time), zeolite dose (D), initial dye concentration (C_0), and ionic strength (I) are investigated for Congo red adsorption under batch mode. It was found that the adsorption process was greatly affected by the initial pH of the dye solution. The removal efficiency decreased from 97.68 to 5.22 % when the pH varied from 3 to 5; thus, acidic conditions clearly improve Congo red adsorption on zeolite. At pH 3, an increase in C_0 and I and decrease in D resulted in an increase in the adsorption capacity q_e. The effects of these three parameters and their interactions were also investigated using the 2^3 full factorial design experiments approach where q_e was chosen as the response. The results obtained from this method followed by the analysis of variance and the Student's *t*-test show that, the influence of these parameters on dye adsorption process are in the order $I < C_0 < D$. The kinetic studies revealed that adsorption follows a pseudo-second-order kinetic model. The adsorption isotherms experimental data were analyzed using the Langmuir, Freundlich, and Temkin isotherms models. The Freundlich isotherm was the best-fit model to the experimental data. The fitting of kinetics and isotherm models was evaluated by using non-linear modeling, R^2, MSE, and RMSE.

Keywords: Congo red dye; adsorption; batch mode; zeolite; kinetics; isotherm; full factorial design experiments

1. **Introduction**

Considerable volumes of waste effluents containing synthetic dyes are generated by several industries such as textiles, paper, printing, cosmetics, plastics, leather, etc. [1]. Their release into the hydrosphere poses significant environmental risks, giving undesirable color to the receiving water media and inhibiting sunlight penetration, thus limiting photosynthetic activity and increasing the organic matter charge in water, thereby creating a severe imbalance in aquatic ecosystems [2]. In addition, synthetic dyes also have adverse effects on human health due to their mutagenic and carcinogenic nature [3]. Therefore, it is essential to treat these effluents at their point of origin prior to release them into the mainstream.

Currently, several conventional and advanced treatment processes have been proposed in the literature and some of them have been industrially implemented for the treatment of this type of effluent, such as biodegradation [4,5], coagulation-flocculation [6-9], electro-

coagulation [10], membrane filtration [11,12], ion-exchange resin [13,14], Fenton oxidation [15], ozonation [16], photocatalysis [17], and adsorption [18]. Nonetheless, certain approaches have limitations in terms of bacterial growth inhibition, sludge production, not being appropriate for all dyes, short life of the applied technique, high operating cost, slow kinetics, and byproduct formation [19]. Over the past decade or so, research efforts have focused on dye removal adsorption technology [20]. This technique has several benefits owing to its simplicity, low cost, great efficacy, and ability to manage relatively large flow rates while generating high-quality effluent [2].

Activated carbon is the favored adsorbent in air [21-23] and wastewater treatment because of its large specific surface area and adsorption capacity; however, its poor selectivity, regeneration difficulties with a loss of adsorption capacity and high cost have prompted many researchers to test and develop new adsorbents with an improved cost ratio and for specific effluents [24]. In this regard, Crini in 2006 [25] identified in a seminal review a broad range of conventional and non-conventional adsorbents evaluated on some dyestuffs and their adsorption capacities. This effort has been extended by other authors to make this list more exhaustive [26]. Among low-cost adsorbent materials, zeolites are superior to activated carbon owing to their microporous solid state, well-defined crystalline structure, ion-exchange capacity, high specific surface area, selectivity, and, most importantly, their availability in large mineable deposits at relatively low costs [27-29].

In this study, the removal of Congo red (CR) from aqueous solution by zeolite was investigated. Initially, experimental and modeling methods were used to assess the adsorption behavior of CR on zeolites. To study the adsorption of CR, both kinetic and isotherm adsorption models were examined, and nonlinear fitting was employed. Furthermore, it was demonstrated in this study how adsorbent dosage (D), initial dye concentration C_0, and ionic strength (I) interacted and ultimately influenced CR adsorption capacity. A 2^3 full factorial design experiments approach was used to study the removal of CR. Finally, within the parameters' range of variation, a linear model yielding $q = f(D, C_0, I)$ was established.

2. Materials and Methods

2.1. Materials

Zeolite material was purchased from sigma Aldrich with commercial code 96096 and was utilized just as supplied. Congo red, an anionic diazo direct dye (C.I. 22120, MW = 696.68 g/mol) was of analytical grade and purchased from Merck Company (Darmstadt, Germany).

The chemical structure of this dye is shown in Figure V.1. The CR dye stock solution (1 g/l) was prepared in deionized water and the required pH value of the aqueous dye solutions was adjusted by using either 0.1 M HCl or NaOH solutions. These chemicals were purchased from sigma Aldrich Chemical Company, Burlington, MA, USA.

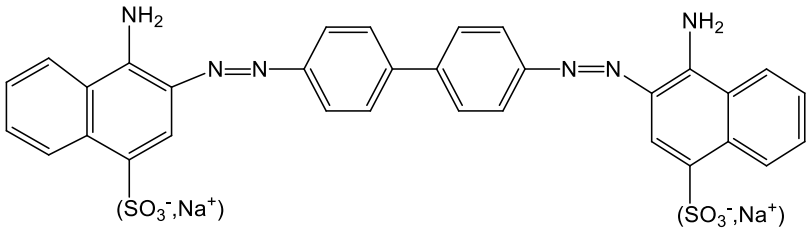

Fig V.1. Chemical structure of CR.

2.2. Analytical Measurements

CR concentrations in aqueous solution were measured using a UV-visible spectrophotometer (BECKMAN DU® 520), due to the color change of CR as a function of solution pH (Figures V.2 and V.3), three calibration curves at pH = 2, pH = 3, and pH = 5 with respect to their λ_{max} were constructed. After the solid-liquid separation and prior to the dye analysis, the samples are scanned in the visible spectrum region to determine which of the calibration curves to employ. In contrast, it is relevant to note that the pH of fresh solutions of the dye with initial concentrations such as those used in this work, is naturally around 8. A pH meter (hanna instruments, Portugal) supplied with a combined glass electrode was used for pH measurements. Separation of phases (solid/liquid) before dye analysis in aqueous solution was performed by centrifugation (EBA-20 Model, Andreas Hettich GmbH& Co, KG, Tuttlingen, Germany).

Fig V.2. CR colors solutions at different initial pHs, C_0 = 20 mg/L.

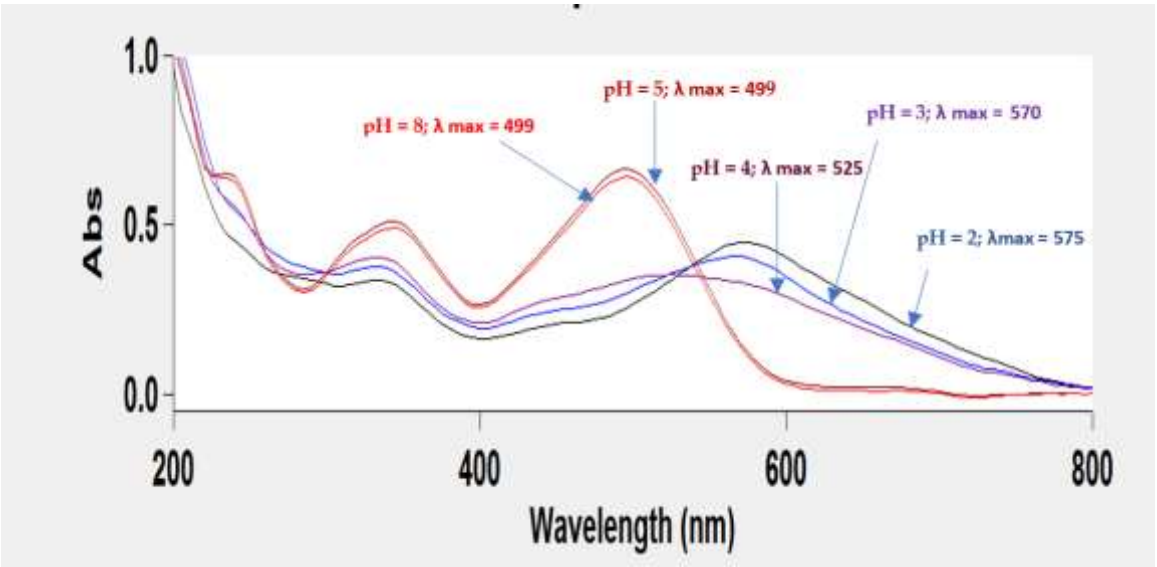

Fig V.3. λ_{max} (nm) values obtained at different initial dye solution pH, C_0 = 20 mg/L.

2.3. Adsorption Experiments

The aqueous CR solutions for adsorption tests were prepared by diluting the stock solution in deionized water to the required concentrations. Batch adsorption experiments were carried out in 100 mL conical flasks with glass stoppers placed in a C76 shaking water bath (New Brunswick Scientific, Edison, NJ, USA) operating at 200 rpm. A volume of 50 mL of dye solution with different initial concentrations were placed in the conical flasks and combined with a known amount of adsorbent at a constant temperature of 25°C and a required pH value. The effect of initial pH on the removal of CR was investigated over the range of 2 to 11. The pH at equilibrium (pH_{eq} or the final pH) was also measured in this stage, and for the experiments conducted at an initial pH of 3 and with the initial dye concentrations and zeolite dosages used, the final pH values are close to 5. The effect of the adsorbent dose (D) was studied throughout a 0.04 to 0.18 g/L range. To study the effect of the ionic strength on CR adsorption, experiments were performed by using varied concentrations (0 to 9.1 mg/L) of sodium sulfate salt (Na_2SO_4). Adsorption kinetics were investigated by measuring dye adsorption at various time intervals using CR solutions at initial concentrations of 25 and 30 mg/L. Based on the kinetic experiments, a time contact of 100 min was set for all subsequent isotherm tests to achieve a steady-state or pseudo-equilibrium, and dye solutions with initial concentrations ranging from 8 to 40 mg/L were used for this purpose at 25°C. All assays were carried out in triplicate and the average values were presented. The maximum difference between the three values was less than 3% of the mean. The dye removal efficiency E (%), and the adsorption capacity q_t (mg/g) at the time t (min), were calculated using the following equations

$$E\ (\%) = \frac{(C_0 - C_t).100}{C_0} \qquad (1)$$

$$q_t = \frac{(C_0 - C_t).V}{m} \qquad (2)$$

where C_0, C_t, m, and V are the initial and the actual CR concentration (mg/L), the used adsorbent dried amount (g), and the dye solution volume (L), respectively. At equilibrium ($t = t_{eq}$), C_t and q_t are named C_{eq} and q_{eq}, respectively.

2.4. The Factorial Design

Adsorbent dose (D), initial dye concentration (C_0), and the ionic strength (I) were taken as independent variables (factors) and adsorption capacity q_e as a response. A full 2^3 factorial design of experiments [30] was considered to evaluate the main effects and interactions in CR adsorption process. Three factors to be investigated at two levels of 2^3 factorial design having 8 experiments with all possible combinations of variables were conducted in duplicate which gives a total of 16 trials. Low (−1) and high (+1) levels of the factors are given in Table V.1. The factorial design matrix and q_e obtained are shown in Table V.2. To avoid systematic errors, the order in which the experiments were conducted was randomized and the results were analyzed with Minitab17® software. In the range of parameter variation, it is useful to develop the response-factors relationship in terms of a mathematical model such as the response function. The use of variance analysis and factorial design of experiments allowed to express the adsorption capacity as a polynomial regression model. The codified model employed for full 2^3 factorial designs was as follows:

$$\widehat{Y} = a_0 + a_1 D + a_2 C_0 + a_3 I + a_{12} D\ C_0 + a_{13} D\ I + a_{23} C_0\ I + a_{123} D\ C_0\ I + \varepsilon \qquad (3)$$

where $\widehat{Y}$, a_0, and a_i represent the model predicted response, the global mean, and the regression coefficient corresponding to the main factor effects and interactions, respectively. The term ε is the random error component. In this model, the factors are in codes terms and can take values from −1 or +1. To convert the real values of the parameter X_i to the coded values (or vice versa), the following equations can be used [31]:

$$x = \frac{X - X_m}{\Delta X} \qquad (4)$$

where

$$X_m = \frac{X_{+1} + X_{-1}}{2} \quad (5)$$

$$\Delta X = \frac{X_{+1} - X_{-1}}{2} \quad (6)$$

x is the dimensionless coded value, X is the real value of the factor, and X_{+1} and X_{-1} are the maximum and minimum values of the factor X_i, in the range of variation studied. The effects, regression coefficients, and the associated standard errors for CR adsorption are shown in Table V.3.

Table V.1. Experimental parameters and their levels.

Factors	**Real Unit**	**Low Level (−1)**	**High Level (+1)**
D	g/L	0.02	0.1
C_0	mg/L	8.3	25.9
I	mg Na_2SO_4/L	0	9.1

Table V.2. 2^3 full factorial design matrix of experiments.

		Coded Experiments Matrix			**q_e (mg/g)**		
Std Order	**Run Order**	**D**	**C_0**	**I**	**Observed**	**Predicted**	**Residual**
16	1	+1	+1	+1	238.5	239.93	-1.43
4	2	+1	+1	-1	230.8	232.34	-1.56
7	3	-1	+1	+1	1175.3	1170.34	5.00
10	4	+1	-1	-1	73.7	75.28	-1.56
1	5	-1	-1	-1	289.5	286.86	2.60
9	6	-1	-1	-1	284.3	286.86	-2.60
12	7	+1	+1	-1	233.9	232.34	1.56
6	8	+1	-1	+1	77.4	77.65	-0.29
5	9	-1	-1	+1	339.7	333.98	5.71
2	10	+1	-1	-1	76.8	75.28	1.56
8	11	+1	+1	+1	241.4	239.93	1.43
3	12	-1	+1	-1	1146.1	1148.08	-1.95
14	13	+1	-1	+1	77.9	77.65	0.29
13	14	-1	-1	+1	328.3	333.98	-5.71
15	15	-1	+1	+1	1165.3	1170.34	-5.00
11	16	-1	+1	-1	1150.0	1148.08	1.95

Table V.3. Coded coefficients.

Term	**Effect (ω_i)**	**Coefficient (a_i)**	**Standard Error (SE)**
Constant		445.56	1.08
D	-578.51	-289.26	1.08
C_0	504.23	252.12	1.08
I	19.83	9.92	1.08
D.C_0	-344.56	-172.28	1.08
D.I	-14.86	-7.43	1.08
C_0.I	-4.91	-2.45	1.08
D.C_0.I	7.52	3.76	1.08

2.5. Kinetics and Isotherm Studies

Adsorption behavior of CR was also investigated by the isotherm and kinetic studies at a constant temperature of 25°C. The fitting of the considered models was evaluated by using nonlinear modeling performed by OriginPro8® software, and same error functions were defined to establish the fit of the model to the experimental data. These error functions are calculated on the basis of three following functions: the sum of squared difference between the experimentally obtained adsorption capacities (Y_i) to their mean ($\overline{Y}$); the sum of squared deviation between the model-predicted capacities ($\widehat{Y}_i$) to ($\overline{Y}$); and finally, from the sum of the squared residual between experimental (Yi) and predicted ($\widehat{Y}_i$) capacities. The total sum of squares (TSS) calculates the variation between data points and the mean. In least-squares fitting, the TSS can be divided into two parts: the variation explained by regression (RSS) and that not explained by regression (SSE). From (n) number of the adsorption experiments, TSS, RSS, and SSE were computed as follows [32]:

$$TSS = \sum_{i=1}^{n} (Y_i - \overline{Y})^2 \qquad (7)$$

$$RSS = \sum_{i=1}^{n} \left(\widehat{Y}_i - \overline{Y}\right)^2 \qquad (8)$$

$$SSE = \sum_{i=1}^{n} \left(Y_i - \widehat{Y}_i\right)^2 \qquad (9)$$

The ratio of RSS to TSS can be used as one measure of the quality of the regression model. This quantity termed the coefficient of determination is computed as:

$$R^2 = \frac{RSS}{TSS} = 1 - \frac{SSE}{TSS} \qquad (10)$$

From the above equation, we can see that when using a good fitting model, R^2 value should be close to 1.

The value of SSE averaged with the degree of freedom (DF) can measure the mean square error (MSE) which gives the variance of the random errors between the fitted model and the observed data according to the following equation [33,34]:

$$MSE = \frac{SSE}{DF} \qquad (11)$$

and

$$DF = n - p \qquad (12)$$

where n is the number of observed data Y_i (i = 1 to n), and p is the number of parameters of the model. It should be noted that the models being compared in this part of the study have the same number of parameters. The last goodness of fit criteria is the root-MSE (root mean sum of square error) which can be calculated as:

$$RMSE = \sqrt{MSE} = \sqrt{\frac{SSE}{DF}} \qquad (13)$$

Small MSE and RMSE values, close to zero, and large R^2 value, close to 1, indicate better agreement of experimental data with the model.

2.5.1. Adsorption Kinetics

During adsorption, investigations of the kinetics of the adsorption process give insight into the reaction rate and the sorption mechanism including mass transfer, diffusion, and reaction on the adsorbent surface [35]. They are also essential for determining the adsorbent-adsorbate minimum contact time required to reach the steady-state or pseudo-equilibrium for the system, which is of tremendous practical value to ultimately save time and energy. The most popular kinetic models applied in aqueous-phase adsorption are the pseudo-first order (PFO), pseudo-second-order (PSO), and the intraparticle diffusion (IPD) [36,37].

The pseudo-first-order kinetic rate equation (PFO) is expressed as follows:

$$q_t = q_e\left(1 - e^{-k_1 t}\right) \qquad (14)$$

where q_t and q_e (mg/g) are the adsorption capacities at any contact time t (min) and at equilibrium, respectively; and k_1 (min^{-1}) is the rate constant of the PFO model.

The pseudo-second kinetic model (PSO) is:

$$q_t = \frac{k_2 q_e^2 t}{1 + k_2 q_e t} \qquad (15)$$

where k_2 (g/mg min) is the pseudo-second order rate constant.

The intra-particle diffusion model (IPD) is presented as follows:

$$q_t = k_{id}\, t^{0.5} + C_i \qquad (16)$$

where k_{id} (mg/g min) is the rate constant of the intra-particle diffusion model and C_i (mg/g) is a constant associated with the thickness of the boundary layer, where a higher value of C_i corresponds to a greater effect on the limiting boundary layer.

The kinetic parameters of the different models tested can be obtained by solving the nonlinear equations by iterative methods using the Gauss-Newton algorithm integrated in Origin Pro8® (OriginLab Corp, USA) software with a judicious choice of the initial vectors.

2.5.2. Adsorption isotherm

The adsorption process continues until the adsorbate uptake amount on the adsorbent surface and the residual amount in the solution reach a dynamic equilibrium. The connection between these two values at a constant and defined temperature, known as the adsorption isotherm, is fundamental in describing the interactive behavior of solutes and adsorbents and is critical in the design of adsorption systems [38]. In this work, three extensively used adsorption isotherm models were employed to characterize the CR adsorption process onto zeolite [35,36,39].

The Langmuir isotherm assumes that the adsorbate molecules cover a monolayer on the homogeneous surface of adsorbent, without interaction between adsorbed molecules owing to constant enthalpies and sorption activation energy; the corresponding nonlinear equation is as follows:

$$q_e = \frac{K_L C_e q_{max}}{1 + K_L C_e} \qquad (17)$$

where C_e is the equilibrium concentration of the adsorbate (mg/L), C_0 the initial concentration of the adsorbate (mg/L), and q_{max} (mg/g) and K_L (L/mg) are the maximum adsorption capacity and a constant related to the energy of adsorption, respectively. One can also introduce a separation factor (R_L):

$$R_L = \frac{1}{1 + K_L C_0} \qquad (18)$$

This is a useful dimensionless constant which can determine the operating conditions:
$R_L > 1$, unfavorable adsorption; $R_L = 1$, linear adsorption; $R_L = 0$, irreversible adsorption; $0 < R_L < 1$, favorable adsorption.

Freundlich's adsorption isotherm is an empirical model that assumes a heterogeneous adsorption surface with molecular interaction. The applicable nonlinear equation is as follows:

$$q_e = K_F C_e^n \qquad (19)$$

where K_F (mg/g)/(mg/L)^n is the Freundlich constant, which characterizes the strength of adsorption and n (dimensionless; $0 < n < 1$) is a Freundlich intensity parameter that reflects the magnitude of the adsorption driving force or surface heterogeneity (the adsorption isotherm becomes linear when n =1, favorable when $n < 1$, and unfavorable when $n > 1$).

Unlike the two previous isotherms, Temkin isotherm considers that the decrease in the heat of adsorption of all molecules in the surface layer is linear with uniform distribution of binding energies. The corresponding nonlinear equation is:

$$q_e = \beta_T \ln(A_T C_e) \qquad (20)$$

where A_T is an equilibrium binding constant and β_T refers to a Temkin isotherm constant. If $\beta_T < 8$ kJ mol^{-1}, the adsorption is physical in nature.

3. Results and Discussion

3.1. Effect of Contact Time and Initial Dye Concentration

To determine the optimal shaking time to reach pseudo-equilibrium in the process, the adsorption of CR on zeolite as a function of time was performed with initial CR concentrations of 25 and 30 mg/L at pH 3. The corresponding data are shown in Figure V.4, the q_t value

increased dramatically in the first six min where it attained 219.2 and 289.4 mg/g for the corresponding initial concentrations of 25 and 30 mg/L, respectively; this demonstrates that the adsorption rate was very fast in this time interval. This can be attributed to the abundant availability of the sorptive active sites on the zeolite surface at the beginning. After this time and as these sites are gradually occupied, adsorption slows and ultimately levels off, hence, the plateau becomes evident. The pseudo-equilibrium steady state was reached at about 100 min of contact time. As is evident, raising the initial concentration might provide the driving force necessary to overcome the mass transfer resistances between the aqueous and solid phases, resulting in an increase in the q_e values [40]. Experiments involving CR adsorption on other adsorbents, such as activated carbon [41], zeolitic imidazolate framework-67 [42], and reduced graphene oxide [43], have previously demonstrated strong similarities.

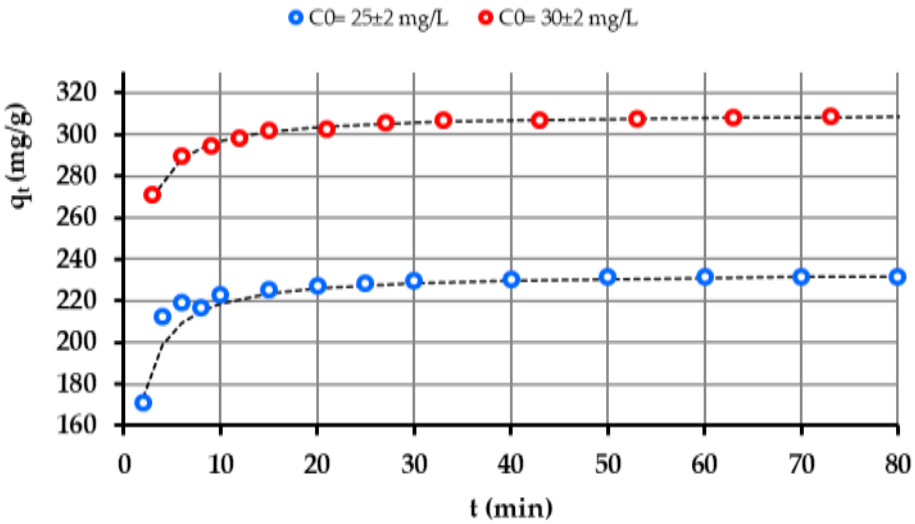

Fig V.4. Kinetic of CR adsorption on zeolite (pH = 3, D = 0.1 g/L, T = 25°C, ……PSO model).

3.2. Effect of pH

The efficiency of dye adsorption processes is greatly influenced by the pH of the solution. It affects the surface electrical charge of the adsorbent, the degree of ionization of adsorbate molecules in aqueous solution, and the dissociation of different functional groups on the active sites of the adsorbent, either independently or in conjunction [44]. In most cases, pH is termed as the 'master variable'. The effect of initial solution pH on CR removal is shown in Figure V.5. It can be observed that the maximum adsorption of CR took place at relatively very low initial solution pH (between pH 2 and 3). The removal efficiency E decreased significantly from 96.5 to 5.2% as the initial solution pH was increased from 3 to 5. It can be also noticed

that, in the initial pH range from 5 to 8, the dye uptake was very weak and the E values began to rise after pH 9. This result can be explained by the following scenario:

CR is an anionic dye containing SO_3 functional groups (see Figure V.1), its dissociation in water gives its sulphonate groups ($-SO_3^-$) that are negatively charged in aqueous solution as it is shown in Equation (21).

$$\text{dye} - (SO_3^-, Na^+) \xrightarrow{\text{Water}} \text{dye} - SO_{3\,(aq)}^- + Na_{(aq)}^+ \qquad (21)$$

At an acidic initial pH, the active surface functional groups of zeolite which are mainly the Silanol (Si-OH) and Aluminol groups (Al-OH) become protonated, as it is shown by the consecutive reactions provided in Equations (22) and (23) [45].

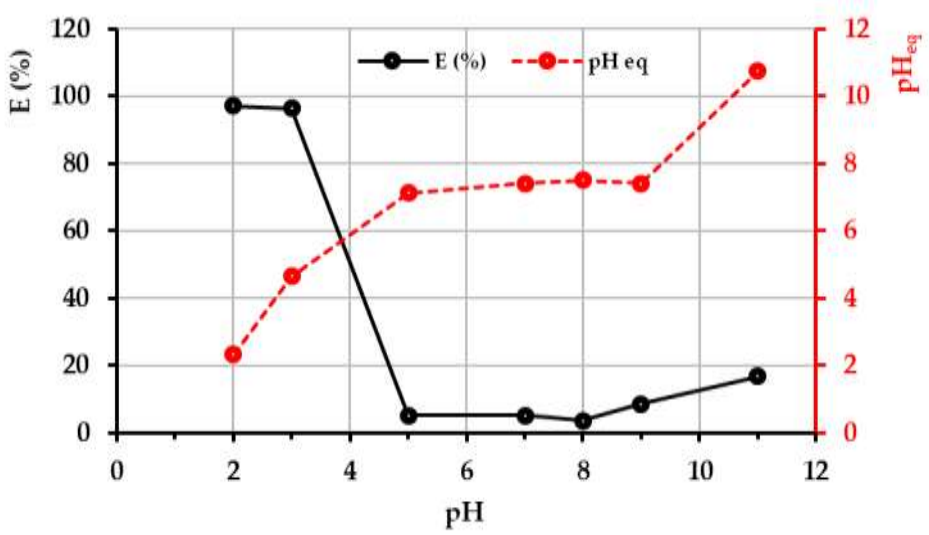

Fig V.5. Effect of initial solution pH on CR removal efficiency (C_0 = 26.9 mg/L, D = 0.1 g/L, T = 25°C).

Ion exchange reaction:

$$[S - OM]_Z + H_{(aq)}^+ \leftrightarrow [S - OH]_Z + M_{(aq)}^+ \qquad (22)$$

adsorption on neutral surface:

$$\underbrace{[S - OH]_Z}_{\text{Neutral surface}} + H_{(aq)}^+ \leftrightarrow \underbrace{[S - OH_2^+]_Z}_{\text{Protonated surface}} \qquad (23)$$

where S is surface central metal (Si, Al) of zeolite, and M is the metal cation balancing the charge of zeolitic framework. The adsorption of $H^{+}_{(aq)}$ on the zeolite surface caused an increase in the solution pH as seen in this investigation and illustrated in Figure V.5.

Under such conditions, the ionic attraction between ($-SO_3^-$) and ($SiOH_2^+$, $AlOH_2^+$) is the possible adsorption mechanism of CR dye on the zeolite as it is shown in Equation (24).

$$\underbrace{[S-OH_2^+]_Z}_{\text{Protonated surface}} + SO_3^- - \text{dye}_{(aq)} \leftrightarrow \underbrace{[S-OH_2^+]_Z}_{\text{Protonated surface}} \ldots\ldots SO_3^- - \text{dye} \quad (24)$$

Similar results have been reported by several studies about adsorption of anionic dyes on zeolite and clay materials [46,47].

3.3. Influence of Adsorbent Dose

In order to investigate the effect of zeolite dose on CR removal at pH 3, a series of experiments were undertaken with different adsorbent doses at initial dye concentration of 25 mg/L. The results obtained are depicted in Figure V.6. Examination of this figure revealed that adsorbed amount of CR decreased with increasing adsorbent dose, while the removal efficiency E increased until the plateau is reached beyond the adsorbent dose of 0.1 g/L which corresponds to the value of 98.7%. At these conditions, further additional amount of adsorbent has little influence on the improvement of E. The highest value of q_e obtained was 610.2 mg/g at adsorbent dose of 0.04 g/L.

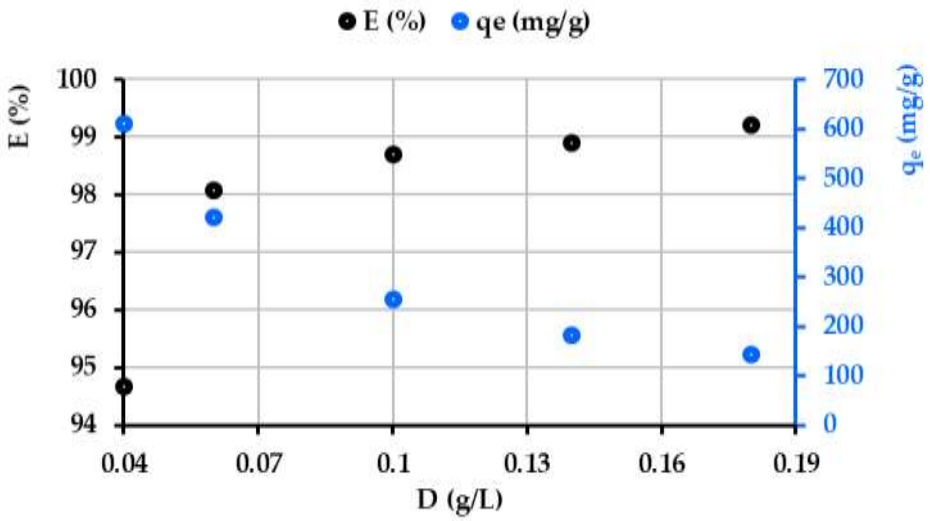

Fig V.6. Effect of zeolite dose on CR removal efficiency and the adsorption capacity (C_0 = 25 ± 2 mg/L, pH = 3, T = 25°C).

3.4. Effect of Ionic Strength

Many electrolytes generated by the dissolution of sodium salts may occur in wastewater because they are often utilized as a stimulator in the dyeing industry. As can be observed in Figure V.7, ionic strength has a positive effect on CR molecules uptake by adsorbent material. The adsorption capacity increased from 230 to 244.9 mg/g, as the concentration of Na_2SO_4 was increased from 0 to 9.1 mg/L. The enhanced removal of CR dye with an increase in Na_2SO_4 concentration can be attributed to the increase in surface positive charge of the adsorbents [48]. These results are in good agreement with those reported by other authors on removal of CR by reduced graphene oxide [43].

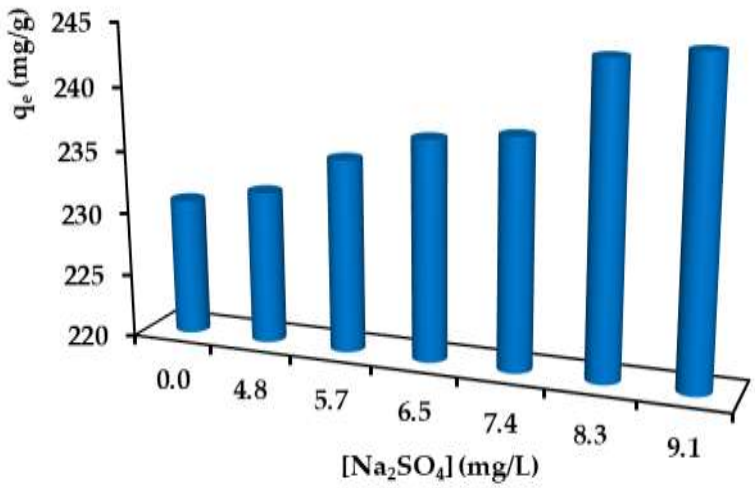

Fig V.7. Effect of Na_2SO_4 concentration on the adsorption of CR (C_0 = 25 ± 2 mg/L, D = 0.1 g/L, pH = 3, T = 25°C).

3.5. The Factorial Design

There are numerous significant issues with the conventional one-variable-at-a-time technique, in which we change one variable at a time while keeping all other variables in the experiment fixed. This type of experimentation requires substantial resources to obtain a limited amount of information about the process. In addition, this method's trials are often inaccurate, inefficient, time-consuming, and may provide false optimal conditions for the process. An experiment is known as a factorial experiment if the treatments include every possible combination of several levels of factors. It displays the influence of process variable interactions and enhances process optimization. The impact of a factor is the change in the average value of

the response caused by a shift from a lower (-1) to a higher (+1) level of a factor. According to the Yates algorithm, the effect ω can be calculated by the following expression [30,31].

$$\omega_i = \underbrace{\frac{\sum q_{e\,exp}}{n}}_{+1} - \underbrace{\frac{\sum q_{e\,exp}}{n}}_{-1} \qquad (25)$$

where ω_i is the effect of the factor i, $q_{e\ exp}$ the measured response, and n is the number of experiments at each level (+1) or (-1). By replacing the response $\widehat{Y}$ by $\widehat{q_e}$, and the coefficients a_i in Equation (3) with their values given in Table V.3, we obtain:

$$\widehat{q_e}\left(^{mg}/_{g}\right) = 445.56 - 289.26\ D + 252.12\ C_0 + 9.92\ I - 172.28\ D.C_0 - 7.43\ D.I - 2.45\ C_0.I + 3.76\ D.C_0.I \qquad (26)$$

According to the data reported in Table V.3, we can observe that the main effects of factors C_0 and I have a positive sign for CR adsorption. This indicates that q_e increases as these factors' levels rise throughout the adsorption process. In contrast, the effect of D is negative and high levels of this factor reduce q_e values.

Statistical analysis of variance (ANOVA) was also performed to determine which process parameters are statistically significant. Fisher F-test is a tool for assessing which process factors have a significant impact on the value of CR adsorption capacity. The F-value for each process parameters is simply a ratio of mean of the squared deviations to the mean of the squared error. Usually, the larger the F-value, the greater the effect on q_e value due to the change of the process parameter. The results of variance analysis are given in Table V.4. From these data, one can observe that the main effects of the three factors studied as well as 2-way and 3-way interactions are statistically significant (*p*-values < 0.05) at 95% of confidence interval except C_0–I interaction which has a *p*-value > 5%. According to the greatest F-value, the adsorbent dosage (D) has the most significant effect on CR adsorption compared to the other factors, the three parameters effect are listed in the following order: effect (D) > effect (C_0) >> effect (I).

Pareto charts were used to determine the relative significance of the main effects and their interactions (Figure V.8). A Student's *t*-test was employed to determine whether the calculated effects were significantly different from zero and the values for each effect and interaction are represented by horizontal columns in Pareto chart [49,50]. It was observed that for a 95% confidence level and eight freedom degrees, the *t*-value is 2.306. The vertical line in the chart indicates the minimum statistically significant effect magnitude for 95% confidence level.

According to the results of the statistical study given below, Equation (26) giving the response as a function of the terms that are statistically significant can be simplified to:

$$\widehat{q_e}\left(^{mg}/_{g}\right) = 445.56 - 289.26\,D + 252.12\,C_0 + 9.92\,I - 172.28\,D.C_0 - 7.43\,D.I + 3.76\,D.C_0.I \qquad (27)$$

Table V.4. Analysis of variance (ANOVA) for full factorial experimental design.

Source	Degrees of Freedom (DF)	Sum of Squares (SS)	Mean Square (MS)	F-Value	*p*-Value
D	1	1,338,717	1,338,717	71,317.01	0.000
C_0	1	1,016,998	1,016,998	54,178.17	0.000
I	1	1573	1573	83.80	0.000
D.C_0	1	474,895	474,895	25,298.92	0.000
D.I	1	883	883	47.04	0.000
C_0.I	1	96	96	5.14	0.053
D.C_0.I	1	226	226	12.05	0.008
Error	8	150	19		
Total	15	2,833,538			

S = 4.33259; R^2 = 99.99%; $R^2_{ajusted}$ = 99.99%; $R^2_{predicted}$ = 99.98%.

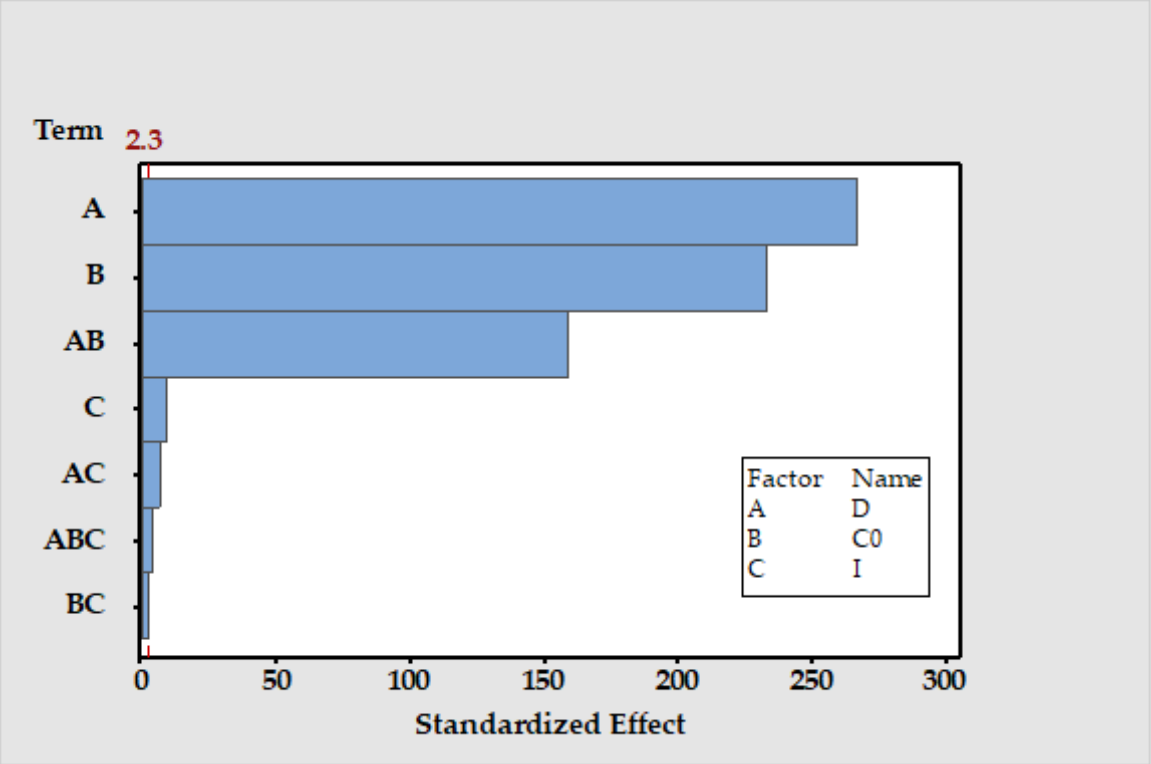

Fig V.8. Pareto chart of the standardized effects (response is q_e (mg/g), α = 0.05).

3.6. CR adsorption Kinetics and Isotherm Studies

3.6.1. Adsorption Kinetics

Table V.5 shows the parameters obtained for the adsorption kinetics models examined. Based on the fitting criteria adopted, the IPD model is inadequate for representing the CR adsorption kinetics on our material at the two dye initial concentrations. The PFO model, on the other hand, does not describe the entire range of adsorption time and is only restricted to the initial time range. The experimental data fit the PSO model very well. The values of R^2, MSE, and RMSE obtained are 0.98973, 2.19716, and 1.48228 for C_0 = 24 ± 2 mg/L, and 0.99094, 1.01749, and 1.00871 for C_0 = 31 ± 2 mg/L, respectively. On the other hand, the $q_{e,cal}$ values obtained are in agreement with $q_{e,exp}$ (see Table V.5). This trend was also observed in other studies [42,46].

3.6.2. Adsorption Isotherm

The findings in Table V.6 indicate that the adsorption of CR onto zeolite at 25°C followed the Freundlich model since R^2, MSE, and RMSE values found are better than those obtained for the Langmuir and Temkin isotherm models, thus, suggesting the heterogeneity of the zeolite particles' adsorption sites. According to Table V.6, the mean value of "n" obtained from the Freundlich isotherm is equal to 0.61, which is lower than unity and indicating favorable adsorption [36,51]. In addition, the value of K_F for Congo red adsorption is 126.31. These findings suggest that zeolite has a high capacity for adsorbing anionic Congo red dye in solution.

Table V.5. Parameters of kinetic models tested for CR removal on zeolite at 25°C using nonlinearized equations.

Model	C_0 (mg/L)	$q_{e,exp}$ (mg/g)	$q_{e,cal}$ (mg/g)	k_1 (min^{-1})	k_2 (g/mg min)	k_{id} (mg/g min)	C_i(mg/g)	R^2	MSE	RMSE
PFO			228.2 ± 1.3	0.666 ± 0.044	-	-	-	0.865	28.735	5.360
PSO	24 ± 2	232.0	233.8 ± 0.4	-	$0.006 \pm 2 \times 10^{-4}$	-	-	0.989	2.197	1.482
IPD			-	-	-	2.948 ± 0.752	204.398 ± 5.736	0.474	112.370	10.600
PFO			305.8 ± 1.4	0.694 ± 0.049	-	-	-	0.725	30.819	5.551
PSO	31 ± 2	311.2	310.9 ± 0.3	-	$0.007 \pm 2 \times 10^{-4}$	-	-	0.990	1.017	1.008
IPD			-	-	-	2.668 ± 0.509	285.737 ± 3.672	0.646	39.711	6.301

Table V.6. Non-linear isotherm models fitting to experimental data (D = 0.1 g/L, pH = 3, T = 25°C).

Model	q_{max} (mg/g)	K_L(L/mg)	K_F(mg/g)/(mg/L)^n	n	β_T	A_T	R^2	MSE	RMSE
Langmuir	666.5 ± 71.6	0.205 ± 0.039	-	-	-	-	0.985	122.374	11.062
Freundlich	-	-	126.319 ± 3.604	0.613 ± 0.020	-	-	0.996	29.614	5.441
Temkin	-	-	-	-	138.942 ± 13.031	2.160 ± 0.38	0.966	285.500	16.896

4. Conclusions

The analysis of variance and the 2^3 full factorial design of experiments for batch adsorption of Congo red dye using zeolite was studied. The effects of three factors, adsorbent dose D (0.02-0.1 g/L), initial dye concentration C_0 (8.3-25.9 mg/L), and ionic strength expressed in terms of Na_2SO_4 salt solution I (0-9.1 mg/L) on adsorption capacity were identified. The main effects of factors C_0 and I have a positive sign for CR adsorption, indicating that q_e increases as these factors' levels rise throughout the adsorption process. In contrast, the effect of D is negative, and high levels of this factor reduce q_e values.

The statistical analysis confirmed that the one order polynomial equation gave a reasonably good fit with an R^2 = 99.99% and adjusted R^2 = 99.99%. According to the significance effect obtained in variance analysis and by means of Pareto charts, the adsorbent dose was the most significant factor in this process followed by C and I.

For all examined concentrations, the adsorption rate conformed to pseudo-second-order kinetics with a strong determination coefficient ($R^2 \simeq 0.99$) and favorable MSE and RMSE values. The Freundlich isotherm better described the adsorption process occurring in this study. Moreover, it is shown that the planar shape of CR and the appropriate number of sulfonic groups are essential for its successful adsorption under acidic conditions (pH = 3).

All of the findings show that zeolite, which is an eco-friendly material, may be used efficiently to remove CR dye from aqueous solutions in a batch system.

Author Contributions: Conceptualization, A.I. and L.M.; methodology, A.I., L.M., S.C. and A.H.; validation, J.-C.B., A.A. and L.M.; formal analysis, A.I., S.C. and A.M.; investigation, A.I.; resources, L.M., H.T. and A.A.; data curation, A.I., L.M., N.H. and A.M.; writing—original draft preparation, A.I.; writing—review and editing, A.I., A.H., L.M., N.H., J.-C.B., H.T. and S.C.; visualization, A.I., L.M., J.-C.B. and A.A.; supervision, L.M., A.A. and J.-C.B.; project administration, L.M. and J.-C.B.

All authors have read and agreed to the published version of the manuscript.

Funding: This research received no external funding.

Institutional Review Board Statement: Not applicable.

Informed Consent Statement: Not applicable.

Data Availability Statement: Not applicable.

Acknowledgments: The authors wish to thank all who assisted in conducting this work.

Conflicts of Interest: The authors declare no conflict of interest.

References

1. de Luna, M.D.G.; Flores, E.D.; Genuino, D.A.D.; Futalan, C.M.; Wan, M.-W. Adsorption of Eriochrome Black T (EBT) dye using activated carbon prepared from waste rice hulls—Optimization, isotherm and kinetic studies. *J. Taiwan Inst. Chem. Eng.* **2013**, *44*, 646–653. https://doi.org/10.1016/j.jtice.2013.01.010.
2. Gupta, V.; Kumar, R.; Nayak, A.; Saleh, T.; Barakat, M. Adsorptive Removal of Dyes from Aqueous Solution onto Carbon Nanotubes: A Review. *Adv. Colloid Interface Sci.* **2013**, *193–194*, 24–34. https://doi.org/10.1016/j.cis.2013.03.003.
3. Mittal, H.; Babu, R.; Dabbawala, A.; Stephen, S.; Alhassan, S. Zeolite-Y Incorporated Karaya Gum Hydrogel Composites for Highly Effective Removal of Cationic Dyes. *Colloids Surf. Physicochem. Eng. Asp.* **2019**, *586*, 124161. https://doi.org/10.1016/j.colsurfa.2019.124161.
4. van der Zee, F.; Villaverde, S. Combined Anaerobic–Aerobic Treatment of Azo Dyes—A Short Review of Bioreactor Studies. *Water Res.* **2005**, *39*, 1425–1440. https://doi.org/10.1016/j.watres.2005.03.007.
5. Franca, R.; Vieira, A.; Mata, A.M.T.; Carvalho, G.; Pinheiro, H.; Lourenco, N. Effect of an Azo Dye on the Performance of an Aerobic Granular Sludge Sequencing Batch Reactor Treating a Simulated Textile Wastewater. *Water Res.* **2015**, *85*, 327–336. https://doi.org/10.1016/j.watres.2015.08.043.
6. Gurses, A.; Yalçin, M.; Doğar, Ç. Removal of Remazol Red Rb by Using Al (III) as Coagulant-Flocculant: Effect of Some Variables on Settling Velocity. *Water Air Soil Pollut.* **2003**, *146*, 297–318. https://doi.org/10.1023/A:1023994822359.
7. Yang, Z.; Lu, X.; Gao, B.; Wang, Y.; Yue, Q.; Chen, T. Fabrication and Characterization of Poly(Ferric Chloride)-Polyamine Flocculant and Its Application to the Decolorization of Reactive Dyes. *J. Mater. Sci.* **2014**, *49*, 4962–4972. https://doi.org/10.1007/s10853-014-8197-0.
8. Hadadi, A.; Imessaoudene, A.; Bollinger, J.-C.; Cheikh, S.; Assadi, A.A.; Amrane, A.; Kebir, M.; Mouni, L. Parametrical Study for the Effective Removal of Mordant Black 11 from Synthetic Solutions: Moringa oleifera Seeds' Extracts Versus Alum. *Water* **2022**, *14*, 4109. https://doi.org/10.3390/w14244109.

9. Hadadi, A.; Imessaoudene, A.; Bollinger, J.-C.; Assadi, A.A.; Amrane, A.; Mouni, L. Comparison of Four Plant-Based Bio-Coagulants Performances against Alum and Ferric Chloride in the Turbidity Improvement of Bentonite Synthetic Water. *Water* **2022**, *14*, 3324. https://doi.org/10.3390/w14203324.
10. Hendaoui, K.; Ayari, F.; Ben Rayana, I.; Ben Amar, R.; Darragi, F.; Trabelsi-ayadi, M. Real Indigo Dyeing Effluent Decontamination Using Continuous Electrocoagulation Cell: Study and Optimization Using Response Surface Methodology. *Process Saf. Environ. Prot.* **2018**, *116*, 578–589. https://doi.org/10.1016/j.psep.2018.03.007.
11. Derouich, G.; Younssi, S.; Bennazha, J.; Cody, J.; Ouammou, M.; El Rhazi, M. Development of Low-Cost Polypyrrole/Sintered Pozzolan Ultrafiltration Membrane and Its Highly Efficient Performance for Congo Red Dye Removal. *J. Environ. Chem. Eng.* **2020**, *8*, 103809. https://doi.org/10.1016/j.jece.2020.103809.
12. Tavangar, T.; Karimi, M.; Rezakazemi, M.; Reddy, R.; Aminabhavi, T. Textile Waste, Dyes/Inorganic Salts Separation of Cerium Oxide-Loaded Loose Nanofiltration Polyethersulfone Membranes. *Chem. Eng. J.* **2020**, *385*, 123787. https://doi.org/10.1016/j.cej.2019.123787.
13. Wawrzkiewicz, M. Removal of C.I. Basic Blue 3 Dye by Sorption onto Cation Exchange Resin, Functionalized and Non-Functionalized Polymeric Sorbents from Aqueous Solutions and Wastewaters. *Chem. Eng. J.* **2013**, *217*, 414–425. https://doi.org/10.1016/j.cej.2012.11.119.
14. Wu, J.; Li, Q.; Li, W.; Li, Y.; Wang, G.; Li, A.; Li, H. Efficient Removal of Acid Dyes Using Permanent Magnetic Resin and Its Preliminary Investigation for Advanced Treatment of Dyeing Effluents. *J. Clean. Prod.* **2020**, *251*, 119694. https://doi.org/10.1016/j.jclepro.2019.119694.
15. Torrades, F.; García-Montaño, J. Using Central Composite Experimental Design to Optimize the Degradation of Real Dye Wastewater by Fenton and Photo-Fenton Reactions. *Dyes Pigments.* **2014**, *100*, 184–189. https://doi.org/10.1016/j.dyepig.2013.09.004.
16. Muniyasamy, A.; Sivaporul, G.; Gopinath, A.; Lakshmanan, R.; Altaee, A.; Achary, A.; Chellam, P.V. Process Development for the Degradation of Textile Azo Dyes (Mono-, Di-, Poly-) by Advanced Oxidation Process-Ozonation: Experimental & Partial Derivative Modelling Approach. *J. Environ. Manag.* **2020**, *265*, 110397. https://doi.org/10.1016/j.jenvman.2020.110397.

17. Lum, P.; Foo, K.Y.; Zakaria, N.; Palaniandy, P. Ash Based Nanocomposites for Photocatalytic Degradation of Textile Dye Pollutants: A Review. *Mater. Chem. Phys.* **2019**, *241*, 122405. https://doi.org/10.1016/j.matchemphys.2019.122405.
18. Mouni, L.; Belkhiri, L.; Bollinger, J.-C.; Bouzaza, A.; Assadi, A.; Tirri, A.; Dahmoune, F.; Madani, K.; Remini, H. Removal of Methylene Blue from Aqueous Solutions by Adsorption on Kaolin: Kinetic and Equilibrium Studies. *Appl. Clay Sci.* **2018**, *153*, 38–45. https://doi.org/10.1016/j.clay.2017.11.034.
19. Raman, C.; Kanmani, S. Textile Dye Degradation Using Nano Zero Valent Iron: A Review. *J. Environ. Manag.* **2016**, *177*, 341–355. https://doi.org/10.1016/j.jenvman.2016.04.034.
20. Khanday, W.; Asif, M.; Hameed, B. Cross-Linked Beads of Activated Oil Palm Ash Zeolite/Chitosan Composite as a Bio-Adsorbent for the Removal of Methylene Blue and Acid Blue 29 Dyes. *Int. J. Biol. Macromol.* **2016**, *95*, 895–902. https://doi.org/10.1016/j.ijbiomac.2016.10.075.
21. Ma, C.; Bai, J.; Hu, X.; Jiang, Z.; Wang, L. Nitrogen-doped porous carbons from polyacrylonitrile fiber as effective CO_2 adsorbents. *J. Environ. Sci*. **2023**, *125*, 533–543. https://doi.org/10.1016/j.jes.2022.03.016.
22. Huang, J.; Bai, J.; Demir, M.; Hu, X.; Jiang, Z.; Wang, L. Efficient N-Doped Porous Carbonaceous CO_2 Adsorbents Derived from Commercial Urea-Formaldehyde Resin. *Energy Fuels*. **2022**, *36*, 5825–5832. https://doi.org/10.1021/acs.energyfuels.2c00748.
23. Ma, C.; Bai, J.; Demir, M.; Hu, X.; Liu, S.; Wang, L. Water chestnut shell-derived N/S-doped porous carbons and their applications in CO_2 adsorption and supercapacitor. *Fuel* **2022**, *326*, 125119. https://doi.org/10.1016/j.fuel.2022.125119.24.
24. Gupta, V.; Suhas, D. Application of Low-Cost Adsorbents for Dye Removal—A Review. *J. Environ. Manag.* **2009**, *90*, 2313–2342. https://doi.org/10.1016/j.jenvman.2008.11.017.
25. Crini, G. Non-Conventional Low-Cost Adsorbents for Dye Removal: A Review. *Bioresour. Technol.* **2006**, *97*, 1061–1085. https://doi.org/10.1016/j.biortech.2005.05.001.
26. Moradi, O.; Sharma, G. Emerging novel polymeric adsorbents for removing dyes from wastewater: A comprehensive review and comparison with other adsorbents. *Environ. Res*. **2021**, *201*, 111534. https://doi.org/10.1016/j.envres.2021.111534.
27. Humelnicu, I.; Baiceanu, A.; Ignat, M.-E.; Viorica, D. The Removal of Basic Blue 41 Textile Dye from Aqueous Solution by Adsorption onto Natural Zeolitic Tuff: Kinetics

and Thermodynamics. *Process Saf. Environ. Prot.* **2016**, *105*, 274–287. https://doi.org/10.1016/j.psep.2016.11.016.

28. Ouki, S.; Cheeseman, C.R.; Perry, R. Natural Zeolite Utilisation in Pollution Control: A Review of Applications to Metals' Effluents. *J. Chem. Technol. Biotechnol.* **1994**, *59*, 121–126. https://doi.org/10.1002/jctb.280590202.
29. Hernández-Beltrán, N.; Olguín, M.; Rosas Aburto, A. Effect of Acid Phosphate Media on the Stability of Clinoptilolite-Rich Tuff. *J. Incl. Phenom.* **2008**, *61*, 93–100. https://doi.org/10.1007/s10847-007-9399-8.
30. Goupy, J. *Plans D'expériences Pour Surfaces de Réponse;* Dunod: Paris, France, 1999.
31. Jiju Antony, J. *Design of Experiments for Engineers and Scientists*; Elsevier Ltd.: Amsterdam, The Netherlands, 2003.
32. Zhang, K.; Cheung, W.H.; Valix, M. Roles of physical and chemical properties of activated carbon in the adsorption of lead ions. *Chemosphere.* **2005**, *60*, 1129–1140. https://doi.org/10.1016/j.chemosphere.2004.12.059.
33. Vuono, D.; Catizzone, E.; Aloise, A.; Policicchio, A.; Agostino, R.G.; Migliori, M.; Giordano, G. Modelling of adsorption of textile dyes over multi-walled carbon nanotubes: Equilibrium and kinetic. *Chin. J. Chem. Eng*. **2017**, *25*, 523–532. https://doi.org/10.1016/j.cjche.2016.10.021.
34. Tanzifi, M.; Yaraki, M.T.; Karami, M.; Karimi, S.; Kiadehi, A.D.; Karimipour, K.; Wang, S. Modelling of dye adsorption from aqueous solution on polyaniline/carboxymethylcellulose/TiO_2 nanocomposites. *J. Colloid Interface Sci*. **2018**, *519*, 154–173. https://doi.org/10.1016/j.jcis.2018.02.059.
35. Krstic, V. Role of zeolite adsorbent in water treatment. Chapter 14. In *Handbook of Nanomaterials for Wastewater Treatment*, Elsevier: Amsterdam, The Netherlands, 2021; pp. 417–481.
36. Tran, H.N.; You, S.J.; Hosseini-Bandegharaei, A.; Chao, H.P. Mistakes and inconsistencies regarding adsorption of contaminants from aqueous solutions: A critical review. *Water Res*. **2017**, *120*, 88–116. https://doi.org/10.1016/j.watres.2017.04.014.
37. Lima, E.C.; Sher, F.; Guleria, A.; Saeb, M.R.; Anastopoulos, I.; Tran, H.N.; Hosseini-Bandegharaei, A. Is one performing the treatment data of adsorption kinetics correctly? *J. Environ. Chem Eng*. **2021**, *9*, 104813. https://doi.org/10.1016/j.jece.2020.104813.
38. Chahkandi, M. Mechanism of Congo red adsorption on new sol-gel-derived hydroxyapatite nano-particle. *Mater. Chem. Phys.* **2017**, *202*, 340–351. https://doi.org/10.1016/j.matchemphys.2017.09.047.

39. Tran, H.N.; Lima, E.C.; Juang, R.S.; Bollinger, J.C.; Chao, H.P. Thermodynamic parameters of liquid–phase adsorption process calculated from different equilibrium constants related to adsorption isotherms: A comparison study. *J. Environ. Chem. Eng.* **2021**, *9*, 106674. https://doi.org/10.1016/j.jece.2021.106674.
40. Imessaoudene, A.; Cheikh, S.; Bollinger, J.-C.; Belkhiri, L.; Tiri, A.; Bouzaza, A.; El Jery, A.; Assadi, A.; Amrane, A.; Mouni, L. Zeolite Waste Characterization and Use as Low-Cost, Ecofriendly, and Sustainable Material for MalachiteGreen and Methylene Blue Dyes Removal: Box–Behnken Design, Kinetics, and Thermodynamics. *Appl. Sci*. **2022**, *12*, 7587. https://doi.org/10.3390/app12157587.
41. Purkait, M.K.; Maiti, A.; DasGupta, S.; De, S. Removal of congo red using activated carbon and its regeneration. *J. Hazard. Mater.* **2007**, *145*, 287–295. https://doi.org/10.1016/j.jhazmat.2006.11.021.
42. Tu, N.T.T.; Thien, T.V.; Du, P.D.; Chau, V.T.T.; Mau, T.X.; Khieu, D.Q. Adsorptive removal of congo red from aqueous solution using zeolitic imidazolateframework–67. *J. Environ. Chem. Eng.* **2018**, *6*, 2269–2280. https://doi.org/10.1016/j.jece.2018.03.031.
43. Wu, Z.; Yuana, X.; Zhong, H.; Wang, H.; Jiang, L.; Zeng, G.; Wang, H.; Liu, Z.; Li, Y. Highly efficient adsorption of Congo red in single and binary water with cationic dyes by reduced graphene oxide decorated NH2-MIL-68(Al). *J. Mol. Liq.* **2017**, *247*, 215–229. https://doi.org/10.1016/j.molliq.2017.09.112.
44. Banerjee, S.; Chattopadhyaya, M.C. Adsorption characteristics for the removal of a toxic dye, tartrazine from aqueous solutions by a low cost agricultural by-product. *Arab. J. Chem.***2017**, *10*, S1629–S1638. https://doi.org/10.1016/j.arabjc.2013.06.005.
45. Polatoglu, I.; Cakicioglu-Ozkan, F. Aqueous interactions of zeolitic material in acidic and basic solutions. *Microporous Mesoporous Mater*. **2010**, *132*, 219–225. https://doi.org/10.1016/j.micromeso.2010.03.001.
46. Vimonses, V.; Lei, S.; Jin, B.; Chow, C.W.K.; Saint, C. Kinetic study and equilibrium isotherm analysis of Congo Red adsorption by clay materials. *J. Chem. Eng.* **2009**, *148*, 354–364. https://doi.org/10.1016/j.cej.2008.09.009.
47. Djomgoue, P.; Siewe, M.; Djoufac, E.; Kenfack, P.; Njopwouo, D. Surface modification of Cameroonian magnetite rich clay with Eriochrome BlackT. Application for adsorption of nickel in aqueous solution. *Appl. Surf. Sci*. **2012**, *258*, 7470– 7479. https://doi.org/10.1016/j.apsusc.2012.04.065.

48. Debnath, S.; Kitinya, J.; Onyango, M.S. Removal of Congo red from aqueous solution by two variants of calcium and iron based mixed oxide nano-particle agglomerates. *J. Ind. Eng. Chem*. 2014, *20*, 2119–2129. https://doi.org/10.1016/j.jiec.2013.09.041.
49. Carmona, M.E.R.; da Silva, M.A.P.; Ferreira Leite, S.G. Biosorption of chromium using factorial experimental design. *Process Biochem*. **2005**, *40*, 779–788. https://doi.org/10.1016/j.procbio.2004.02.024.
50. Bingol, D.; Tekin, N.; Alkan, M. Brilliant Yellow dye adsorption onto sepiolite using a full factorial design. *Appl. Clay Sci.* **2010**, *50*, 315–321. https://doi.org/10.1016/j.clay.2010.08.015.
51. Tran, H.N.; You, S.J.; Chao, H.P. Fast and efficient adsorption of methylene green 5 on activated carbon prepared from new chemical activation method. *J. Environ. Manag*. **2017**, *188*, 322–336. http://doi.org/10.1016/j.jenvman.2016.12.003.

Chapter VI. Synthesis of a TiO_2/zeolite composite: Evaluation of adsorption-photodegradation synergy for the removal of Malachite Green

The findings of this study have been published in the journal "*Nano-Structures & Nano-Objects*"

Ali Imessaoudene, Omar Mechraoui, Boubekeur Aberkane, Abderrahim Benabbas, Amar Manseri, Younes Moussaoui, Jean-Claude Bollonger, Abdeltif Amrane, Abdelhalim Zoukel and Lotfi Mouni. Synthesis of a TiO_2/zeolite composite: Evaluation of adsorption-photodegradation synergy for the removal of Malachite Green. *Nano-Structures & Nano-Objects*. **2024**, 38, *101191*

https://doi.org/10.1016/j.nanoso.2024.101191

Introduction

In this part of the thesis, based on the high adsorptive properties demonstrated by the LTA-type zeolite in Chapter V, this material was employed as a support for the TiO_2 semiconductor. The goal was to synthesize a versatile and sustainable composite capable of simultaneously functioning as both an adsorbent and photocatalyst for dye removal. This composite (TiO_2-Zeo) was synthesized using the solid-state dispersion method and thoroughly characterized. Characterization findings, showed that, for TiO_2-Zeo catalyst, the zeolitic matrix preserved its initial structure without any alteration, while its gap energy of 3.23 eV was similar to that of the starting TiO_2 material, showing that TiO_2 nanoparticles were simply deposited on the surface of the zeolite support. The main conclusions of this research are: (i) zeolite-supported TiO_2 phocatalysts proved to be more efficient than TiO_2 nanoparticles for the photo-discoloration of Malachite Green solution, without being too sensitive to the pH of the medium, (ii) due to their high adsorption properties, the introduction of zeolite in the composite can facilitate the migration and the preconcentration of dye molecules near the photoactive surface sites of TiO_2 to increase the photodegradation efficiency, and (iii) the adsorption and photodegradation processes in the TiO_2-Zeo photocatalyst exhibit a synergistic interaction, significantly enhancing the overall efficiency of organic pollutant removal. Therefore, it represents a promising photocatalyst for the abatement of organic pollution in water.

Chapter VI. Synthesis of a TiO_2/zeolite composite: Evaluation of adsorption-photodegradation synergy for the removal of Malachite Green

Abstract

Preparing by a simple method a versatile and sustainable material that can simultaneously perform effectively as an adsorbent/photocatalyst is a real challenge in wastewater treatment technology. In this work, a composite with 10% (wt%) TiO_2 nanoparticles supported on zeolite (TiO_2-Zeo) was synthesized by a facile-solid-state dispersion method, and characterized for their physicochemical, phase structure, microstructure, and optical properties. Characterization findings, showed that, for TiO_2-Zeo catalyst, the zeolitic matrix preserved its initial structure without any alteration, while its gap energy of 3.23 eV was similar to that of the starting TiO_2 material, showing that TiO_2 nanoparticles were simply deposited on the surface of the zeolite support. TiO_2-Zeo photocatalyst, as well as commercial TiO_2 nanoparticles, tested here as a photocatalyst model in view of comparison, were used for the removal of Malachite Green dye (MG) from aqueous solution. The adsorption and photodegradation potential of the catalysts was evaluated under the same operating conditions. It was found that the adsorption kinetics for the two materials were relatively slow, and the pseudo-first-order model can describe accurately the adsorption kinetics data. The equilibrium states were reached after 140 min and 150 min for MG/TiO_2-Zeo and MG/TiO_2 systems. At 0.5 $g.L^{-1}$ dose of TiO_2-Zeo, the adsorption capacity of MG at equilibrium, and the removal efficiency obtained with 25 $mg.L^{-1}$ and 35 $mg.L^{-1}$ were 41.2 $mg.g^{-1}$ (82.3%), and 46.9 $mg.g^{-1}$ (65.6%), respectively. Whereas, after 240 min UV irradiation, the obtained values in synergistic adsorption-photodegradation dye removal were superior, namely 47.4 $mg.g^{-1}$ (92.7%) and 63.6 $mg.g^{-1}$ (90.2%), respectively. On the other hand, within the range of operating conditions considered, the overall kinetic rate of synergistic adsorption-photodegradation was also simulated using the modified Elovich heterogeneous kinetic model in the two following scenarios: for strong and weak adsorption. Based on the goodness-of-fit criteria values obtained with the two used catalysts, the model appeared globally very consistent with kinetic data in both cases, with a perfect agreement in the strong adsorption case.

Keywords: TiO_2/zeolite composite; TiO_2 nanoparticles; Synergistic adsorption-photodegradation; Malachite Green removal; Kinetic modeling

1. Introduction

Nowadays, the rapid development of the world's industrial sector has led to more and more toxic contaminants in terms of quality and quantity, that are released in the natural water cycle, posing a serious problem for the aquatic ecosystem and humanity [1-4]. Dyes, potentially toxic metals and metalloids, pesticides, pharmaceutical compounds, organic solvents, and other pollutants are commonly identified in factory effluents [5-7]. Various types of synthetic dyes are manufactured in large quantities for the textile, paper, cosmetic and printing industries [8,9]. These industries are major consumers of water and are therefore considered to be the main sources of dyes hydrosphere pollution [10]. Dye substances in waters poses a significant threat to human health and aquatic ecosystems due to their recalcitrant, carcinogenicity, highly poisonous, and non-bio-degradable nature [11,12]. Therefore, it is crucial to treat dye effluents at their point of origin before discharging them into the mainstream. Since 1967, heterogeneous photocatalysis has been promoted as a viable technique for degrading organic refractive pollutants and for environmental remediation [13,14]. TiO_2 is the most extensively employed photocatalyst among the various types of semiconductors owing to its high photocatalytic activity, corrosion resistance, low toxicity, and inexpensive cost [15]. It is one of the simplest and most powerful catalysts for the removal of dyes and phenolic compounds from aqueous media [14]. However, the primary disadvantages of introducing TiO_2 nanoparticles into a slurry system (suspended TiO_2 particles) are their propensity to agglomerate into large particles in suspension, resulting in a decrease in the effective surface area and the catalytic efficiency, as well as the difficulties encountered in its effective recovery by filtration for further reuse [16]. Hence, a number of research investigated in depth the immobilization of TiO_2 nanoparticles on a variety of supports in order to overcome these shortcomings, enhance durability, and minimize treatment costs. Among others, activated carbon [17], glass beads [18], polymeric material [19], oxidized CS-GLA layer [20], clay [21], alginate-Bentonite beads [22]), silica nanofibers [23] and zeolite [24,25] might be mentioned.

Zeolite is an important kind of aluminosilicate porous material. It features uniform nano-sized pores and channels, superior adsorptive properties, relatively low cost and an eco-friendly nature [26,27]. Among the many application benefits of this mineral as photocatalysts support is that the cages and channels in crystalline zeolite can be used as constrained systems for the preparation of semiconductors (TiO_2) with controlled particle size and shape as well as the preconcentration of the substrate near the photoactive sites [28]. Zeolites are amphoteric in nature. The aluminum ions in the framework and charge balancing cations function as electron

acceptors (Lewis acids), while the oxygens in the framework, particularly Al (Si-O-Al oxygen), act as electron donors (Lewis bases) [29]. As a result, zeolitic matrix may be useful in controlling photo-induced charge transfer reactions [30]. Furthermore, the high electric field present in the zeolitic matrix may significantly contribute to delaying the back electron transfer reaction, which is the reason of poor quantum efficiency in most photocatalytic reactions [31].

In the photocatalysis process with TiO_2-supported catalysts, the adsorption and photodegradation synergy has been well recognized; nevertheless, regarding kinetics studies, to our knowledge, the overall removal rate of the target molecule with this hybrid process has not been previously investigated. When studying the photocatalysis removal kinetics of organic pollutants using this kind of photocatalyst, most researchers have either ignored or excluded adsorption kinetics, assuming that the adsorption-desorption process reached an equilibrium state. However, at least from a theoretical point of view, adsorption-desorption equilibria cannot be reached in photocatalytic reactions because the active species generated by photo-induced carriers continuously destroy the adsorbed molecules [32].

In the light of the previous discussion on the appropriate properties of TiO_2 as a photocatalyst and zeolite as a carrier, the present work aimed to synthesize zeolite-supported titania composite (TiO_2-Zeo) through a facile and efficient method, namely a solid-state dispersion method. To examine its physicochemical, phase structure, microstructure, and optical properties, various analytical methods were employed including X-ray diffraction (XRD), Fourier transform infrared (FT-IR) spectroscopy, scanning electron microscopy (SEM), energy dispersive X-ray spectroscopy (EDS), and diffuse reflectance spectroscopy (DRS). On the other hand, TiO_2-Zeo composite, alongside TiO_2 nanoparticles used as a photocatalyst model in view of comparison, were investigated for the removal of Malachite Green (MG) dye from aqueous solution in the same operating conditions. In addition, the kinetics of the adsorption-photodegradation synergy, adsorption, and photodegradation were measured independently to elucidate the interaction between adsorption and photodegradation, and the respective contribution of each of them to the overall synergy. Another specific objective of this study was to model the kinetics of MG removal by a synergistic process combining adsorption and photodegradation.

2. Materials and methods

2.1. Materials

Zeolite (Product Code 96096-100 G, Sigma-Aldrich, St. Louis, MO, USA) was utilized as received. TiO_2 powder and Malachite Green Oxalate (C.I. 42000) were purchased from Biochem Chemopharma (Cosne-Cours-sur-Loire, France). All other chemicals used in this work were of analytical grade and were obtained either from Sigma-Aldrich or Biochem Chemopharma. The working MG solutions were prepared by diluting the stock solution (1 $g.L^{-1}$) to the desired concentrations in deionized water. The natural pH of these solutions approximatively 4.0 and was not adjusted during experiments unless otherwise stated (effect of pH). Batch reactor of 1.25 L of capacity equipped with a cooling jacket was used in adsorption and photocatalytic experiments, and the UV light radiations was generated by 3 UV lamps (model PL-S 9w/10/2P Hg - Philips, made in Poland).

2.2. Photocatalyst preparation

A photocatalyst, zeolite-supported TiO_2 (TiO_2-Zeo) was prepared by the solid-state dispersion method that has been reported elsewhere [33] with a few modifications. First, in two separate beakers, 3 g of zeolite was added to 45 mL of ethanol and in the second 0.3 g of TiO_2 in 15 mL of ethanol. The two mixtures were agitated under ultrasonic (FALC Instruments, Italy) action for 30 min. Then, the two suspensions were mixed together and magnetically stirred for 4 h at room temperature to obtain a homogeneous mixture. The solvent was evaporated, and the obtained residue was dried at 110°C in an oven then calcined in a muffle furnace (Nabertherm, Germany) at 400°C for 6 h. This photocatalyst was prepared in such a way that the loaded amount of TiO_2 in zeolite was 10% (wt%).

2.3. Characterization

Characterization of zeolite and supported titania photocatalysts were conducted via different analytical techniques. The structure of the materials was investigated by X-ray Diffractometer (Malvern Panalytical, Empyrean, UK) operating at 45 kV and 40 mA, with a Ni filter and CuKα (λ = 1.54 Å) radiation. FT-IR spectroscopy was run with a Shimadzu IRAffinity-1 model (Japan) using the pressed KBr pellets method. The morphology of zeolite (Zeo) and zeolite-supported TiO_2 (TiO_2-Zeo) powders was characterized by using a Schottky field emission scanning electron microscope JEOL JSM-7610FPlus (Tokyo, Japan). The selected SEM parameters: beam energy, probe current and working distance, allowed us to

reveal the nanometer-scale surface structures. For the elemental analysis, we used the EDS (Energy Dispersive X-Ray Spectroscopy) system attached to the SEM: Bruker Quantax-200 (Berlin, Germany). The latter is composed by a silicon drift detector (SDD) XFlash-6/10 and Esprit 2.1 Software. Diffuse reflectance spectroscopic studies were carried out using Analytik Jena Specord 210 plus (Germany) equipped with an integrated sphere in a wavelength range from 280 to 900 nm at room temperature.

2.4. Green Malachite removal, preliminary tests

The effect of initial pH on the photo-discoloration of the dye solution was examined over a pH range from 4 to 10 under UV irradiation; the pHs at the end of the reaction (pH_f) were also measured. The initial pH was adjusted to the desired value by adding either HCl or NaOH solutions (0.1 M). On the other hand, at the natural MG solution pH (around 4.0), the Malachite Green removal effectiveness either by photolysis (with UV irradiation and without TiO_2-Zeo), adsorption (without UV and with TiO_2-Zeo), and photocatalysis (with UV and TiO_2-Zeo) process were evaluated and compared. In this study, all experiments were performed in duplicate, the results obtained were reproducible, and the maximum difference between the two response values was less than 3% of the mean. The mean values were reported here.

2.5. Evaluation of adsorption and photocatalytic performance

In the dark, adsorption experiments were carried out at 25°C in the batch reactor described above. One liter of dye solution of initial concentrations 25 $mg.L^{-1}$ and 35 $mg.L^{-1}$ was contacted with known amounts of the synthetized catalyst powder (0.1 g and 0.5 g). The suspensions were magnetically stirred at 500 rpm. Samples (5 mL) of the mixture were withdrawn at regular intervals and centrifuged at 1459 g-force for 10 min before MG concentration measurement at the absorbance of 618 nm using UV-vis spectrophotometer (Agilent Technologies Cary 60 UV–vis, USA). TiO_2 nanoparticles were also used in this section of the study as a model photocatalyst, and tested under the same operating conditions as those conducted for TiO_2-Zeo. The adsorption capacity q_t ($mg.g^{-1}$) and the discoloration efficiency E (%) at any time t were calculated using the equations Eq. (S1, S2) in the Supporting Data file.

The photocatalytic experiments were conducted at 25°C in which 1 L of MG solutions (25 $mg.L^{-1}$ and 35 $mg.L^{-1}$) and the photocatalysts (0.1 g and 0.5 g) were contacted and immediately stirred (500 rpm) and UV irradiated in the presence of bubbling oxygen to assure oxygen saturation. During the UV irradiation, 5 mL of the mixture was taken out at given time intervals and centrifuged for MG solution analysis. Here, the combined adsorption-

photodegradation performances were evaluated and the overall MG removal kinetics rate was examined.

For photocatalytic degradation of adsorbed MG on TiO_2-Zeo and TiO_2 surfaces, after 3 h dark adsorption, 5 mL solution was sampled at selected time intervals in the next 150 min under UV irradiation. For all the experiments, the initial pH of the MG solutions was around 4 and not adjusted.

The reusability of TiO_2-Zeo photocatalyst was evaluated over 3 consecutive cycles of use. After each cycle, the used catalyst was recovered after solid-liquid separation by filtration through 0.22 µm pore size membrane. The collected solid was then washed several times with ethanol and deionized water, and finally dried in an oven, stored in the desiccator until its next use.

3. Results and discussion

3.1. Photocatalyst characterization

Fig VI.1 shows the X-ray diffraction pattern of the synthesized zeolite-supported titania catalyst (TiO_2-Zeo), and for comparative purposes, the diffractogram of zeolite support (Zeo) was also included. As shown in Fig VI.1, practically the titania loading has not affected the zeolite crystallinity in the TiO_2-Zeo matrix. The characteristic XRD peaks of titania phases observed were preponderantly those attributed to anatase (ICSD: 063711) at 2Θ = 25.31° (101), 48.04° (200) and 55.07° (211). Importantly, no signal can be assigned to the rutile phase. On the other hand, the peaks identified in the zeolite support were those specific to LTA-type zeolite (ICSD: 024901). FT-IR spectra of the zeolite and TiO_2-Zeo materials were investigated in the wavenumber range of 400-4000 cm^{-1} and only the results in the range of 400-1800 cm^{-1} are shown in Fig VI.2. For the two samples, the absorption bands in the region from 1663 to 3700 cm^{-1} indicated the presence of water molecules or OH group in zeolite [34]. As illustrated in Fig VI.2, all these materials showed characteristic vibrations assigned to the zeolitic structure. The strongest wide vibration peak observed at 945-1120 cm^{-1}, the absorption band from 651 to 684 cm^{-1} and from 449 to 482 cm^{-1} can be attributed to the T-O (T= Si or Al) asymmetrical stretching mode, to the symmetrical stretching and to (O-T-O) deformation mode of the internal bonds of TO_4 tetrahedra, respectively [35,36]. Moreover, peaks assigned to the external bonds of the TO_4 tetrahedra can also be noticed in the region from 515 to 592 cm^{-1} which became relatively broader for TiO_2-Zeo. These vibrations were assigned to those of double rings consisting of four and six atoms [35]. The peak of low intensity that appeared only

in the spectrum of TiO_2-Zeo at 418 cm^{-1} can be reasonably assigned to Ti-O-Ti bending vibration [37]. Therefore, it is clear that TiO_2 nanoparticles were simply deposited on the surface of the zeolite rather than the Ti being incorporated into the zeolitic framework.

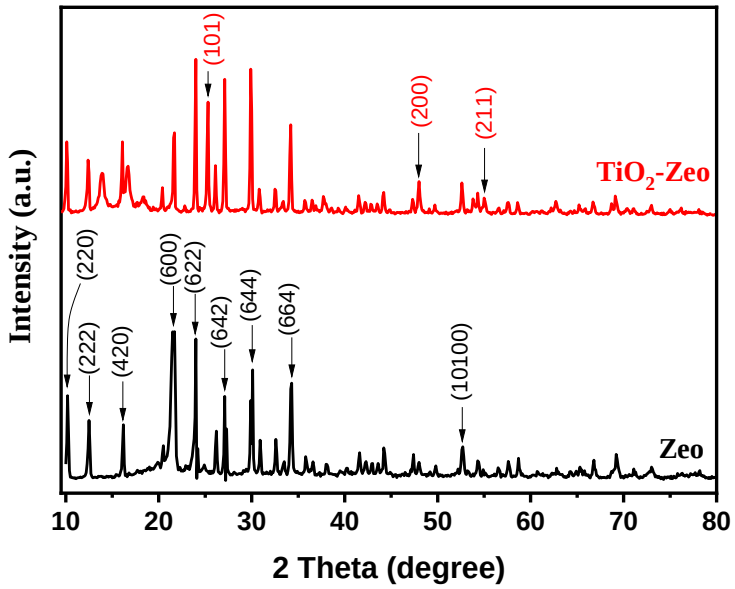

Fig VI.1. XRD patterns of the TiO_2-Zeo catalyst and zeolite.

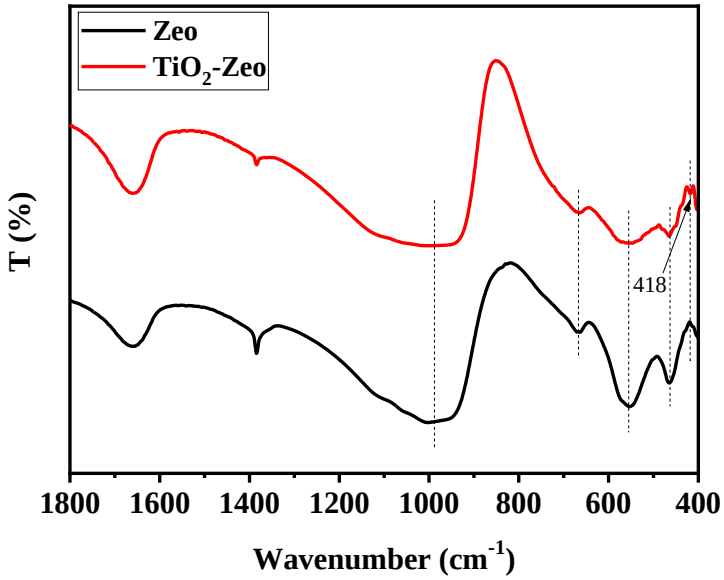

Fig VI.2. FT-IR spectra of the TiO_2-Zeo catalyst and zeolite.

Fig VI.3 shows the SEM micrographs of the zeolite and zeolite-supported titania materials. The micrographs of the two solids (Fig VI.3(a) and (b)) showed micrometer-sized zeolitic particles with a cubic morphology, which are typical of a LTA-type zeolite [38]. This remark was well in agreement with that of the characteristics of zeolite XRD pattern. In addition, the distribution of TiO_2 nanometer-sized particles on the external surface of the zeolite support was roughly uniform (Fig VI.3(b)) which is advantageous for the photocatalytic properties of the TiO_2-Zeo material. The pure TiO_2 was composed of nanoparticles of different sizes (Fig VI.3(b)). The calcination stage during composite synthesis can have an effect on particle growing. Although LTA-type zeolite in the composite was coated with 10% TiO_2, the shape of LTA-type zeolite was maintained intact in TiO_2-Zeo. The EDS spectra of Zeo and TiO_2-Zeo given in Fig VI.3(c)-(d) and the surface elemental composition in wt% of these materials (Table VI.1) demonstrated that the TiO_2 nanoparticles have been well dispersed/attached on the external surface of the zeolite particles and the Ti content is 10.02%.

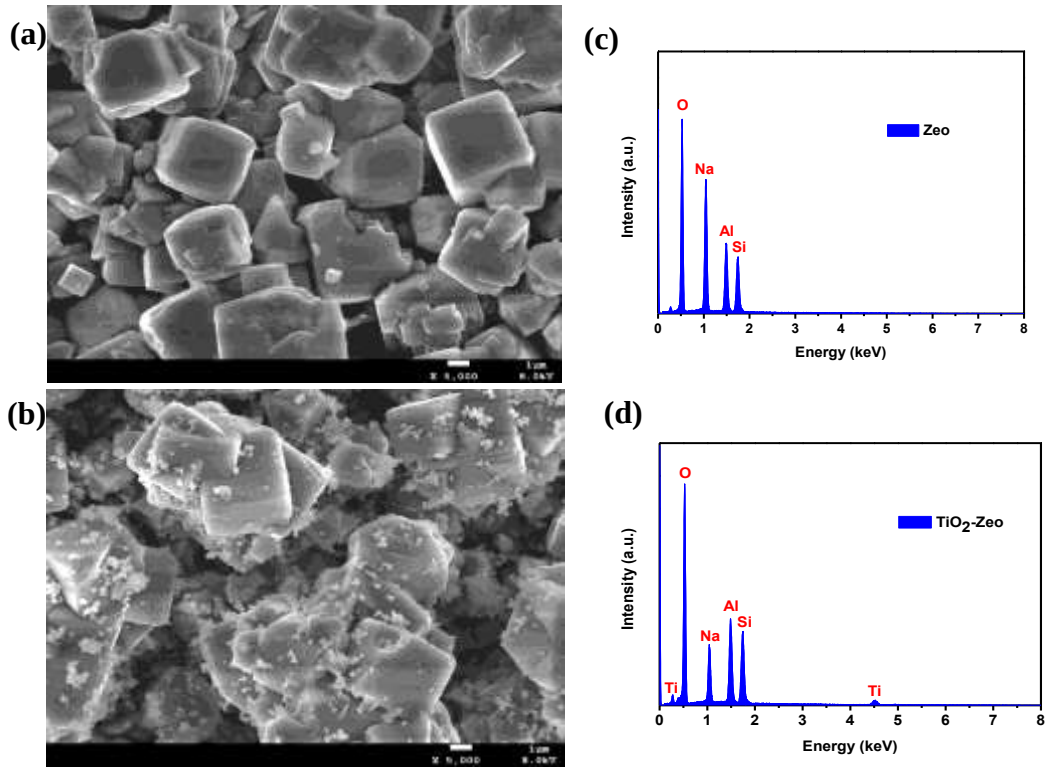

Fig VI.3. SEM micrographs and EDS images of zeolite (a), (c), and TiO_2-Zeo catalyst (b), (d).

Fig VI.4(a) displays UV–vis diffuse reflectance spectra of the zeolite, TiO_2 and zeolite-supported TiO_2. As clearly shown in this illustration, there was a close spectral profile similarity between TiO_2 and TiO_2-Zeo with a very slight shift of the TiO_2-Zeo spectrum towards the short wavelengths as has been shown by other researchers [34]. Also, one can notice that for $\lambda > 400$ nm, practically most of radiation was reflected by TiO_2 and TiO_2-Zeo materials. On the other hand, for $\lambda < 320$ nm, the R (%) values were the lowest which means that the incident radiations are almost completely absorbed and have sufficient energy for the electron/hole pair generation. The band-gap energy for TiO_2 and TiO_2-Zeo semiconductors were estimated using the reflectance data given in Fig VI.4(a). For this purpose, F(R), the Kubelka-Munk function was used Eq. (1) [39].

$$F(R) = \frac{(1-R)^2}{2R} \qquad (1)$$

where R is taken here as the measured absolute reflectance of the photocatalysts.

On the other side, the incident photon energy E can be calculated as (Eq. (2)):

$$E(eV) = \frac{1240.7}{\lambda\,(nm)} \qquad (2)$$

where λ is the incident radiation wavelength (nm). The optical band gap energy value can be calculated from the linear fitting by a straight line of $(F(R) \times E)^{1/2}$ vs. E (Fig VI.4(b)). The obtained gap energies for the two materials were practically identical and equal to 3.23 eV (384 nm) which is the typical anatase gap energy [40]. This result is also consistent with those discussed previously, showing that TiO_2 nanoparticles are simply deposited on the surface of zeolite microparticles.

Table VI.1
Surface elemental composition of Zeo and TiO_2-Zeo materials (wt%).

Elements	O	Si	Na	Al	Ti	Total
Zeo	42.46	21.70	21.48	14.36	-	100 %
TiO_2-Zeo	46.96	21.54	8.63	12.85	10.02	100 %

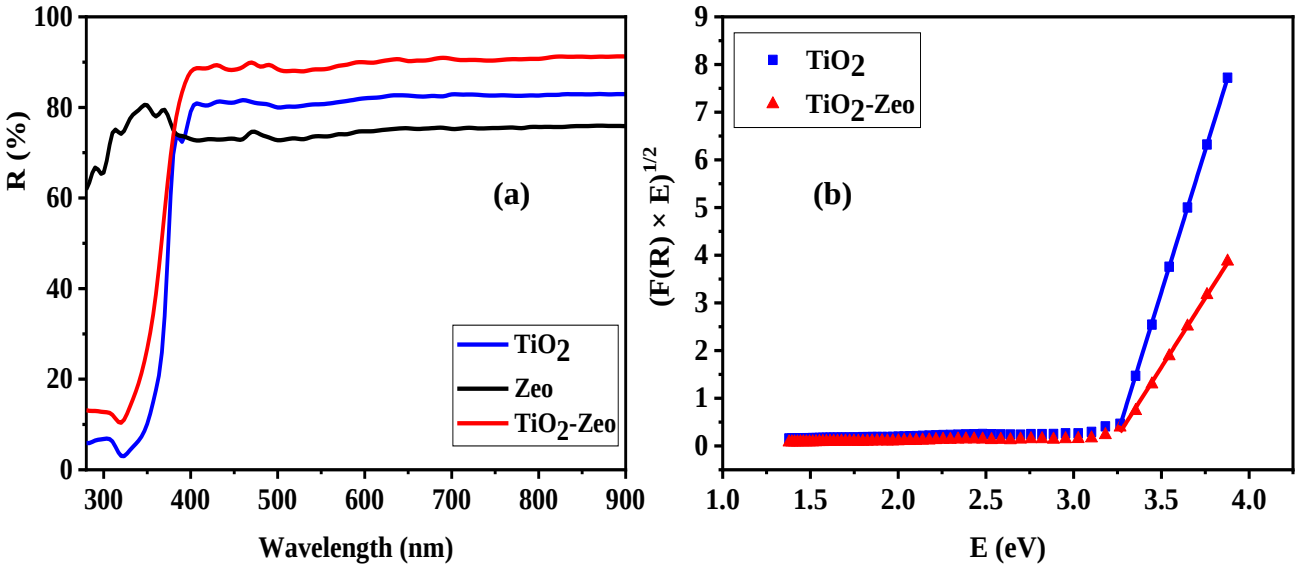

Fig VI.4. Diffuse reflectance spectra of TiO_2 nanoparticles, zeolite and TiO_2-Zeo catalyst.

3.2. Preliminary tests results

According to the results obtained from the investigation of the effect of the pH (Fig VI.5), it can be seen that the photo-discoloration of the dye solution using TiO_2-Zeo catalyst was not strongly affected by the initial pH of the MG solution. The photo-discoloration efficiencies obtained with 25 $mg.L^{-1}$ of the initial concentration of the MG solution at the initial pH values of 4, 7 and 10 were 86.4%, 97.9% and 91.6%, respectively. This finding can be explained considering the intrinsic characteristics of the zeolitic support [41]. When the zeolite is contacted with the aqueous solution at acidic pH, it can easily exchange its own Na^+ ions with H_3O^+ ions, resulting an increase in the final pH (pH_f) of the mixture. On the other hand, at an alkaline pH of the solution, the OH^- ions can neutralize the neutral zeolite surface, leading to a decrease in the final pH (see blue columns in Fig VI.5). Therefore, the zeolite material can act as a moderator of the pH of the medium, offering another major advantage as a carrier for pH-sensitive catalyst.

The one-on-one testing of the MG removal by photolysis, adsorption, and photocatalysis gives the results shown in Fig VI.6. According to this figure, without the catalyst, only about 3.7% of MG was degraded in the blank control after 240 min of illumination indicating negligible self-photodegradation of MG; the dye is stable under UV irradiation. However, at this time, about 86.4% of the dye was removed by TiO_2-Zeo under light against 66.7% in the dark, indicating that the MG photo-discoloration activity is mainly connected to adsorption

ability on the TiO_2-Zeo surface. As also reported by Luo et al. [42], the improvement of the adsorption of the target molecule on the catalyst was very beneficial for the photocatalytic degradation reaction due to the fact that photocatalytic reactions occur mainly on the catalyst surface. Hypothetical schemes for dye elimination in the above-mentioned applications are described in the Supplementary Information.

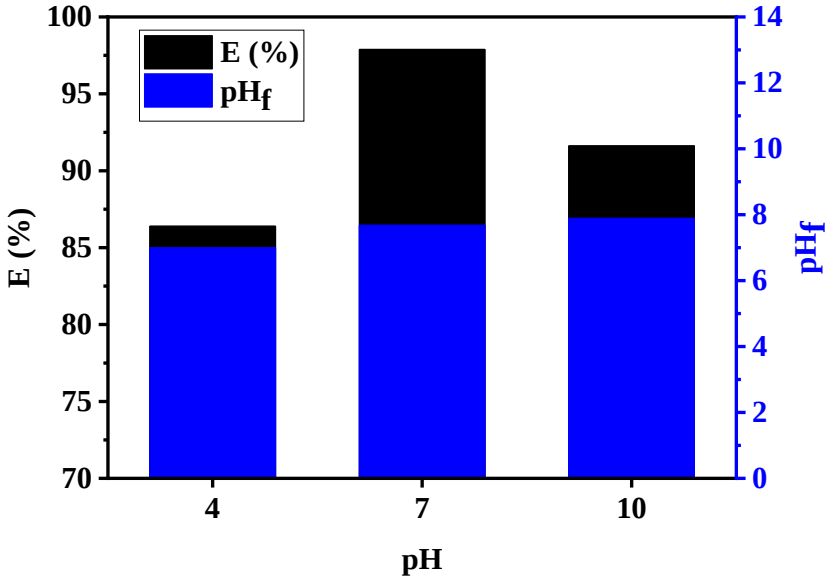

Fig VI.5. Effect of initial solution pH on MG photo-discoloration: C_0 = 25 mg.L^{-1}, TiO_2-Zeo photocatalyst dose = 0.1 g.L^{-1}, t = 240 min, T = 25°C and under UV irradiation.

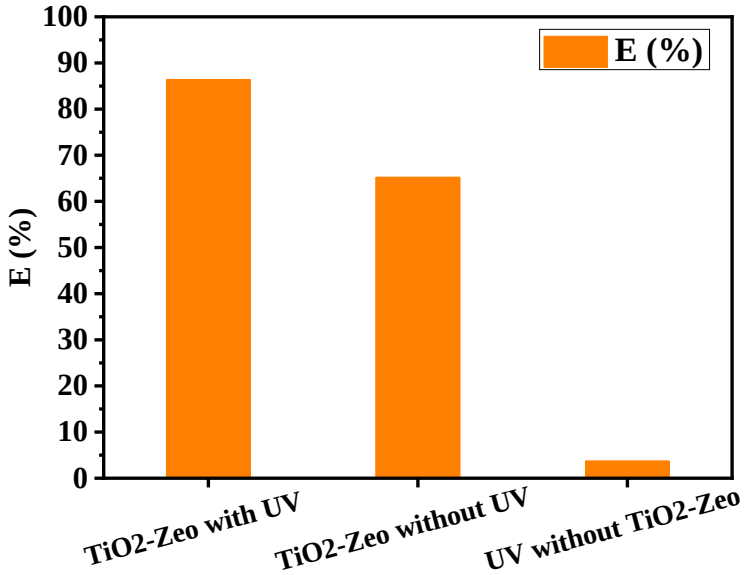

Fig VI.6. MG removal efficiency in photocatalysis, adsorption, and photolysis cases: C_0 = 25 mg.L^{-1}, TiO_2-Zeo dose = 0.1 g.L^{-1}, pH = 4, T = 25°C at t = 240 min.

3.3. Adsorption studies

In aqueous phase adsorption, the pseudo-first-order kinetic model (PFOM) is mostly used by the authors to mathematically describe the intrinsic adsorption rate constant [43]. This model can be described in differential form by the following adsorption rate equation:

$$r_{ads} = -dC_t/dt = k_{ads}(C_t - C_e) \qquad (3)$$

where r_{ads} is the adsorption rate and k_{ads} is the adsorption rate constant (min^{-1}). C_0, C_t, and C_e are the MG concentrations in the bulk solution at time 0, *t*, and equilibrium, respectively.

Origin 2019b® software was employed in this work to simulate nonlinear fittings of experimental data to the integrated form of the corresponding kinetic models and for constants calculation. The models' fit was assessed using R^2, RMSE and Chi-Sqr as goodness-of-fit criteria [44,45], the corresponding equations are shown in Supporting Information (Eq. (S9-S11)). For the MG adsorption experiments under various operating conditions, the obtained results are shown in Table VI.2 and Fig VI.7.

On the basis of R^2, RMSE and Chi-Sqr values obtained, the pseudo-first-order model can describe accurately the adsorption kinetics of MG on TiO_2-Zeo and TiO_2 (Table VI.2). On the other side, according to the k_{ads} values obtained, it can be seen that MG adsorption kinetics on the two solids tested were relatively slow. The equilibrium states were reached after 140 min and 150 min for MG/TiO_2-Zeo and MG/TiO_2 systems, respectively. The adsorption process could be divided into three steps for the two adsorbents [46,47]. In the first contact times, MG uptake sharply increased, this can be related to the number of initially vacant surface sites at the beginning. Over time, repulsive forces between the cationic dye molecules adsorbed and the solution phase make the remaining vacant surface sites more difficult to be occupied; thus, the adsorption slows down and finally levels off. As can be considered obvious, increasing the initial concentration provides more driving force to overcome the mass transfer resistance between the solid and liquid phases, then the q_e values increase [48]. At initial pH of around 4, MG uptake on the surface of TiO_2-Zeo and TiO_2 materials may be due to the interaction that occurred between the protonated SOH_2^+ site (S = Al, Si or Ti atom of the surface) and the amines or aromatic groups of the MG molecules [41,49].

Table VI.2
Pseudo-first-order kinetic constants for MG adsorption on TiO_2-Zeo and TiO_2: pH = 4 and T = 25°C.

Parameters / adsorbents	C_0 (mg.L^{-1})	m (g)	k_{ads} (mn^{-1})	R^2	RMSE	Chi-Sqr
TiO_2-Zeo	25	0.1	1.95×10^{-2}	0.986	6.100	37.209
	25	0.5	2.14×10^{-2}	0.989	1.329	1.766
	35	0.1	1.56×10^{-2}	0.989	6.933	48.067
	35	0.5	1.56×10^{-2}	0.976	2.422	5.864
TiO_2	25	0.1	1.22×10^{-2}	0.956	3.594	12.915
	25	0.5	9.90×10^{-3}	0.974	0.749	0.561
	35	0.1	2.74×10^{-2}	0.998	0.606	0.367
	35	0.5	1.91×10^{-2}	0.985	0.535	0.286

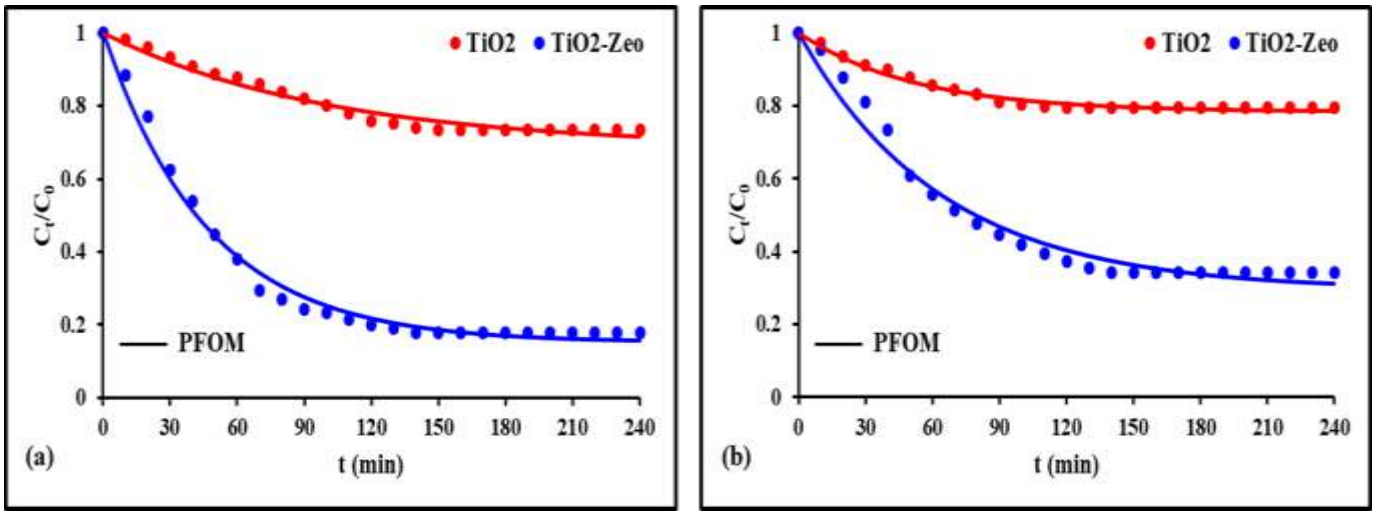

Fig VI.7. PFOM Kinetic model simulation to the adsorption experimental data (symbols) of MG on TiO_2-Zeo and TiO_2 in dark: C_0 = 25 mg.L^{-1} (a) and 35 mg.L^{-1} (b) with 0.5 g.L^{-1} samples dose at pH = 4 and T = 25°C.

3.4. MG removal by the combined adsorption-photodegradation process

Table VI.3 shows the MG removal yields E (%) and the correspondent adsorption capacity q (mg.g^{-1}) obtained at the two initial dye concentrations (25 and 35 mg.L^{-1}) for the two catalysts tested at the dose of 0.1 and 0.5 g.L^{-1}, at pH close to 4, and after 240 min of solid samples / dye solutions contact time, under light exposure or in the dark.

According to Table VI.3, with 0.1 g.L^{-1} samples dose and under UV irradiation, TiO_2-Zeo exhibited a high photo-discoloration activity of MG solutions even at relatively high initial concentrations, removing 86.4% and 85.6% of the dye at initial concentrations of 25 and 35 mg.L^{-1}, respectively, compared to 74.7% and 69.1% with the suspended TiO_2. According to the findings of trials conducted in the dark, TiO_2-Zeo demonstrated remarkable MG adsorption capacity. These results can be explained by the fact that the synthesized catalyst TiO_2-Zeo

contains a significant amount of zeolite, which is known to be a powerful MG adsorbent even for solutions at pH about 4 [50,51]. In contrast, the adsorption of MG on the surface of TiO_2 nanoparticles was relatively poor. This result is consistent with the findings of the adsorption kinetics investigation (Fig VI.7) and those of other authors [49]. At a relatively high dosage of samples (0.5 $g.L^{-1}$), the combined adsorption-photodegradation performance of both catalysts towards the target molecule were substantial and comparable. In addition, the q_{240} values (for a 240 min contact time) of TiO_2-Zeo and TiO_2 increased dramatically between adsorption (in the dark) and the combined adsorption-photodegradation process experiments for all combinations of operating conditions (Table VI.3). This indicates a significant photodegradation activity of MG molecules by the TiO_2 nanoparticles in TiO_2-Zeo composite under these conditions, showing that dye removal was not mainly due to adsorption but to the synergy between the two processes, photodegradation and adsorption.

Table VI.3
Comparison of MG removal efficiency and the corresponding q_{240} obtained by adsorption and combined process with TiO_2-Zeo and TiO_2 for a 240 min contact time: pH = 4 and T = 25°C.

Samples	Parameters	Samples dose ($g.L^{-1}$)	C_0 = 25 $mg.L^{-1}$		C_0 = 35 $mg.L^{-1}$	
			In the dark	Under UV light	In the dark	Under UV light
TiO_2-Zeo	E_{240} (%)	0.1	66.7	86.4	62.0	85.6
	q_{240} ($mg.g^{-1}$)		165.6	201.9	211.9	279.8
TiO_2	E_{240} (%)		18.6	74.7	14.8	69.1
	q_{240} ($mg.g^{-1}$)		48.0	186.8	53.1	236.3
TiO_2-Zeo	E_{240} (%)	0.5	82.3	92.7	65.6	90.2
	q_{240} ($mg.g^{-1}$)		41.2	47.4	46.9	63.6
TiO_2	E_{240} (%)		26.4	96.7	20.5	89.4
	q_{240} ($mg.g^{-1}$)		13.3	47.9	14.2	61.6

The modeling of MG photo-discoloration kinetics by the combined adsorption-photodegradation process was undertaken and the commonly first-order and modified Elovich kinetic models were used to simulate the overall removal rates of MG by the two photocatalysts in question. The heterogeneous model (modified Elovich) is controlled by multiple processes (i.e., adsorption and photodegradation) [32]. These models' governing equations can be expressed as follows:

- First-order kinetic model

$$r = -dC_t/dt = k_1 C_t \qquad (4)$$

- Modified Elovich kinetic model

$$r = -dC_t/dt = k_e C_0 e^{-\beta(C_0 - C_t)} \qquad (5)$$

where r is the overall photo-discoloration rate of MG; k_1 (min^{-1}), k_e (min^{-1}) represent the rate constants of the first-order, and the modified Elovich models, respectively; β is a constant inversely proportional to the removal capacity, since the more its value is high, the more the MG removal rate decelerates with time. The integrated forms of Eqs. (3, 4, 5) are given by Eq. (S12, S13, S14), respectively. The calculated parameters of Eq. 4 and Eq. 5 are shown in Table VI.4.

Table VI.4
Optimal fitting parameters of first-order and modified-Elovich kinetics models for MG removal by synergistic adsorption-photodegradation with 0.5 $g.L^{-1}$ catalysts dose: pH = 4 and T = 25°C.

Kinetic models		*First-order*	*Modified-Elovich*				
Parameters Materials	C_0 ($mg.L^{-1}$)	k_1 (mn^{-1})	k_e (mn^{-1})	B	R^2	*RMSE*	*Chi-Sqr*
TiO_2-*Zeo*	25	1.41×10^{-2}	/	/	0.992	0.582	0.339
	25	/	2.18×10^{-2}	0.10	0.999	0.199	0.039
TiO_2	25	8.40×10^{-3}	/	/	0.959	1.308	1.712
	25	/	5.84×10^{-3}	5.93×10^{-3}	0.999	0.257	0.066
TiO_2-*Zeo*	35	9.75×10^{-3}	/	/	0.978	1.135	1.287
	35	/	1.58×10^{-2}	7.81×10^{-2}	0.998	0.328	0.107
TiO_2	35	7.68×10^{-3}	/	/	0.968	1.527	2.332
	35	/	5.70×10^{-3}	8.22×10^{-3}	0.994	0.663	0.440

According to Table VI.4 and based on the goodness-of-fit criteria, the modified Elovich model fitted the kinetic data more accurately than the first-order model for both photocatalysts evaluated under various experimental settings. It became clear that MG removal by the photocatalysts was a synergistic process of adsorption and photodegradation, rather than a simple adsorption or photodegradation mechanism. Currently, a number of studies have shown that the modified Elovich model is very efficient to simulate the photocatalysis kinetics data and elucidate this synergy [32,52-57].

As also displayed in Table VI.4, at a dose of 0.5 $g.L^{-1}$, k_e values of TiO_2-Zeo (k_e = 2.18×10^{-2} and 1.58×10^{-2} min^{-1}) were greater than those of TiO_2 (k_e = 5.84×10^{-3} and 5.70×10^{-3} min^{-1}) at 25 $mg.L^{-1}$ and 35 $mg.L^{-1}$, respectively. The initial rate of MG removal by TiO_2-Zeo was 3.73 and 2.77 times higher than with TiO_2 at theses concentrations, respectively. The relatively higher β value obtained at the concentration of 25 $mg.L^{-1}$ with TiO_2-Zeo (β = 0.1) compared to that with TiO_2 (β = 5.93×10^{-3}), did not significantly affect the MG removal rate with TiO_2-Zeo when compared to TiO_2 during the selected reaction time (Fig VI.8(a)). This can be explained by the significant disparity in their initial rates. For a concentration of 35 $mg.L^{-1}$, the obtained values of β were 7.81×10^{-2} with TiO_2-Zeo versus 8.22×10^{-3} with TiO_2; the reaction rates with the two catalysts became closer over the time until becoming equal at t = 137 min (Fig VI.8(b)). Throughout the chosen reaction time, the overall rate of dye removal at 0.5 $g.L^{-1}$ of TiO_2-Zeo was faster than with TiO_2 (Fig VI.8).

Therefore, TiO_2-Zeo material, specifically at 10% mass ratio (TiO_2/Zeolite), is a promising adsorbent/photocatalyst composite system for MG photo-discoloration due to its facile synthesis and excellent removal efficiency with a relatively fast kinetics rate.

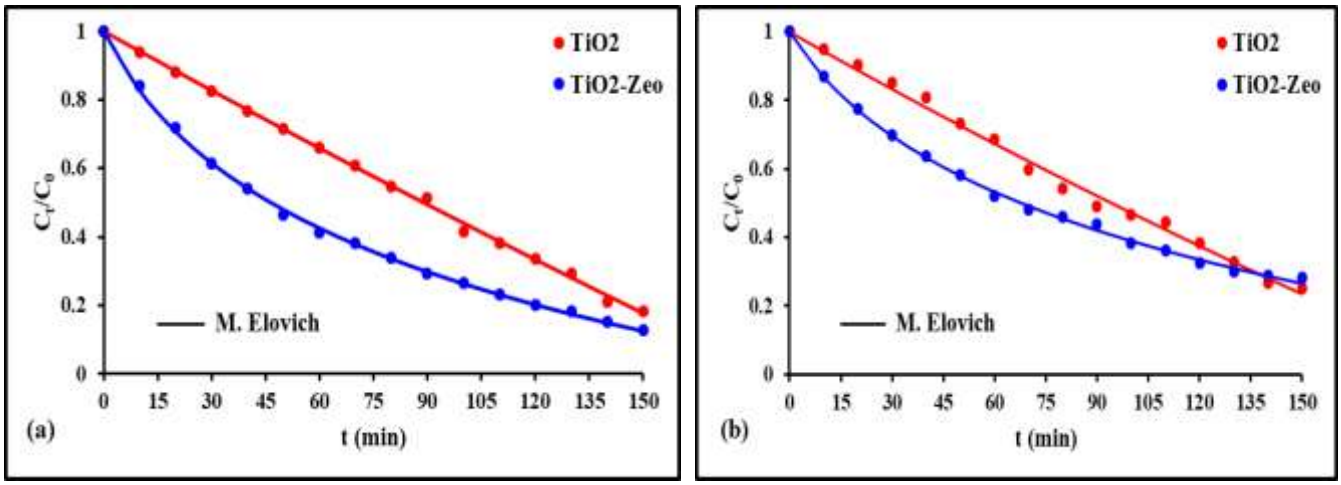

Fig VI.8. Modified-Elovich kinetic model simulation to the experimental data (symbols) of MG removal by synergistic adsorption-photodegradation for the two photocatalysts (0.5 $g.L^{-1}$): C_0 = 25 $mg.L^{-1}$ (a) and 35 $mg.L^{-1}$ (b), pH = 4 and T = 25°C.

3.5. TiO_2-Zeo reusability test

The reusability of TiO_2-Zeo photocatalyst was examined through three consecutive cycles of combined adsorption-photodegradation removal of MG. It was found that the experimental data kinetics for each reuse cycle agreed very well with the modified Elovich model (Fig VI.9) with a good value of R^2, RMSE and Chi-Sqr (Table VI.S2). On the other hand, the photo-discoloration efficiencies (*E)* obtained at 25 $mg.L^{-1}$ of MG solution and after 150 min of

irradiation were 87.1%, 76.1%, and 64.0% for the first, second, and third removal of MG, respectively against 71.7%, 65.9%, and 58.6% at 35 $mg.L^{-1}$. From this, the TiO_2-Zeo catalyst provides stable properties during the photocatalytic process.

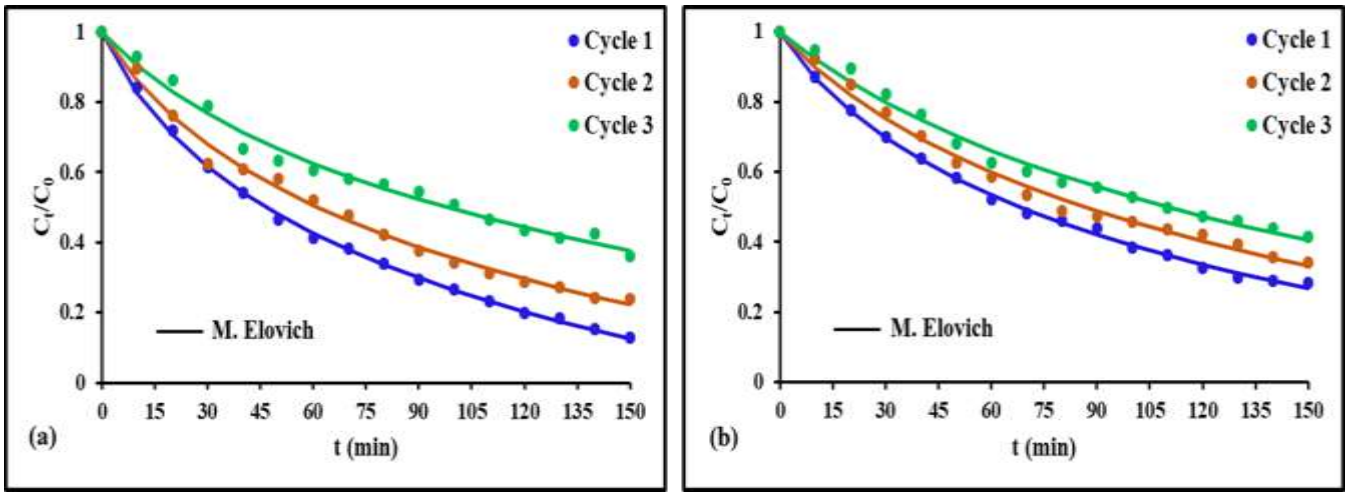

Fig VI.9. Reusability of TiO_2-Zeo with different initial concentration of MG: C_0 = 25 $mg.L^{-1}$ (a) and 35 $mg.L^{-1}$ (b), pH = 4, T = 25°C and photocatalyst dose = 0.5 $g.L^{-1}$.

3.6. Surface MG photodegradation

The change in MG concentration C_t as a function of time was simulated with respect to the models given Eq. 4 and Eq. 5. The obtained results are summarized in Table VI.5. Although the values of the goodness-of-fit criteria obtained for the two models were very satisfactory, they were on the whole relatively better for the first-order model (Table VI.5 and Fig VI.10). In other words, this finding indicates that the MG surface degradation process was dominated by the photodegradation step, which was slower compared to adsorption ($k_1 < k_{ads}$) (see Table VI.2 and Table VI.5). In this study, the performance of modified Elovich's model can also be appreciated in the representation of the kinetics data in a very satisfactory way in the following two extreme situations: when adsorption is strong, as in the case of the combined process, and if adsorption is weak, as in the case of surface photodegradation where the k_e values obtained were close to those of k_1 (Table VI.5).

Table VI.5
Optimal fitting parameters of first-order and Modified-Elovich kinetics models for MG removal by surface MG photodegradation under UV irradiation with 0.5 $g.L^{-1}$ catalysts dose: pH = 4 and T = 25°C.

Kinetics models		First-order	Modified-Elovich				
Parameters / Materials	C_0 ($mg.L^{-1}$)	k_1 (mn^{-1})	k_e (mn^{-1})	β	R^2	*RMSE*	*Chi-Sqr*
TiO_2-Zeo	25	4.51×10^{-3}	/	/	0.996	6.45×10^{-3}	4.16×10^{-5}
	25	/	4.35×10^{-3}	1.74	0.996	6.48×10^{-3}	4.20×10^{-5}
	35	3.79×10^{-3}	/	/	0.986	5.96×10^{-2}	3.55×10^{-3}
	35	/	3.46×10^{-3}	0.20	0.988	5.84×10^{-2}	3.41×10^{-3}
TiO_2	25	4.32×10^{-3}	/	/	0.998	1.56×10^{-1}	2.43×10^{-2}
	25	/	4.46×10^{-3}	6.64×10^{-2}	0.998	1.61×10^{-1}	2.61×10^{-2}
	35	1.6×10^{-3}	/		0.996	1.57×10^{-1}	2.45×10^{-2}
	35	/	1.55×10^{-3}	2.11×10^{-2}	0.996	1.61×10^{-1}	2.58×10^{-2}

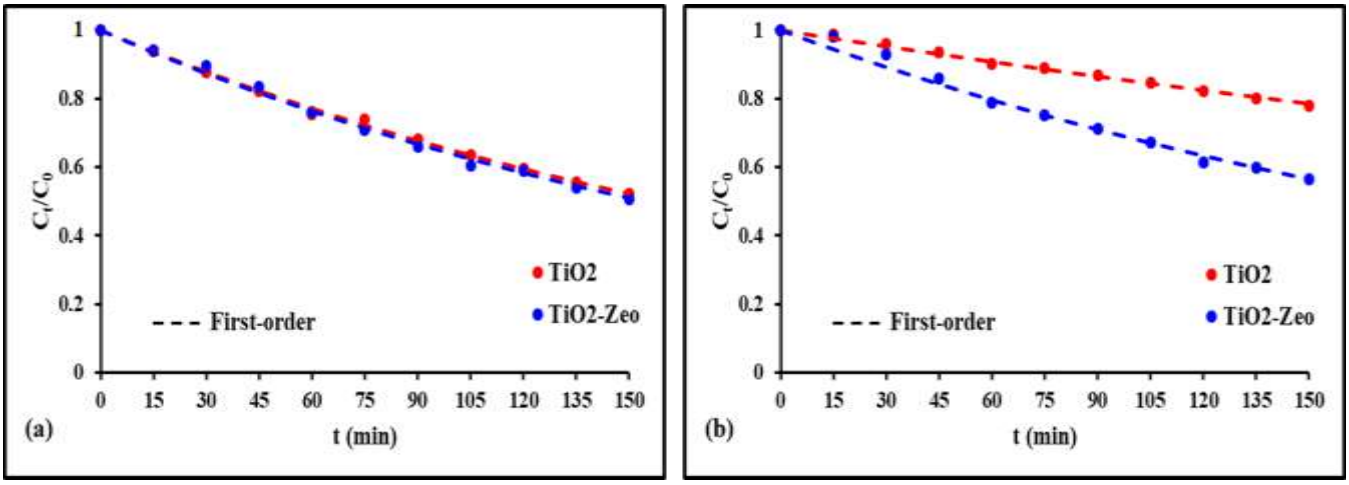

Fig VI.10. Surface degradation kinetics of adsorbed MG by TiO_2-Zeo and TiO_2 under UV irradiation: C_0 = 25 $mg.L^{-1}$ (a) and 35 $mg.L^{-1}$ (b) and with 0.5 $g.L^{-1}$ catalysts dose (pH = 4 and T = 25°C).

4. Conclusions

In conclusion, zeolite-supported TiO_2 catalysts, prepared via the solid-state dispersion method, is a simple way to produce active photocatalysts. Under UV irradiation, it showed to be more efficient than simple adsorption (in the dark) or photochemical degradation for MG solution discoloration, without being too sensitive to the pH of the medium. The optical properties of the synthesized TiO_2-Zeo catalyst and the commercial TiO_2 showed that LTA-type zeolite used as an inert material did not affect the titania band gap. On the other hand, due to its high adsorption properties, the introduction of zeolite can facilitate the migration and the preconcentration of MG molecules near the photoactive surface sites to increase the photodegradation efficiency. The TiO_2-Zeo material showed high synergistic adsorption-

photodegradation performances and hence is a promising photocatalyst for organic pollution abatement in water.

CRediT authorship contribution statement

Omar Mechraoui: Resources, Formal analysis, Data curation. **Ali Imessaoudene:** Writing-review & editing, Writing-original draft, Methodology, Investigation, Formal analysis, Data curation, Conceptualization. **Lotfi Mouni:** Writing-review & editing, Validation, Supervision, Methodology, Formal analysis. **Younes Moussaoui:** Resources, Formal analysis, Data curation. **Amar Manseri:** Resources, Formal analysis, Data curation. **Abderrahim Benabbas:** Resources, Formal analysis, Data curation, Conceptualization. **Boubekeur Aberkane:** Resources, Formal analysis, Data curation. **Abdeltif Amrane:** Writing-review & editing, Validation, Formal analysis. **Jean-Claude Bollinger:** Writing-review & editing, Validation, Formal analysis. **Abdelhalim Zoukel:** Resources, Formal analysis, Data curation.

Declaration of competing interest

The authors declare no conflict of interest.

Data availability

Data is contained within the article or Supplementary data.

Acknowledgements

The authors acknowledge the Center for Scientific and Technical Research in Physicochemical Analysis (CRAPC) located at Bou Ismaïl, Tipaza, Algeria for DRS analysis.

References

[1] Z. Yin, F. Yuan, M. Li, M. Xue, D. Zhou, Y. Chen, X. Liu, Y. Luo, Z. Hong, C. Xie, J. Ou, Self-cleaning, underwater writable, heat-insulated and photocatalytic cellulose membrane for high-efficient oil/water separation and removal of hazardous organic pollutants, Prog. Org. Coat. 157 (2021), 106311, https://doi.org/10.1016/j.porgcoat.2021.106311

[2] Z. Yin, F. Yuan, M. Xue, Y. Xue, Y. Xie, J. Ou, Y. Luo, Z. Hong, C. Xie, A multifunctional and environmentally safe superhydrophobic membrane with superior

oil/water separation, photocatalytic degradation and anti-biofouling performance, J. Colloid Interface Sci. 611 (2022) 93-104, https://doi.org/10.1016/j.jcis.2021.12.070

[3] Z. Yin, M. Li, Z. Li, Y. Deng, M. Xue, Y. Chen, J. Ou, S. Lei, Y. Luo, C. Xie, A harsh environment resistant robust $Co(OH)_2$@stearic acid nanocellulose-based membrane for oil-water separation and wastewater purification, J. Environ. Manag. 342 (2023), 118127, https://doi.org/10.1016/j.jenvman.2023.118127

[4] K. Liu, Z. Yin, R. Luo, B. Qiu, Y. Chen, C. Yang, Y. Luo, Z. Hong, M. Xue, Durable $Co(OH)_2$/stearic acid-based superhydrophobic/superoleophilic nanocellulose membrane for highly efficient oil/water separation and simultaneous removal of soluble dye, Ind. Crops Prod. 203 (2023), 117190, https://doi.org/10.1016/j.indcrop.2023.117190

[5] A. Reghioua, D. Barkat, A.H. Jawad, A.S. Abdulhameed, M.R. Khan, Synthesis of Schiff's base magnetic crosslinked chitosan-glyoxal/ZnO/Fe_3O_4 nanoparticles for enhanced adsorption of organic dye: Modeling and mechanism study, Sustain. Chem. Pharm. 20 (2021), 100379, https://doi.org/10.1016/j.scp.2021.100379

[6] A.H. Jawad, U.K. Sahu, N.A. Jani, Z.A. ALOthman, L.D. Wilson, Magnetic crosslinked chitosan-tripolyphosphate/MgO/Fe_3O_4 nanocomposite for reactive blue 19 dye removal: Optimization using desirability function approach, Surf. Interfaces. 28 (2022), 101698, https://doi.org/10.1016/j.scp.2021.100379

[7] Z. Yin, Z. Li, Y. Deng, M. Xue, Y. Chen, J. Ou, Y. Xie, Y. Luo, C. Xie, Z. Hong, Multifunctional CeO_2-coated pulp/cellulose nanofibers (CNFs) membrane for wastewater treatment: Effective oil/water separation, organic contaminants photodegradation, and anti-bioadhesion activity, Ind. Crops Prod. 197 (2023), 116672, https://doi.org/10.1016/j.indcrop.2023.116672

[8] A. Reghioua, D. Barkat, A.H. Jawad, A.S. Abdulhameed, S. Rangabhashiyam, M.R. Khan, Z.A. ALOthman, Magnetic Chitosan-Glutaraldehyde/Zinc Oxide/Fe_3O_4 nanocomposite: Optimization and adsorptive mechanism of Remazol Brilliant Blue dye removal, J. Polym. Environ. 29 (2021) 3932-3947, https://doi.org/10.1007/s10924-021-02160-z

[9] A.H. Jawad, S. Rangabhashiyam, A.S. Abdulhameed, S.S.A. Syed-Hassan, Z.A. ALOthman, L.D. Wilson, Process optimization and adsorptive mechanism for Reactive Blue 19 dye by Magnetic Crosslinked Chitosan/MgO/Fe3O4 Biocomposite, J. Polym. Environ. 30 (2022) 2759-2773, https://doi.org/10.1007/s10924-022-02382-9

[10] Z. Li, Z. Yin, W. Xiao, Y. Chen, C. Yang, Y. Luo, Z. Hong, M. Xue, Facile construction of robust superhydrophobic ZIF-8@pulp/cellulose nanofiber (CNF) membrane for multifunctional applications, Ind. Crops Prod. 209 (2024), 118001, https://doi.org/10.1016/j.indcrop.2023.118001

[11] Z.M. Zain, A.S. Abdulhameed, A.H. Jawad, Z.A. ALOthman, Z.M. Yaseen, A pH-Sensitive Surface of Chitosan/Sepiolite Clay/Algae Biocomposite for the Removal of Malachite Green and Remazol Brilliant Blue R Dyes: Optimization and Adsorption Mechanism Study, J. Polym. Environ. 31 (2023) 501-518, https://doi.org/10.1007/s10924-022-02614-y

[12] V.K. Gupta, R. Kumar, A. Nayak, T.A. Saleh, M.A. Barakart, Adsorptive removal of dyes from aqueous solution onto carbon nanotubes: A review, Adv. Colloid Interface Sci. 193-194 (2013) 24-34, https://doi.org/10.1016/j.cis.2013.03.003

[13] A. Nezamzadeh-Ejhieh, S. Hushmandrad, Solar photodecolorization of methylene blue by CuO/X zeolite as a heterogeneous catalyst, Appl. Catal. A: Gen. 388 (2010) 149-159, https://doi.org/10.1016/j.apcata.2010.08.042

[14] D. Chen, Y. Cheng, N. Zhou, P. Chen, Y. Wang, K. Li, S. Huo, P. Cheng, P. Peng, R. Zhang, L. Wang, H. Liu, Y. Liu, R. Ruan, Photocatalytic degradation of organic pollutants using TiO_2-based photocatalysts: A review, J. Clean. Prod. 268 (2020), 121725, https://doi.org/10.1016/j.jclepro.2020.121725

[15] A.Y. Shan, T.I.M. Ghazi, S. Abdul Rashid, Immobilisation of titanium dioxide onto supporting materials in heterogeneous photocatalysis: A review, Appl. Catal. A: Gen. 389 (2010) 1-8, https://doi.org/10.1016/j.apcata.2010.08.053

[16] K.P. Gopinath, N.V. Madhav, A. Krishnan, R. Malolan, G. Rangarajan, Present applications of titanium dioxide for the photocatalytic removal of pollutants from water: A review, J. Environ. Manag. 270 (2020), 110906, https://doi.org/10.1016/j.jenvman.2020.110906

[17] L.R. Conde-Rivera, A.F. Suarez-Escobar, J.J. Marin-Perez, M.J. Junco-Rodriguez, F.E. Lopez-Suarez, TiO_2 supported on activated carbon from tire waste for ibuprofen removal, Mater. Lett. 291 (2021), 129590, https://doi.org/10.1016/j.matlet.2021.129590

[18] C. Shen, Y.J. Wang, J.H. Xu, G.S. Luo, Facile synthesis and photocatalytic properties of TiO_2 nanoparticles supported on porous glass beads, Chem. Eng. J. 209 (2012) 478-485, https://doi.org/10.1016/j.cej.2012.08.044

[19] J. Gomes, B. Maniezo, P. Alves, P. Ferreira, R.C. Martins, Immobilization of TiO_2 onto a polymeric support for photocatalytic oxidation of a paraben's mixture, J. Water Process Eng. 46 (2022), 102458, https://doi.org/10.1016/j.jwpe.2021.102458

[20] A.H. Jawad, M.A. Nawi, Characterizations of the Photocatalytically-Oxidized Cross-Linked Chitosan-Glutaraldehyde and its Application as a Sub-Layer in the TiO_2/CS-GLA Bilayer Photocatalyst System, J. Polym. Environ. 20 (2012) 817-829, https://doi.org/10.1007/s10924-012-0434-5

[21] C. Li, L. Sun, J. Niu, A.A. Reka, P. Feng, H. Garcia, Core-shell Bi-containing spheres and TiO_2 nanoparticles co-loaded on kaolinite as an efficient photocatalyst for methyl orange degradation, Catal. Commun. 175 (2023), 106609, https://doi.org/10.1016/j.catcom.2023.106609

[22] S. Chkirida, N. Zari, R. Achour, H. Hassoune, A. Lachehab, A. Qaiss, R. Bouhfid, Highly synergic adsorption/photocatalytic efficiency of Alginate/Bentonite impregnated TiO_2 beads for wastewater treatment, J. Photochem. Photobiol. A: Chem. 412 (2021), 113215, https://doi.org/10.1016/j.jphotochem.2021.113215

[23] X. Tang, Q. Feng, K. Liu, X. Luo, J. Huang, Z. Li, A simple and innovative route to remarkably enhance the photocatalytic performance of TiO_2: Using micro-meso porous silica nanofibers as carrier to support highly-dispersed TiO_2 nanoparticles, Microporous Mesoporous Mater. 258 (2018) 251-261, https://doi.org/10.1016/j.micromeso.2017.09.024

[24] Z. Pan, E.A. Stemmler, H.J. Cho, W. Fan, L.A. LeBlanc, H.H. Patterson, A. Amirbahman, Photocatalytic degradation of 17α-ethinylestradiol (EE2) in the presence of TiO2-doped zeolite, J. Hazard. Mater. 279 (2014) 17-25, https://doi.org/10.1016/j.jhazmat.2014.06.040

[25] S. Tedesco, G. Hurst, A. Imtiaz, M. Ratova, L. Tosheva, P. Kelly, TiO_2 supported natural zeolites as biogas enhancers through photocatalytic pre-treatment of Miscanthus x giganteous crops, Energy 205 (2020), 117954, https://doi.org/10.1016/j.energy.2020.117954

[26] S. Liu, M. Lim, R. Amal, TiO_2-coated natural zeolite: Rapid humic acid adsorption and effective photocatalytic regeneration, Chem. Eng. Sci. 105 (2014) 46-52, https://doi.org/10.1016/j.ces.2013.10.041

[27] A. Nezamzadeh-Ejhieh, E. Shahriari, Photocatalytic decolorization of methyl green using Fe(II)-o-phenanthroline as supported onto zeolite Y, J. Ind. Eng. Chem. 20 (2014) 2719-2726, https://doi.org/10.1016/j.jiec.2013.10.060

[28] Y. Zang, R. Farnood, J. Currie, Photocatalytic activities of AgBr/Y-zeolite in water under visible light irradiation, Chem. Eng. Sci. 64 (2009) 2881-2886, https://doi.org/10.1016/j.ces.2009.03.015

[29] N. Dubey, S.S. Rayalu, N.K. Labhsetwar, R.R. Naidu, R.V. Chatti, S. Devotta, Photocatalytic properties of zeolite-based materials for the photoreduction of methyl orange, Appl. Catal. A: Gen. 303 (2006) 152-157, https://doi.org/10.1016/j.apcata.2006.01.043

[30] R. Chatti, S.S. Rayalu, N. Dubey, N. Labhsetwar, S. Devotta, Solar-based photoreduction of methyl orange using zeolite supported photocatalytic materials, Sol. Energy Mater. Sol. Cells 91 (2007) 180-190, https://doi.org/10.1016/j.solmat.2006.08.009

[31] S. Sankararaman, K.B. Yoon, T. Yabe, J.K. Kochi, Control of Back Electron Transfer from Charge-Transfer Ion Pairs by Zeolite Supercages, J. Am. Chem. Soc. 113 (1991) 1419-1421, https://doi.org/10.1021/ja00004a057

[32] Y. Luo, X. Wei, B. Gao, W. Zou, Y. Zheng, Y. Yang, Y. Zhang, Q. Tong, L. Dong, Synergistic adsorption-photocatalysis processes of graphitic carbon nitrate (g-C3N4) for contaminant removal: Kinetics, models, and mechanisms, Chem. Eng. J. 375 (2019), 122019, https://doi.org/10.1016/j.cej.2019.122019

[33] M. D'Auria, L. Emanuele, R. Racioppi, V. Velluzzi, Photochemical degradation of crude oil: Comparison between direct irradiation, photocatalysis, and photocatalysis on zeolite, J. Hazard. Mater. 164 (2009) 32-38, https://doi.org/10.1016/j.jhazmat.2008.07.111

[34] A.H. Alwash, A.Z. Abdullah, N. Ismail, Zeolite Y encapsulated with Fe-TiO_2 for ultrasound-assisted degradation of amaranth dye in water, J. Hazard. Mater. 233-234 (2012) 184-193, https://doi.org/10.1016/j.jhazmat.2012.07.021

[35] D.I. Petkowicz, R. Brambilla, C. Radtke, C.D.S. da Silva, Z.N. da Rocha, S.B.C. Pergher, J.H.Z. dos Santos, Photodegradation of methylene blue by in situ generated titania supported on a NaA zeolite, Appl. Catal. A: Gen. 357 (2009) 125-134, https://doi.org/10.1016/j.apcata.2008.12.040

[36] A. Nezamzadeh-Ejhieh, M. Karimi-Shamsabadi, Decolorization of a binary azo dyes mixture using CuO incorporated nanozeolite-X as a heterogeneous catalyst and solar irradiation, Chem. Eng. J. 228 (2013) 631-641, https://doi.org/10.1016/j.cej.2013.05.035

[37] W. Zhang, F. Bi, Y. Yu, H. He, Phosphoric acid treating of ZSM-5 zeolite for the enhanced photocatalytic activity of TiO_2/HZSM-5, J. Mol. Catal. A: Chem. 372 (2013) 6- 12, https://doi.org/10.1016/j.molcata.2013.02.002

[38] D.I. Petkowicz, S.B.C. Pergher, C.D.S. da Silva, Z.N. da Rocha, J.H.Z. dos Santos, Catalytic photodegradation of dyes by in situ zeolite-supported titania, Chem. Eng. J. 158 (2010) 505-512, https://doi.org/10.1016/j.cej.2010.01.039

[39] S. Landi, I.R. Segundo, E. Freitas, M. Vasilevskiy, J. Carneiro, C.J. Tavares, Use and misuse of the Kubelka-Munk function to obtain the band gap energy from diffuse reflectance measurements, Solid State Commun. 341 (2022), 114573, https://doi.org/10.1016/j.ssc.2021.114573

[40] M.I. Litter, Heterogeneous photocatalysis: Transition metal ions in photocatalytic systems, Appl. Catal. B: Environ. 23 (1999) 89-114, https://doi.org/10.1016/S0926-3373(99)00069-7

[41] I. Polatoglu, F. Cakicioglu-Ozkan, Aqueous interactions of zeolitic material in acidic and basic solutions, Microporous Mesoporous Mater. 132 (2010) 219-225, https://doi.org/10.1016/j.micromeso.2010.03.001

[42] Y. Luo, Y. Han, M. Xue, Y. Xie, Z. Yin, C. Xie, X. Li, Y. Zheng, J. Huang, Y. Zhang, Y. Yang, B. Gao, Ball-milled bismuth oxybromide/biochar composites with enhanced removal of reactive red owing to the synergy between adsorption and photodegradation, J. Environ. Manage. 308 (2022), 114652, https://doi.org/10.1016/j.jenvman.2022.114652

[43] É.C. Lima, M.A. Adebayo, F.M. Machado, Kinetic and equilibrium models of adsorption. In: Bergmann, C., Machado, F. (Eds), Carbon Nanomaterials as Adsorbents for Environmental and Biological Applications, Carbon Nanostructures, Springer International Publishing, Switzerland, 2015, pp. 33-69, https://doi.org/10.1007/978-3-319-18875-1_3

[44] A. Imessaoudene, S. Cheikh, A. Hadadi, N. Hamri, J.C. Bollinger, A. Amrane, H. Tahraoui, A. Manseri, L. Mouni, Adsorption Performance of Zeolite for the Removal of Congo Red Dye: Factorial Design Experiments, Kinetic, and Equilibrium Studies, Separations 10 (2023), 57, https://doi.org/10.3390/separations10010057

[45] H.N. Tran, S.J. You, H.P. Chao, Fast and efficient adsorption of methylene green 5 on activated carbon prepared from new chemical activation method, J. Environ. Manage. 188 (2017) 322-336, https://doi.org/10.1016/j.jenvman.2016.12.003

[46] S. Cheikh, A. Imessaoudene, J.C. Bollinger, A. Manseri, A. Bouzaza, A. Hadadi, N. Hamri, A. Amrane, L. Mouni, Adsorption behavior and mechanisms of the emerging antibiotic pollutant norfloxacin on eco-friendly and low-cost hydroxyapatite: Integrated experimental and response surface methodology optimized adsorption process, J. Mol. Liq. 392 (2023), 123424, https://doi.org/10.1016/j.molliq.2023.123424

[47] N. Hamri, A. Imessaoudene, A. Hadadi, S. Cheikh, A. Boukerroui, J.C. Bollinger, A. Amrane, H. Tahraoui, H.N. Tran, A.O. Ezzat, H.A. Al-Lohedan, L. Mouni, Enhanced adsorption capacity of Methylene Blue dye onto kaolin through acid treatment: Batch adsorption and machine learning studies, Water 16 (2024), 243, https://doi.org/10.3390/w16020243

[48] A. Hadadi, A. Imessaoudene, J.C. Bollinger, S. Cheikh, A. Manseri, L. Mouni, Dual valorization of Potato Peel (Solanum tuberosum) as a versatile and sustainable agricultural waste in both bioflocculation of Eriochrome Black T and biosorption of Methylene Blue, J. Polym. Environ. 31 (2023), 2983-2998, https://doi.org/10.1007/s10924-023-02780-7

[49] C.C. Chen, C.S. Lu, Y.C. Chung, J.L. Jan, UV light induced photodegradation of malachite green on TiO2 nanoparticles, J. Hazard. Mater. 141 (2007) 520-528, https://doi.org/10.1016/j.jhazmat.2006.07.011

[50] R. Han, Y. Wang, Q. Sun, L. Wang, J. Song, X. He, C. Dou, Malachite green adsorption onto natural zeolite and reuse by microwave irradiation, J. Hazard. Mater. 175 (2010) 1056-1061, https://doi.org/10.1016/j.jhazmat.2009.10.118

[51] A. Imessaoudene, S. Cheikh, J.C. Bollinger, L. Belkhiri, A. Tiri, A. Bouzaza, A. El Jery, A. Assadi, A. Amrane, L. Mouni, Zeolite Waste Characterization and Use as Low-Cost, Ecofriendly, and Sustainable Material for Malachite Green and Methylene Blue Dyes Removal: Box–Behnken Design, Kinetics, and Thermodynamics, Appl. Sci. 12 (2022), 7587, https://doi.org/10.3390/app12157587

[52] X. Wei, X. Wang, Y. Pu, A. Liu, C. Chen, W. Zou, Y. Zheng, J. Huang, Y. Zhang, Y. Yang, M. Naushad, B. Gao, L. Dong, Facile ball-milling synthesis of CeO_2/g-C_3N_4 Z-scheme heterojunction for synergistic adsorption and photodegradation of methylene blue: Characteristics, kinetics, models, and mechanisms, Chem. Eng. J. 420 (2021), 127719, https://doi.org/10.1016/j.cej.2020.127719

[53] F. Yu, F. Tian, H. Zou, Z. Ye, C. Peng, J. Huang, Y. Zheng, Y. Zhang, Y. Yang, X. Wei, B. Gao, ZnO/biochar nanocomposites via solvent free ball milling for enhanced

adsorption and photocatalytic degradation of methylene blue, J. Hazard. Mater. 415 (2021), 125511, https://doi.org/10.1016/j.jhazmat.2021.125511

[54] Y. Luo, Y. Han, M. Xue, Y. Xie, Z. Yin, C. Xie, X. Li, Y. Zheng, J. Huang, Y. Zhang, Y. Yang, B. Gao, Ball-milled bismuth oxybromide/biochar composites with enhanced removal of reactive red owing to the synergy between adsorption and photodegradation, J. Environ. Manage. 308 (2022) 114652, https://doi.org/10.1016/j.jenvman.2022.114652

[55] Y. Luo, A. Zheng, M. Xue, Y. Xie, S. Yu, Z. Yin, C. Xie, Z. Hong, W. Tan, W. Zou, L. Dong, B. Gao, Ball-milled Bi_2MoO_6/biochar composites for synergistic adsorption and photodegradation of methylene blue: Kinetics and mechanisms, Ind. Crops Prod. 186 (2022), 115229, https://doi.org/10.1016/j.indcrop.2022.115229

[56] Y. Luo, Y. Han, Y. Hua, M. Xue, S. Yu, L. Zhang, Z. Yin, X. Li, X. Ma, H. Wu, T. Liu, Y. Shen, B. Gao, Step scheme nickel-aluminium layered double hydroxides/biochar heterostructure photocatalyst for synergistic adsorption and photodegradation of tetracycline, Chemosphere 309 (2022), 136802, https://doi.org/10.1016/j.chemosphere.2022.136802

[57] D. Ning, J. Li, Y. Lan, H.Y. Sohn, J. Yang, C. Chen, Z. Chu, X. Mao, Molten salt synthesis of Z-scheme CeO_2/C_3N_4 photocatalysts with excellent properties for removal of organic pollutants: Characterization, kinetics and mechanisms, J. Rare Earths. 41 (2023) 1153-1162, https://doi.org/10.1016/j.jre.2022.07.021

Supporting Information

Chapter VI. Synthesis of a TiO_2/zeolite composite: Evaluation of adsorption-photodegradation synergy for the removal of Malachite Green

The adsorption capacity at any time was calculated by the straightforward equation:

$$q_t(mg.L^{-1}) = \frac{(C_0 - C_t).V}{m} \qquad (S1)$$

Whereas, the discoloration efficiency *E* (%) has been calculated as:

$$E\ (\%) = \frac{(C_0 - C_t).100}{C_0} \qquad (S2)$$

where q_t is the adsorption capacity at a contact time *t* (min), C_0 (mg.L^{-1}) and C_t (mg.L^{-1}) are the initial MG concentrations and at time *t*, respectively, V (L) is the volume of the dye solution, and *m* (g) is the dried weight of the solid.

Preliminary tests results

At initial pH of around 4, the active surface functional groups of zeolite which are mainly the Silanol (Si-OH) and Aluminol groups (Al-OH) become protonated, as it is shown by the consecutive reactions provided in Eq. (S3, S4) [1].

Ion exchange reaction:

$$[S-ONa]_Z + H^+_{(aq)} \leftrightarrow [S-OH]_Z + Na^+_{(aq)} \qquad (S3)$$

adsorption on neutral surface:

$$\underbrace{[S-OH]_Z}_{Neutral\ surface} + H^+_{(aq)} \leftrightarrow \underbrace{[S-OH_2^+]_Z}_{Protonated\ surface} \qquad (S4)$$

where S is surface central metal (Si, Al) of zeolite, and Na^+ is the metal cation balancing the electrical charge of LTA-type zeolite framework. On the other side, considering the amphoteric character of TiO_2 in aqueous solution, at pH near 4, the surface hydroxyl groups (Ti-OH) in TiO_2-Zeo surface composite can also be easily protonated as follows [2]:

$$\underbrace{[Ti-OH]_Z}_{Neutral\ surface} + H^+_{(aq)} \leftrightarrow \underbrace{[Ti-OH_2^+]_Z}_{Protonated\ surface} \qquad (S5)$$

Therefore, the interaction that occurred between the protonated sites $SiOH_2^+$, $AlOH_2^+$, and $TiOH_2^+$ of the surface of TiO_2-Zeo, and the amines or aromatic groups of the MG molecules is the probable mechanism of dye uptake [3].

In the case of photocatalysis, the overall photodegradation reaction of MG by TiO_2-Zeo under UV irradiation can be simplified as shown in step 11 (Table VI.S1). MG photodegradation reaction is initiated when a photoexcited electron transits from the filled valence band to the empty conduction band of TiO_2 as the absorbed photon energy, *hv*, equals or exceeds the band gap of the semiconductor [4]. Therefore, a strongly reducing electron (e_{cb}^-) and strongly oxidizing hole (h_{vb}^+) pairs will be generated (Table VI.S1, step 1). The chain reactions (step 2-8) are the separation and trapping of electrons and holes to reducing sites and oxidizing sites on the surface of TiO_2-Zeo, followed by generation of reactive species such as $OH^\bullet$ radicals, $O_2^{\bullet-}$ radicals, and H_2O_2 [5]. Finally, MG degradation can take place via direct oxidation by the hole (step 9), since the hole is a strong oxidizing agent, and through radical reactions (step 10), giving CO_2 and H_2O as products [6].

Table VI.S1
Photodegradation mechanism [5].

Step 1	$TiO_2 \xrightarrow{hv \geq 3.23\ eV} TiO_2^\bullet (e_{cb}^- + h_{vb}^+)$
Step 2	$h_{vb}^+ + H_2O \longrightarrow OH^\bullet + H^+$
Step 3	$e_{cb}^- + O_2 \longrightarrow O_2^{\bullet-}$
Step 4	$O_2^{\bullet-} + H_2O \longrightarrow OH^- + HO_2^\bullet$
Step 5	$O_2^{\bullet-} + HO_2^\bullet + H^+ \longrightarrow H_2O_2 + O_2$
Step 6	$O_2 + 2e_{cb}^- + H^+ \longrightarrow H_2O_2$
Step 7	$2h_{vb}^+ + 2H_2O \longrightarrow 2H_2O_2 + 2\ H^+$
Step 8	$H_2O_2 + e_{cb}^- \longrightarrow OH^- + OH^\bullet$
Step 9	$h_{vb}^+ + MG \longrightarrow intermediate\ products + CO_2 + H_2O$
Step 10	$OH^\bullet + MG \longrightarrow intermediate\ products \longrightarrow CO_2 + H_2O$
Step 11	$MG + O_2 \xrightarrow{hv, TiO_2-Zeo} CO_2 + H_2O$

In MG removal by photolysis, the following conventional mechanism of direct photolysis can describe the dye decomposition reactions [7]:

$H_2O + hv \longrightarrow OH^\bullet + H^+$ (S6)

$MG + OH^\bullet \longrightarrow products$ (S7)

Initially, the water molecule is cleaved under UV irradiation and transformed into hydrogen and hydroxyl radicals, then the dye molecules react with free radicals to produce the decomposition products. The overall photolysis reaction of MG can be schematized as follows

$$MG + O_2 \xrightarrow{h\nu} produts \qquad (S8)$$

R^2, RMSE and Chi-Sqr formulas

The coefficient of determination (R^2), root mean sum of square error (*RMSE*), and *Chi-Sqr* as goodness-of-fit criteria can be computed as:

$$R^2 = 1 - \frac{\sum_{i=1}^{n}\left(Y_{i,exp} - Y_{i,Cal}\right)^2}{\sum_{i=1}^{n}\left(Y_{i,exp} - Y_{mean}\right)^2} \qquad (S9)$$

$$RMSE = \sqrt{\frac{\sum_{i=1}^{n}\left(Y_{i,exp} - Y_{i,Cal}\right)^2}{n-p}} \qquad (S10)$$

$$Chi - Sqr = \sum_{i=1}^{n} \frac{\left(Y_{i,exp} - Y_{i,Cal}\right)^2}{Y_{i,Cal}} \qquad (S11)$$

where n is the number of observed data $Y_{i,exp}$ (i = 1 to i = n), and Y_{mean} is their mean. $Y_{i,Cal}$ is the predicted value by the model, and p is the number of parameters of the model.

Small *RMSE* and *Chi-Sqr* values, close to zero, and large R^2 value, close to 1, indicate better agreement of experimental data with the model.

Integrated forms of differential models

The integrated form of the pseudo-first-order kinetic model (Eq. 3) for boundary conditions (t = 0, $C_t = C_0$ and t = t, $C_t = C_t$) leads to the nonlinear equation:

$$C_t = C_e + (C_0 - C_e).e^{-k_{ads}.t} \qquad (S12)$$

The integrated form of the first-order kinetic model (Eq. 4) and the modified Elovich model (Eq. 5) for the same boundary conditions gives Eq. (S13) and Eq. (S14), respectively.

$$C_t = C_0.e^{-k_1.t} \qquad (S13)$$

$$C_t = C_0 - {}^{1}/_{\beta}.\ln(1 + \beta.k_e.C_0.t) \qquad (S14)$$

Table VI.S2
Reusability of TiO_2-Zeo and the best-fit parameters of modified-Elovich's kinetics model for each cycle: pH = 4, T = 25°C and photocatalyst dose = 0.5 $g.L^{-1}$.

Parameters / Material	C_0 ($mg.L^{-1}$)	m (g)	Cycles time	k_e (mn^{-1})	β	R^2	RMSE	Chi-Sqr
TiO_2-Zeo	25	0.5	1	2.18×10^{-2}	0.1000	0.999	0.199	0.039
			2	1.66×10^{-2}	0.1009	0.993	0.523	0.274
			3	1.09×10^{-2}	0.1061	0.986	0.607	0.369
	35	0.5	1	1.58×10^{-2}	0.0781	0.998	0.328	0.107
			2	1.16×10^{-2}	0.0715	0.992	0.673	0.453
			3	8.65×10^{-3}	0.0666	0.989	0.727	0.528

References

[1] Polatoglu, F. Cakicioglu-Ozkan, Aqueous interactions of zeolitic material in acidic and basic solutions, Microporous Mesoporous Mater. 132 (2010) 219-225, https://doi.org/10.1016/j.micromeso.2010.03.001

[2] B. Ohtani, Y. Okugawa, S. Nishimoto, T. Kagiya, Photocatalytic activity of TiO_2, powders suspended in aqueous silver nitrate solution. Correlation with pH-dependent surface structures, J. Phys. Chem. 91 (1987) 3550-3555, https://doi.org/10.1021/j100297a017

[3] C.C. Chen, C.S. Lu, Y.C. Chung, J.L. Jan, UV light induced photodegradation of malachite green on TiO2 nanoparticles, J. Hazard. Mater. 141 (2007) 520-528, https://doi.org/10.1016/j.jhazmat.2006.07.011

[4] U.I. Gayaa, A.H. Abdullah, Heterogeneous photocatalytic degradation of organic contaminants over titanium dioxide: A review of fundamentals, progress and problems, J. Photochem. Photobiol. C Photochem. Rev. 9 (2008), 1-12, https://doi.org/10.1016/j.jphotochemrev.2007.12.003

[5] Z. Pan, E.A. Stemmler, H.J. Cho, W. Fan, L.A. LeBlanc, H.H. Patterson, A. Amirbahman, Photocatalytic degradation of 17α-ethinylestradiol (EE2) in the presence of TiO2-doped zeolite, J. Hazard. Mater. 279 (2014) 17-25, https://doi.org/10.1016/j.jhazmat.2014.06.040

[6] S. Cheikh, A. Imessaoudene, J.C. Bollinger, A. Hadadi, A. Manseri, A. Bouzaza, A. Assadi, A. Amrane, M. Zamouche, A. El Jery, L. Mouni, Complete elimination of the ciprofloxacin antibiotic from water by the combination of adsorption-photocatalysis process using natural hydroxyapatite and TiO_2, Catalysts 13 (2023), 336, https://doi.org/10.3390/catal13020336

[7] S.M. Anisuzzaman, C.G. Joseph, C.K. Pang, N.A. Affandi, S.N. Maruja, V. Vijayan, Current trends in the utilization of photolysis and photocatalysis treatment processes for

the remediation of dye wastewater: A short review, ChemEngineering 6, 2022, 58, https://doi.org/10.3390/chemengineering6040058

General conclusion

General conclusion

Ensuring water quality remains a major challenge for humanity, given the complexity of modern life and the growing diversity of pollution sources. Many countries have implemented stricter water pollution control regulations, requiring compliance with rigorous new standards, which has driven significant progress in the research and development of advanced water treatment technologies.

Among the proposed solutions, several techniques have been considered, including adsorption and heterogeneous photocatalysis, both of which are cost-effective methods with distinct advantages and limitations. The first technique has the significant advantage of treating large volumes of effluent with a high organic pollutant load; however, its limitation lies in merely transferring pollutants from the liquid phase to a solid phase without actual degradation. In contrast, the second technique effectively degrades organic pollutants but is limited to treating effluents with relatively low pollutant concentrations.

The combination or coupling of adsorption and photocatalysis within a single unit operation could be an ideal solution to overcome the limitations of each technique while maximizing the advantages of the process.

The main objective of this study was to enhance the performance of adsorption and photocatalytic processes through a hybrid system in which these processes operate synergistically. The key to this hybrid process is the development of a versatile and sustainable composite, designed to function simultaneously and efficiently as both an adsorbent and a photocatalyst for the effective removal of textile dyes. To evaluate the effectiveness of the newly developed composite, we investigated the removal and degradation of various model dye pollutants in water.

In the first part of our work, we evaluated the adsorption performance of zeolite for the removal of cationic dyes, specifically methylene blue (MB) and malachite green (MG). An LTA-type zeolite from the TFT gas complex (Sonatrach), previously used in multiple natural gas dehydration cycles and considered solid waste by the complex, was appropriately treated and then employed as an adsorbent, referred to here as 4AZW. This approach aimed to valorize the waste and implement the “treat waste with waste” strategy. After thorough characterization, the 4AZW material largely retained the crystalline structure of LTA-type zeolite, which provides a significant advantage in this study. The initial pH of the solution is a crucial factor affecting dye adsorption performance. For methylene blue, the highest adsorption capacities were

observed within the pH range of 5 to 10, reaching a maximum efficiency of 99% at pH 8.5. In the case of malachite green, a consistently high adsorption capacity was maintained between pH 5 and 11, with a peak efficiency of 99.5% at pH 8. Notably, the near-total removal of both dyes occurs at the same or very similar pH values, representing an additional advantage of this adsorbent. However, a key limitation is its relatively low maximum adsorption capacity, measured at 9.95 mg/g for MB and 45.64 mg/g for MG.

In the second part of the thesis, a virgin commercial LTA-type zeolite was utilized to explore its superior adsorption properties. Congo Red was selected as the model molecule to examine the adsorption behavior of LTA-type zeolite toward anionic dyes. The key findings of this study are: (i) the adsorption process occurs at a relatively fast rate, and (ii) the adsorbent demonstrates excellent performance in Congo Red removal, achieving up to 98.7% dye removal even at low doses of 0.1 g/L, with an exceptionally high maximum adsorption capacity of 666.5 mg/g.

In the final part of this work, building on the high adsorption properties demonstrated by the LTA-type zeolite in the second part, this material was used as a support for the TiO_2 semiconductor. The goal was to synthesize a versatile and sustainable composite capable of simultaneously functioning synergistically as both an adsorbent and photocatalyst for dye removal. The TiO_2-Zeo composite was synthesized using the solid-state dispersion method and thoroughly characterized. The characterization results revealed that the zeolitic matrix retained its original structure without any significant alteration. Additionally, the measured band gap energy of 3.23 eV was comparable to that of the pristine TiO_2, indicating that the TiO_2 nanoparticles were merely deposited on the surface of the zeolite support. The main conclusions drawn from this part are as follows: (i) zeolite-supported TiO_2 photocatalysts demonstrated higher efficiency than TiO_2 nanoparticles alone in the photodecolorization of Malachite Green solution, with minimal sensitivity to the pH of the medium; (ii) owing to their excellent adsorption properties, the incorporation of zeolite into the composite promotes the migration and preconcentration of dye molecules near the photoactive sites of TiO_2, thereby enhancing photodegradation efficiency; and (iii) the adsorption and photodegradation processes within the TiO_2-Zeo photocatalyst exhibit a synergistic interaction that significantly improves the overall removal efficiency of organic pollutants. Consequently, this composite represents a promising material for the treatment of organic contaminants in water.

Abstract:

This study addresses the challenge of wastewater contamination by synthetic dyes, particularly from the textile industry. A three-phase approach was undertaken to develop an efficient dye removal system. In the first phase, an LTA-type zeolite repurposed from industrial waste (4AZW) was evaluated for cationic dye adsorption, though its low adsorption capacity remained a limitation. The second phase focused on a commercial LTA-type zeolite, which demonstrated exceptional adsorption performance for anionic dyes, with a maximum capacity of 666.5 mg/g. In the final phase, a zeolite-supported TiO_2 composite (TiO_2-Zeo) was synthesized to function synergistically as both an adsorbent and a photocatalyst. Key findings revealed that TiO_2-Zeo outperformed TiO_2 nanoparticles alone in dye degradation, facilitated dye molecule migration to photoactive sites, and enhanced overall pollutant removal through combined adsorption and photodegradation. This composite presents a promising solution for wastewater treatment and organic pollution abatement.

Résumé:

Cette étude s'inscrit dans le cadre de la lutte contre la contamination des eaux usées par les colorants synthétiques, notamment ceux émis par l'industrie textile. Une stratégie en trois étapes a été mise en œuvre afin de concevoir un système performant d'élimination des colorants. Dans un premier temps, une zéolite de type LTA, valorisée à partir de déchets industriels (4AZW), a été testée pour l'adsorption de colorants cationiques, bien que sa faible capacité d'adsorption ait constitué un facteur limitant. La deuxième phase a examiné les performances d'une zéolite commerciale de type LTA, qui s'est distinguée par une excellente capacité d'adsorption des colorants anioniques, atteignant un maximum de 666.5 mg/g. Enfin, la troisième phase a consisté en la synthèse d'un composite TiO_2-Zeo, associant du TiO_2 à une matrice zéolitique, afin de combiner les propriétés d'adsorption et de photocatalyse. Les résultats ont mis en évidence que ce composite surpassait les nanoparticules de TiO_2 seules en termes de dégradation des colorants, en facilitant la migration des molécules vers les sites photoactifs et en renforçant l'efficacité globale de l'élimination des polluants grâce à l'action synergique des mécanismes d'adsorption et de photodégradation. Ce matériau représente ainsi une solution prometteuse pour le traitement des eaux usées et la réduction de la pollution organique.

ملخص:

تتناول هذه الدراسة مشكلة تلوث مياه الصرف الصناعي بالأصباغ الاصطناعية، لا سيما تلك الناتجة عن صناعة النسيج. تم اعتماد نهج من ثلاث مراحل لتطوير نظام فعال لإزالة الأصباغ. في المرحلة الأولى، تم تقييم أداء الزيوليت من النوعLTA، المعاد تدويره من النفايات الصناعية والمستخدم كممتزات (4AZW) ، في إزالة الأصباغ الكاتيونية، رغم أن قدرته المنخفضة على الامتزاز شكلت قيدًا رئيسيًا. ركزت المرحلة الثانية على زيوليت تجاري من النوع LTA، حيث أظهر أداءً استثنائيًا في امتزاز الأصباغ الأنيونية، بقدرة قصوى بلغت 666.5 ملغ/غ. أما في المرحلة الأخيرة، فقد تم تصنيع مركب من أكسيد التيتانيوم (TiO_2) مدعوم على الزيوليت (TiO_2-Zeo) ، ليعمل بشكل متكامل كممتزومحفز ضوئي في آنٍ واحد. كشفت النتائج الرئيسية أن TiO_2-Zeo تفوق على جزيئات TiO_2 النانوية وحدها في تحلل الأصباغ، كما سهلت عمليةً انتقال جزيئات الصبغة نحو المواقع الفعالة ضوئيًا، مما عزز كفاءة إزالة الملوثات من خلال آليتي االامتزاز والتحلل الضوئي. وبالتالي، يمثل هذا المركب حلاً واعدًا لمعالجة مياه الصرف الصناعي والحد من التلوث العضوي.